

# LIMDD: A Decision Diagram for Simulation of Quantum Computing Including Stabilizer States

Lieuwe Vinkhuijzen<sup>\*,1</sup>, Tim Coopmans<sup>\*,1,2</sup>, David Elkouss<sup>2,3</sup>, Vedran Dunjko<sup>1</sup>, and Alfons Laarman<sup>1</sup>

<sup>1</sup>Leiden University, The Netherlands

<sup>2</sup>Delft University of Technology, The Netherlands

<sup>3</sup>Networked Quantum Devices Unit, Okinawa Institute of Science and Technology Graduate University, Okinawa, Japan

Efficient methods for the representation and simulation of quantum states and quantum operations are crucial for the optimization of quantum circuits. Decision diagrams (DDs), a well-studied data structure originally used to represent Boolean functions, have proven capable of capturing relevant aspects of quantum systems, but their limits are not well understood. In this work, we investigate and bridge the gap between existing DD-based structures and the stabilizer formalism, an important tool for simulating quantum circuits in the tractable regime. We first show that although DDs were suggested to succinctly represent important quantum states, they actually require exponential space for certain stabilizer states. To remedy this, we introduce a more powerful decision diagram variant, called Local Invertible Map-DD (LIMDD). We prove that the set of quantum states represented by poly-sized LIMDDs strictly contains the union of stabilizer states and other decision diagram variants. Finally, there exist circuits which LIMDDs can efficiently simulate, but which cannot be efficiently simulated by two state-of-the-art simulation paradigms: the Clifford +  $T$  simulator and Matrix-Product States. By uniting two successful approaches, LIMDDs thus pave the way for fundamentally more powerful solutions for simulation and analysis of quantum computing.

---

\* These authors contributed equally.  
 Lieuwe Vinkhuijzen\*: [l.t.vinkhuijzen@liacs.leidenuniv.nl](mailto:l.t.vinkhuijzen@liacs.leidenuniv.nl)  
 Tim Coopmans\*: [t.j.coopmans@tudelft.nl](mailto:t.j.coopmans@tudelft.nl)  
 David Elkouss: [d.elkousscoronas@tudelft.nl](mailto:d.elkousscoronas@tudelft.nl), <https://www.davidelkouss.com>  
 Vedran Dunjko: [v.dunjko@liacs.leidenuniv.nl](mailto:v.dunjko@liacs.leidenuniv.nl), <https://liacs.leidenuniv.nl/~dunjko>  
 Alfons Laarman: [a.w.laarman@liacs.leidenuniv.nl](mailto:a.w.laarman@liacs.leidenuniv.nl), <https://alfons.laarman.com>

# Contents

<b>1</b>	<b>Introduction</b>	<b>3</b>
<b>2</b>	<b>Preliminaries: decision diagrams and the stabilizer formalism</b>	<b>4</b>
2.1	Decision diagrams . . . . .	4
2.2	Pauli operators and stabilizer states . . . . .	5
<b>3</b>	<b>Main results</b>	<b>6</b>
3.1	The LIMDD data structure . . . . .	6
3.2	Exponential separations of LIMDDs with the Clifford + T simulator, QMDDs and Matrix Product States . . . . .	8
3.3	Simulating Quantum Circuits with Pauli-LIMDDs . . . . .	11
<b>4</b>	<b>Canonicity: how to keep a LIMDD fully reduced during simulation</b>	<b>17</b>
4.1	LIMDD canonical form . . . . .	17
4.2	The MAKEEDGE subroutine: Maintaining canonicity during simulation . . . . .	20
4.3	Dynamic programming in the APPLYGATE algorithm . . . . .	22
<b>5</b>	<b>Related work</b>	<b>23</b>
<b>6</b>	<b>Discussion</b>	<b>23</b>
<b>7</b>	<b>Acknowledgements</b>	<b>24</b>
<b>A</b>	<b>Efficient linear-algebra algorithms for stabilizer subgroups</b>	<b>28</b>
<b>B</b>	<b>Proof that cluster states and coset states need exponentially-large QMDDs</b>	<b>29</b>
<b>C</b>	<b>How to write graph states, coset states and stabilizer states as Tower-LIMDDs</b>	<b>32</b>
<b>D</b>	<b>Efficient algorithms for choosing a canonical high label</b>	<b>37</b>
D.1	Constructing the stabilizer subgroup of a LIMDD node . . . . .	39
D.2	Efficiently finding a minimal LIM by multiplying with stabilizers . . . . .	42
<b>E</b>	<b>Advanced algorithms</b>	<b>44</b>
E.1	Measuring an arbitrary qubit . . . . .	44
E.2	Applying Hadamards to stabilizer states in polynomial time . . . . .	46
<b>F</b>	<b>LIMDDs prepare the W state efficiently</b>	<b>48</b>
<b>G</b>	<b>Numerical search for the stabilizer rank of Dicke states</b>	<b>52</b>

# 1 Introduction

Classical simulation of quantum computing is useful for circuit design [1, 2] and studying noise resilience in the era of Noisy Intermediate-Scale Quantum (NISQ) computers [3]. Moreover, identifying classes of quantum circuits that are classically simulatable, helps in excluding regions where a quantum computational advantage cannot be obtained. For example, circuits containing only Clifford gates (a non-universal quantum gate set), using an all-zero initial state, only compute the so-called ‘stabilizer states’ and can be simulated in polynomial time [4–8]. Stabilizer states, and associated formalisms for expressing them, are fundamental to many quantum error correcting codes [6] and play a role in measurement-based quantum computation [9]. In fact, simulation of general quantum circuits is fixed-parameter tractable in the number of non-Clifford gates [10], a principle on which many modern simulators are based [10–15].

Another method for simulating universal quantum computation is based on decision diagrams (DDs) [16–19], including Algebraic DDs [20–23], Quantum Multi-valued DDs [24–26] and Tensor DDs [27]. A DD is a directed acyclic graph (DAG) in which each path represents a quantum amplitude, enabling the succinct representation of many quantum states through the combinatorial nature of this structure. Various manipulation operations for DDs exist which implement any quantum gate operation. Together with other DD operations that can be used for measurement, strong simulation is easily implemented using a DD data structure [24, 25, 27]. Indeed, DD-based simulation was empirically shown to be competitive with state-of-the-art simulators [19, 25, 28] and is used in several simulator and circuit verification implementations [29, 30]. DDs and the stabilizer formalism are introduced in Sec. 2.

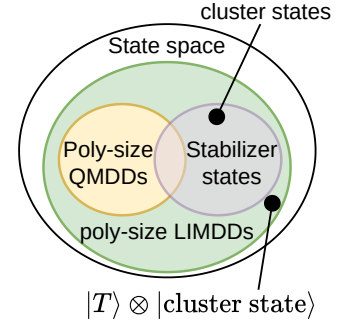


Figure 1: The set of stabilizer states and states represented as poly-sized LIMDDs (this work) and QMDDs.

QMDDs are currently the most succinct DD supporting quantum simulation, but in this paper we show that they require exponential size to represent a type of stabilizer state called a cluster state [31]. In order to unite the strengths of DDs and the stabilizer formalism and inspired by SLOCC (Stochastic Local Operations and Classical Communication) equivalence of quantum states [32, 33], in Sec. 3, we propose LIMDD: a new DD for quantum computing simulation using local invertible maps (LIMs). Specifically, LIMDDs eliminate the need to store multiple states which are equivalent up to LIMs, allowing more succinct DD representations. We prove that the set of quantum states that can be represented by poly-sized LIMDDs is larger than those that can be expressed in either the stabilizer formalism or by poly-sized QMDDs. Fig. 1 shows the resulting separation.

Further, we give algorithms for simulating quantum circuits using LIMDDs in the special case where the LIMs are strings of Pauli gates. We continue by investigating the power of these algorithms compared to state-of-the-art simulation algorithms other than DDs: Matrix Product States [34, 35] and the simulation method for Clifford +  $T$ -gate circuits by performing exponentially many stabilizer-state simulations in the original circuit’s number of  $T$  gates [5, 10–12]. We find circuit families which Pauli-LIMDD can efficiently simulate, which stands in stark contrast to the exponential space that both Matrix Product States and the Clifford+ $T$  simulator are known to require (assuming the Exponential Time Hypothesis [36]). This is the first analytical comparison between decision diagrams and matrix product states.

The crucial ingredients for decision diagrams in both the classical [37] and quantum [2] regimes have been *dynamic programming* (storing the result of each intermediate computation) and *canonicity* (each quantum state has a unique, smallest representative as a LIMDD). We provide algorithms for both in Sec. 4. Indeed, the main technical contribution of this paper is to introduce and formulate a canonical form for Pauli-LIMDDs, and develop an algorithm for bringing a Pauli-LIMDD into this canonical form. By interleaving this algorithm with the circuit simulation algorithms, we ensure that the LIMDDs that the algorithms act upon are always canonical, i.e., as small as possible.

The canonicity algorithm effectively determines whether two quantum states, each represented by a LIMDD node, are equivalent up to single-qubit Pauli operators. We proceed as follows to find such a Pauli operator  $P = P_{\text{first}} \otimes P_{\text{rest}}$ , which maps  $|\varphi\rangle$  to  $|\psi\rangle$  and to which we refer as an isomorphism between  $|\varphi\rangle$  and  $|\psi\rangle$ . First, we take out one qubit and write the states as, e.g.,  $|\varphi\rangle = c_0 |0\rangle |\varphi_0\rangle + c_1 |1\rangle |\varphi_1\rangle$  for complex coefficients  $c_0, c_1$ . Ignoring scalars for now, we then realize that  $P_{\text{rest}}$  must map the pair  $(|\varphi_0\rangle, |\varphi_1\rangle)$  to either  $(|\psi_0\rangle, |\psi_1\rangle)$  or  $(|\psi_1\rangle, |\psi_0\rangle)$  (in case  $P_{\text{first}}$  is a diagonal or antidiagonal single-qubit Pauli operator, respectively). Hence  $P_{\text{rest}}$  is a member of the intersection of the two sets of isomorphisms. Next, we realize that the set of all isomorphisms, e.g. mapping  $|\varphi_0\rangle$  to  $|\psi_0\rangle$ , is a coset  $\pi \cdot G$  of the stabilizer group  $G$  of  $|\varphi_0\rangle$  (i.e. the set of isomorphisms mapping  $|\varphi_0\rangle$  to itself) where  $\pi$  is a single isomorphism  $|\varphi_0\rangle \rightarrow |\psi_0\rangle$ . Thus, to find a (canonical) isomorphism between  $n$ -qubit states  $|\varphi\rangle \rightarrow |\psi\rangle$  (or determine no such isomorphism exists), we need three algorithms: to find (a) an isomorphism between  $(n-1)$ -qubit states, (b) the stabilizer group of an  $(n-1)$ -qubit state (in fact: the group generators, which form an efficient description), (c) the intersection of two cosets in the Pauli group (solving the *Pauli coset intersection problem*). Task (a) and (b) are naturally formulated as recursive algorithms on the number of qubits, which invoke each other in the recursion step. For (c) we provide a separate algorithm which first rotates the two cosets such that one is a member of the Pauli  $Z$  group, hence isomorphic to a binary vector space, followed by using existing algorithms for binary coset (hyperplane) intersection. Having characterized all isomorphisms  $|\varphi\rangle \rightarrow |\psi\rangle$ , we select the lexicographical minimum to ensure canonicity. We emphasize that the algorithm works for arbitrary quantum states, not only stabilizer states.

## 2 Preliminaries: decision diagrams and the stabilizer formalism

Here, we briefly introduce two methods to manipulate and succinctly represent quantum states: decision diagrams and the stabilizer formalism. Here and throughout the paper, we will omit the normalization factor of quantum states for readability.

### 2.1 Decision diagrams

The state  $|\varphi\rangle$  of  $n$  qubits is described by a function  $f: \{0, 1\}^n \rightarrow \mathbb{C}$  as

$$|\varphi\rangle = \sum_{x_1, x_2, \dots, x_n \in \{0, 1\}} f(x_1, x_2, \dots, x_n) |x_1\rangle \otimes |x_2\rangle \otimes \dots \otimes |x_n\rangle \quad (1)$$

where  $\otimes$  denotes the tensor product. A *partial assignment* ( $x_n = a_n, x_{n-1} = a_{n-1}, \dots, x_k = a_k$ ) to the variables induces a *subfunction*  $f_a$ , defined as  $f_a(x_{k-1}, \dots, x_1) \triangleq f(a_n, \dots, a_k, x_{k-1}, \dots, x_1)$ .

The Quantum Multi-valued Decision Diagram (QMDD) [24] is a data structure which can succinctly represent functions of the form  $f: \{0, 1\}^n \rightarrow \mathbb{C}$ , as above. See Fig. 2 for an example. Here each path from the root to the leaf visits nodes representing the variables  $x_3, x_2, x_1$ ; one variable at each level of the diagram. A QMDD is a rooted DAG with a unique leaf node. Each node has two outgoing edges, called its *low edge* and its *high edge*. A node is labeled with (the index of) a variable. The value  $f(x_n, \dots, x_1)$  is found by traversing the diagram, starting at the root and then following the low edge (dashed line) when  $x_i = 0$ , and the high edge (solid line) when  $x_i = 1$ , and multiplying the values on the edges of the path (shown in boxes), so, e.g.,  $f(1, 1, 0) = \frac{1}{2} \cdot 1 \cdot -\sqrt{2} \cdot 1 = -\frac{1}{\sqrt{2}}$  in Fig. 2. The nodes are divided into horizontal *levels*: the root node is at level  $n$ , its children are at level  $n-1$ , etc.

It will be convenient to denote an edge to node  $v$  labeled with  $\ell$  pictographically as  $\xrightarrow{\ell} \textcircled{v}$ . Each QMDD node on level  $k$  represents a (not necessarily normalized)  $k$ -qubit state. Namely, if a

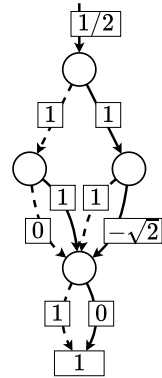


Figure 2: A QMDD representing the 3-qubit quantum state  $[0, 0, \frac{1}{2}, 0, \frac{1}{2}, 0, -\frac{1}{\sqrt{2}}, 0]^\top$ . Edge weights are shown in boxes. Adapted from Fig 2(b) in [25].

node has low edge  $\xrightarrow{\alpha} \textcircled{v_0}$  and high edge  $\xrightarrow{\beta} \textcircled{v_1}$ , then it represents the state  $\alpha |0\rangle \otimes |v_0\rangle + \beta |1\rangle \otimes |v_1\rangle$ . Each node represents a subfunction of  $f$ , up to a complex factor. Two nodes which represent functions which are equal up to a factor can be *merged*; when all eligible nodes have been merged, the QMDD is *reduced*. A reduced QMDD is a *canonical* representation: a given function has a unique reduced QMDD. QMDDs can represent any quantum state or matrix, and there are algorithms which multiply a matrix with a (state) vector in QMDD form. Therefore, QMDDs can simulate any quantum circuit, although they may become exponentially large (in the number of qubits), or take exponential time.

## 2.2 Pauli operators and stabilizer states

In contrast to decision diagrams, the stabilizer formalism forms an efficiently simulatable subset of quantum computation. Stabilizer states on  $n$  qubits are the states outputted by a circuit composed of the Hadamard gate  $H \triangleq |0\rangle\langle 0| + |1\rangle\langle 0| + |0\rangle\langle 1| - |1\rangle\langle 1|$ , the phase gate  $S \triangleq |0\rangle\langle 0| + i|1\rangle\langle 1|$  and CNOT  $\triangleq |00\rangle\langle 00| + |01\rangle\langle 01| + |10\rangle\langle 11| + |11\rangle\langle 10|$  (generators of the Clifford set) on input state  $|0\rangle^{\otimes n}$ . Equivalently, an  $n$ -qubit stabilizer state  $|\varphi\rangle$  is uniquely specified as the common (+1)-eigenvector of a maximal abelian subgroup  $G$  of Pauli operators, i.e.  $G := \{A|\varphi\rangle = |\varphi\rangle \mid A \in \text{PAULI}_n\}$ , where  $\text{PAULI}_n$  is the group generated by  $n$ -qubit tensor products of the single-qubit Pauli operators:

$$\mathbb{I}_2 \triangleq \begin{pmatrix} 1 & 0 \\ 0 & 1 \end{pmatrix}, X \triangleq \begin{pmatrix} 0 & 1 \\ 1 & 0 \end{pmatrix}, Y \triangleq \begin{pmatrix} 0 & -i \\ i & 0 \end{pmatrix}, Z \triangleq \begin{pmatrix} 1 & 0 \\ 0 & -1 \end{pmatrix}$$

where  $i$  is the complex unit. An  $n$ -qubit stabilizer group  $G$  contains  $2^n$  elements, succinctly represented by  $n$  independent generators, each of which requires  $\mathcal{O}(n)$  bits, yielding  $\mathcal{O}(n^2)$  bits in total. Updating a stabilizer state's generators after application of a Clifford gate or a single-qubit computational-basis measurement can be done in polynomial time in  $n$  [4, 5]. Graph states on  $n$  qubits are the output states of circuits with input state  $(|0\rangle + |1\rangle)^{\otimes n}$  followed by only CZ  $\triangleq |00\rangle\langle 00| + |01\rangle\langle 01| + |10\rangle\langle 10| - |11\rangle\langle 11|$  gates, and form a strict subset of all stabilizer states [38].

In this work we will also consider states which are not stabilizer states. In that case, we extend the notion of stabilizer group to mean simply the set  $\text{Stab}(|\varphi\rangle)$  of Pauli operators  $P$  which stabilize the state, i.e.,  $P|\varphi\rangle = |\varphi\rangle$ . In general, we will refer to an abelian subgroup of  $\text{PAULI}_n$ , not containing  $-\mathbb{I}_2^{\otimes n}$ , as an  $n$ -qubit *stabilizer subgroup*; such a group has  $\leq n$  generators. Such objects are also studied in the context of simulating mixed states [39] and quantum error correction [6]. Examples of stabilizer subgroups are  $\{\mathbb{I}_2\}$  for  $|0\rangle + e^{i\pi/4}|1\rangle$ ,  $\langle -Z \rangle$  for  $|1\rangle$  and  $\langle X \otimes X \rangle$  for  $(|00\rangle + |11\rangle) + 2(|01\rangle + |10\rangle)$ . Thus, in contrast to stabilizer states, a state is not uniquely identified by its stabilizer subgroup in this case. We also define  $\text{PAULILIM}_n$  as the group of  $n$ -qubit operators  $\lambda P_n \otimes \dots \otimes P_1$  for  $\lambda \in \mathbb{C} - \{0\}$  and where each  $P_j$  is a single-qubit Pauli operator.

Various efficient algorithms exist for manipulating stabilizer (sub)groups  $G$ , including testing membership (is  $A \in \text{PAULI}_n$  a member of  $G$ ?) and finding a generating set of the intersection of two stabilizer (sub)groups. These algorithms predominantly use standard linear algebra techniques, e.g., Gauss-Jordan elimination. See App. A for details.

Stabilizer rank-based methods [10–15] extend the stabilizer formalism to families of Clifford circuits with arbitrary input states  $|\varphi_n\rangle$ , enabling the simulation of universal quantum computation [40]. By decomposing the  $n$ -qubit state  $|\varphi_n\rangle$  as linear combination of  $\chi$  stabilizer states followed by simulating the circuit on each of the  $\chi$  stabilizer states, the measurement outcomes can be computed in time  $\mathcal{O}(\chi^2 \cdot \text{poly}(n))$ , where the least  $\chi$  is referred to as the *stabilizer rank* of  $|\varphi_n\rangle$ . Therefore, stabilizer-rank based methods are efficient for any family of input states  $|\varphi_n\rangle$  whose stabilizer rank grows polynomially in  $n$ .

A specific method for obtaining a stabilizer decomposition of the output state of an  $n$ -qubit circuit is by writing the circuit into Clifford gates and  $T = |0\rangle\langle 0| + e^{i\pi/4}|1\rangle\langle 1|$  gates (a universal gate set). Next, each of the  $T$  gates can be converted into an ancilla qubit initialized to the state  $T|+\rangle$  where  $|+\rangle = |0\rangle + |1\rangle$ ; thus, an  $n$ -qubit circuit containing  $t$   $T$  gates will be converted into an  $n + t$ -qubit Clifford circuit with input state  $|\varphi\rangle = |0\rangle^{\otimes n} \otimes (T|+\rangle)^{\otimes t}$  [10]. We will refer to the resulting

*specific* stabilizer-rank based simulation method as the ‘Clifford +  $T$  simulator’, whose simulation runtime scales with  $\chi = \chi((T|+)\otimes^t)$ , the number of stabilizer states in the decomposition of  $|\varphi\rangle$ . Trivially, we have  $\chi \leq 2^t$ , and although recent work has found decompositions smaller than  $2^t$  terms, the scaling of  $\chi$  remains exponential in  $t$ . In particular, Bravyi et al. found  $\chi \leq 2^{0.48t}$  [10], which was later improved to  $\chi \leq 2^{0.23t}$  [11]. We emphasize that the Clifford +  $T$  decomposition is not necessarily optimal, in the sense that the intermediate states of the circuit might have lower stabilizer rank than  $|T\rangle^{\otimes t}$  does. Consequently, if a given circuit contains  $t = \Omega(n)$   $T$ -gates, then the Clifford +  $T$  simulator requires exponential time (in  $n$ ) for simulating this  $n$ -qubit circuit, even if there exist polynomially-large stabilizer decompositions of each of the circuit’s intermediate and output states (i.e., in principle, a different stabilizer rank-based simulator might simulate this circuit in efficiently).

The *Schmidt rank* of a state  $|\varphi\rangle$  on  $n$  qubits, relative to a bipartition of the qubits into two sets  $A$  and  $B$ , is the smallest integer  $m \geq 1$  such that  $|\varphi\rangle$  can be expressed as the superposition  $|\varphi\rangle = \sum_{j=1}^m c_j |a_j\rangle_A |b_j\rangle_B$  for complex coefficients  $c_j$ , where each  $|a_j\rangle_A$  is a state on the qubits  $A$ , and likewise each  $|b_j\rangle_B$  is a state on the qubits  $B$ .

### 3 Main results

#### 3.1 The LIMDD data structure

Where QMDDs only merge nodes representing the same complex vector up to a constant factor, the LIMDD data structure goes further by also merging nodes that are equivalent up to local operations, called Local Invertible Maps (LIMs) (see Definition 1). As a result, LIMDDs can be exponentially more succinct than QMDDs, for example in the case of stabilizer states (see Sec. 3.2). We will call nodes which are equivalent under LIMs, (*LIM-*) *isomorphic*. This definition generalizes SLOCC equivalence (Stochastic Local Operations and Classical Communication); in particular, if we choose the parameter  $G$  to be the linear group, then the two notions coincide (Appendix A of [32]) [33, 41].

**Definition 1** (LIM, Isomorphism). An  $n$ -qubit Local Invertible Map (LIM) is an operator  $\mathcal{O}$  of the form  $\mathcal{O} = \lambda \mathcal{O}_n \otimes \cdots \otimes \mathcal{O}_1$ , where the matrices  $\mathcal{O}_i$  are invertible  $2 \times 2$  matrices and  $\lambda \in \mathbb{C} \setminus \{0\}$ . An *isomorphism* between two  $n$ -qubit quantum states  $|\varphi\rangle, |\psi\rangle$  is a LIM  $\mathcal{O}$  such that  $\mathcal{O}|\varphi\rangle = |\psi\rangle$ . If  $G$  is a group of  $2 \times 2$  invertible matrices and if all  $\mathcal{O}_i \in G$ , then we say that  $\mathcal{O}$  is a  $G$ -isomorphism and that  $|\varphi\rangle$  is  $G$ -isomorphic to  $|\psi\rangle$ , denoted  $|\varphi\rangle \simeq_G |\psi\rangle$ . Note that  $G$ -isomorphism is an equivalence relation.

Before we give the formal definition of LIMDDs in Definition 2, we give a motivating example in Figure 3, which demonstrates how the use of isomorphisms can yield small diagrams for a four-qubit state. In the state’s QMDD, the nodes labeled  $q_1$  and  $q_2$  represent the single-qubit states  $|q_1\rangle = [1, 1]^\top$  and  $|q_2\rangle = [1, -1]^\top$ , respectively. By noticing that these two vectors are related via  $|q_2\rangle = Z|q_1\rangle$ , we may merge node  $q_1$  with node  $q_2$  into node  $\ell_1$  in the LIMDD. The isomorphism  $Z$  is then stored on an incoming edge. A similar reduction can be achieved at the QMDD’s third level, by noticing that  $|q_3\rangle = (Z \otimes \mathbb{I} \otimes Z)|q_4\rangle$ . Therefore, the LIMDD also merges these two nodes, into node  $\ell_2$ , and stores the isomorphism  $Z \otimes \mathbb{I} \otimes Z$  on one of its incoming edges. The resulting data structure is a LIMDD of only six nodes instead of ten. Sec. 3.2 shows that merging isomorphic nodes sometimes leads to exponentially smaller diagrams, while the additional cost of storing the isomorphisms is only polynomial.

**Definition 2.** An  $n$ - $G$ -LIMDD is a rooted, directed acyclic graph (DAG) representing an  $n$ -qubit quantum state (or unitary). Formally, it is a 6-tuple  $(\text{NODE} \cup \{\text{Leaf}\}, \text{idx}, \text{low}, \text{high}, \text{label}, e_{\text{root}})$ , where:

- $\text{NODE}$  is a set of nodes with qubit indices  $\text{idx}(v) \in \{1, \dots, n\}$  for  $v \in \text{NODE}$ ;
- $e_{\text{root}}$  is a root edge without source pointing to the root node  $r \in \text{NODE}$ ;

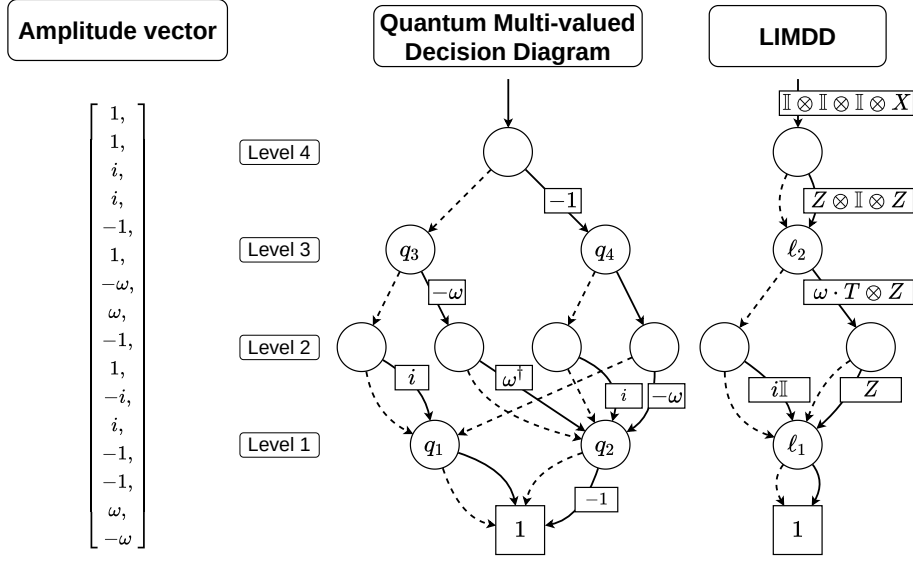


Figure 3: A four-qubit quantum state shown as: an amplitude vector (left), a QMDD and a LIMDD (right). Diagram nodes are horizontally ordered in ‘levels’ with qubit indices 4, 3, 2, 1. Low edges are dashed, high edges solid. Here  $\omega = e^{i\pi/4}$ . By convention, unlabelled edges have label 1 (for QMDD) or  $\mathbb{I}$  (for LIMDD).

- Leaf (a sink) is a unique leaf node with index  $\text{idx}(s) = 0$  representing the number 1;
- $\text{low}, \text{high}: \text{NODE} \rightarrow \text{NODE} \cup \{\text{Leaf}\}$  are the low and high edge functions;
- $\text{label}: \text{low} \cup \text{high} \cup \{e_{\text{root}}\} \rightarrow G\text{-LIM} \cup \{0\}$  is a function labeling edges with LIMs or 0;

Depending on context, we interpret  $\text{low}(v)$  as a node  $v_0$  or an edge  $(v, v_0)$ . We define the semantics of a (non-leaf) node  $v$  and edge  $e$  to node  $v$  by overloading the Dirac notation:

$$|e\rangle \triangleq \begin{cases} \lambda \cdot (\mathcal{Q}_{\text{idx}(v)} \otimes \cdots \otimes \mathcal{Q}_1) \cdot |v\rangle & \text{if } \text{label}(e) = (\lambda, \mathcal{Q}_1, \dots, \mathcal{Q}_{\text{idx}(v)}) \\ [0, \dots, 0]^\dagger & \text{if } \text{label}(e) = 0 \end{cases}$$

$$|v\rangle \triangleq |0\rangle \otimes |\text{low}(v)\rangle + |1\rangle \otimes |\text{high}(v)\rangle$$

Although we define LIMDDs for general LIM groups  $G$ , in this work we will assume that the operators are either diagonal or antidiagonal, i.e., either  $\mathcal{Q}_j = \begin{bmatrix} \alpha & 0 \\ 0 & \beta \end{bmatrix}$ , or  $\mathcal{Q}_j = \begin{bmatrix} 0 & \beta \\ \alpha & 0 \end{bmatrix}$  for all  $j$ .

It is quite simple to find the amplitude of a computational basis state  $\langle x|\psi\rangle$  for a bitstring  $x \in \{0, 1\}^n$ , by traversing the LIMDD of the state  $|\psi\rangle$  from top to bottom, as follows. Suppose that this diagram’s root edge  $e$  is labeled with the LIM  $P = \lambda P_n \otimes \cdots \otimes P_1$  and points to node  $v$ . First, we substitute  $|v\rangle = |0\rangle|v_0\rangle + |1\rangle|v_1\rangle$ , where  $v_0, v_1$  are the low and high edges going out of  $v$ , thus obtaining  $\langle x|e\rangle = \langle x|P(|0\rangle|v_0\rangle + |1\rangle|v_1\rangle)$ . Next, we notice that  $\langle x|P = \lambda \langle x_n|P_n \otimes \cdots \otimes \langle x_1|P_1 = \gamma \langle y|$  for some  $\gamma \in \mathbb{C}$  and a computational basis state  $\langle y|$ . Therefore, letting  $y' = y_{n-1} \dots y_1$ , it suffices to compute  $\langle y_n|y'\rangle(|0\rangle|v_0\rangle + |1\rangle|v_1\rangle)$ , which reduces to either  $\langle y'|v_0\rangle$  if  $y_n = 0$ , or  $\langle y'|v_1\rangle$  if  $y_n = 1$ . By applying this simple rule repeatedly, one walks from the root to the Leaf, encountering one node on each level. Thus, the amplitude  $\langle x|e\rangle$  is found by multiplying together the scalars  $\gamma$  found along this path.

Let us now summarize the representation and manipulation capabilities of the LIMDD data structure. A  $G$ -LIMDD is exact and universal, i.e., for each  $n$ -qubit quantum state  $|\varphi\rangle$  there is a LIMDD with root edge  $e$  such  $|e\rangle = |\varphi\rangle$ , for any choice of parameter  $G$ . In particular, a  $G$ -LIMDD with  $G = \{\mathbb{I}\}$  yields precisely all QMDDs by definition. As all groups  $G$  contain the identity operator  $\mathbb{I}$ , the universality of LIMDDs (i.e. all quantum states can be represented) follows from the universality of QMDDs. Furthermore, for the choice  $G = \text{Pauli}$ , the states that LIMDDs can represent using polynomial space include all stabilizer states, which is a feature that QMDDs and Matrix Product

States do not possess, as shown in Sec. 3.2 and visualized in Fig. 4. Finally, Pauli-LIMDDs can also *manipulate* and measure quantum states, thereby enabling the simulation of quantum circuits, as shown in Sec. 3.3. For many operations, we show that the manipulation is also efficient, i.e., it takes polynomial time in the size of the LIMDD representation of the quantum state/circuit. Specifically, LIMDDs are often faster than QMDDs, and never slower by more than a multiplicative factor  $\mathcal{O}(n^3)$ . Lastly, LIMDDs are a *canonical* representation, i.e., for each state there is a *unique* LIMDD. Canonicity allows the algorithms to employ dynamic programming (because canonicity allows us to immediately detect when a repeated computation is done), which is crucial to obtain efficient algorithms. We treat this subject in Sec. 4.

The bottom line of the algorithmic capabilities of LIMDDs are as follows. There exist algorithms to update a Pauli-LIMDDs after an arbitrary unitary or single-qubit measurement. Although these algorithms are exponential-time in the worst case, they are always efficient for single-qubit Paulis,  $S$  gates and downward CNOTs, and sometimes efficient for the Hadamard gates and upward CNOT. A  $T$ -gate can be efficiently applied to the top qubit. In case the Pauli-LIMDD represents a stabilizer state, the update after any elementary Clifford operation is efficient. In these and many other cases, the LIMDDs of the intermediate states produced by the circuit have polynomial size. For details of the algorithms' runtimes, see Table 1 in Sec. 3.3.

### 3.2 Exponential separations of LIMDDs with the Clifford + T simulator, QMDDs and Matrix Product States

In this section, we show exponential advantages of LIMDDs over three state-of-the-art classical simulation techniques: QMDDs, Matrix Product States (MPS) [34, 42] and the Clifford + T simulator. Specifically, QMDDs and MPS require an exponential amount of time in the number of qubits to simulate a specific stabilizer state—the cluster state—and the Clifford+ $T$  approach fails to efficiently prepare the so-called  $W$  state. All these circuit families are efficiently simulatable by LIMDDs using the algorithms from Sec. 3.3. Intuitively, this is because the intermediate states produced by these circuits all have small LIMDDs, combined with the fact that the algorithms manage to find these small diagrams, as a result of canonicity (see Sec. 4).

#### 3.2.1 LIMDDs are exponentially more succinct than QMDDs

Here, we show that LIMDDs can be exponentially more succinct than the union of QMDDs and stabilizer states (Th. 1), using the facts that the  $n$ -qubit cluster state, a graph state on the two-dimensional grid and hence also a stabilizer state, requires  $2^{\Omega(\sqrt{n})}$  nodes as QMDD (Lemma 3), while each  $n$ -qubit stabilizer states is represented by a Pauli-LIMDD with only  $\mathcal{O}(n)$  nodes (Th. 2). We show that LIMDDs retain this exponential advantage even for  $G$ -LIMDDs with  $G = \langle Z \rangle$  or  $G = \langle X \rangle$  in App. B (QMDD

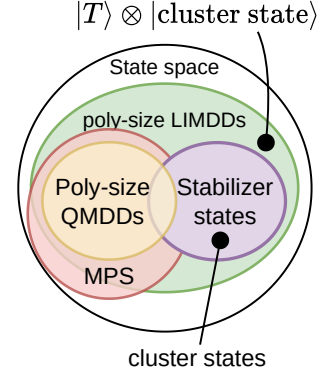


Figure 4: Relations between decision diagrams, stabilizer states and Matrix Product States (MPS). We show in Sec. 3.2.2 that the cluster state has no poly-size MPS. The illustration further shows that MPS contains QMDD, and is incomparable to LIMDD, which we state without proof.

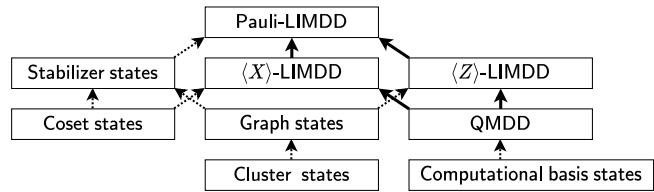


Figure 5: Relations between classes of quantum states and families of polynomial-size decision diagrams. Every arrow denotes a strict inclusion of sets; in particular, each solid arrow  $D_1 \rightarrow D_2$  denotes an exponential separation between two decision diagram families, i.e., some quantum states have polynomial-size diagrams of type  $D_2$ , but have only exponential-size diagrams of type  $D_1$ . The dotted arrows represent inclusion.

lower bounds) and [App. C](#) (LIMDD upper bounds). [Fig. 5](#) visualizes the results from this section. The notation  $\textcircled{v} \xrightarrow{A} \textcircled{w}$  denotes a node with low and high edges labeled with  $A$  and  $B$ , and pointing to nodes  $v$  and  $w$ , respectively.

**Theorem 1** (Exponential separation between Pauli-LIMDD versus QMDD union stabilizer states). The set of quantum states represented by polynomial-size Pauli-LIMDDs is a strict superset of the union of stabilizer states and polynomial-size QMDDs.

*Proof.* The ‘superset’ part follows directly from [Th. 2](#) and the earlier remark that each QMDD is a  $G$ -LIMDD with  $G = \{\mathbb{I}\}$ , i.e., each label is of the form  $\lambda \mathbb{I}$  with  $\lambda \in \mathbb{C}$ . For strictness, consider  $|\varphi\rangle := (|0\rangle + e^{i\pi/4}|1\rangle)/\sqrt{2} \otimes |G_n\rangle$  where  $|G_n\rangle$  is the graph state on the  $n \times n$  grid (the cluster state). This is not a stabilizer state, because each computational-basis coefficient of a stabilizer state is of the form  $z \cdot 1/\sqrt{2}^k$  for  $z \in \{\pm 1, \pm i\}$  and some integer  $k \geq 1$  [[7](#)], while  $\langle 1| \otimes \langle 0|^{\otimes n} |\varphi\rangle = e^{i\pi/4} \cdot \left(\frac{1}{\sqrt{2}}\right)^{n^2+1}$  is not of this form. Its canonical QMDD and Pauli-LIMDD

have root nodes  $\textcircled{G_n} \xrightarrow{1} \textcircled{e^{i\pi/4}} \textcircled{G_n}$  and  $\textcircled{G_n} \xrightarrow{\mathbb{I}} \textcircled{e^{i\pi/4} \mathbb{I}} \textcircled{G_n}$ , where the respective diagram for  $G_n$  is exponentially-large ([Lemma 3](#)) and polynomially small ([Th. 2](#)).  $\square$

**Theorem 2** (Tower Pauli-LIMDDs are stabilizer states). Let  $n > 0$ . Each  $n$ -qubit stabilizer state is represented by a Pauli-LIMDD on  $n$  nodes (a “tower”) with high edge label factors  $\in \{0, \pm 1, \pm i\}$ . Conversely, every such LIMDD represents a stabilizer state.

*Proof sketch of Th. 2.* We give a full proof with induction on  $n$  in [Th. 14](#) in [App. C](#) and give a proof sketch here. The  $n = 1$  case: the six single-qubit states  $|0\rangle, |1\rangle, |0\rangle \pm |1\rangle$  and  $|0\rangle \pm i|1\rangle$  are all represented by a LIMDD with a single node on top of the leaf. The induction step: let  $|\psi\rangle$  be an  $n$ -qubit stabilizer state. First consider the case that  $|\psi\rangle = |a\rangle |\psi'\rangle$  with  $|a\rangle = \alpha|0\rangle + \beta|1\rangle$  (where  $\alpha, \beta \in \{0, \pm 1, \pm i\}$ ) and  $|\psi'\rangle$  stabilizer states on respectively 1 and  $n-1$  qubits. Then  $|\psi\rangle$  is represented by the LIMDD  $\textcircled{\psi} \xrightarrow{\alpha \mathbb{I}} \textcircled{\beta \mathbb{I}} \textcircled{\psi'}$ . In the remaining case,  $|\psi\rangle \propto |0\rangle |\psi_0\rangle + |1\rangle |\psi_1\rangle$ , where both  $|\psi_0\rangle$  and  $|\psi_1\rangle$  are stabilizer states. Moreover, since  $|\psi\rangle$  is a stabilizer state, there is always a set of single-qubit Pauli gates  $P_1, \dots, P_n$  and a  $\lambda \in \{\pm 1, \pm i\}$  such that  $|\psi_1\rangle = \lambda P_n \otimes \dots \otimes P_1 |\psi_0\rangle$ . That is, in our terminology, the states  $|\psi_0\rangle$  and  $|\psi_1\rangle$  are *isomorphic*. Hence  $|\psi\rangle$  can be written as

$$|\psi\rangle = |0\rangle |\psi_0\rangle + \lambda |1\rangle \otimes (P_n \otimes \dots \otimes P_1 |\psi_0\rangle) \quad (2)$$

Hence  $|\psi\rangle$  is represented by the Tower Pauli-LIMDD  $\textcircled{\psi_0} \xrightarrow{\mathbb{I}} \textcircled{\lambda P_n \otimes \dots \otimes P_1} \textcircled{\psi_0}$ . In both cases,  $|\psi'\rangle$  is represented by a Tower Pauli-LIMDD by the induction hypothesis.  $\square$

**Lemma 3.** Denote by  $|G_n\rangle$  the cluster state; a graph state on the  $n \times n$  lattice. Each QMDD representing the cluster state  $|G_n\rangle$  has at least  $2^{\lfloor n/12 \rfloor}$  nodes.

*Proof sketch.* Consider a partition of the vertices of the  $n \times n$  lattice into two sets  $S$  and  $T$  of size  $\frac{1}{2}n^2$ , corresponding to the first  $\frac{1}{2}n^2$  qubits under some variable order. Then there are at least  $\lfloor n/3 \rfloor$  vertices in  $S$  that are adjacent to a vertex in  $T$  [[43](#), Th. 11]. Because the degree of the vertices is small, many vertices on this boundary are not connected and therefore influence the amplitude function independently of one another. From this independence, it follows that, for any variable order, the partial assignments  $\vec{a} \in \{0, 1\}^{\frac{1}{2}n^2}$  induce  $2^{\lfloor n/12 \rfloor}$  different subfunctions  $f_{\vec{a}}$ , where  $f: \{0, 1\}^{n^2} \rightarrow \mathbb{C}$  is the amplitude function of  $|G_n\rangle$ . The lemma follows by noting that a QMDD has a single node per unique subfunction modulo phase. For details see [App. B](#).  $\square$

We note that [Th. 2](#) is a reformulation of the fact that for any  $n$ -qubit stabilizer state  $|\varphi\rangle$ , the  $(n-1)$ -qubit states  $(\langle 0| \otimes \mathbb{I}_{2^{n-1}}) |\varphi\rangle$  and  $(\langle 1| \otimes \mathbb{I}_{2^{n-1}}) |\varphi\rangle$  are not only stabilizer states, but also

Pauli-isomorphic. While we believe this fact is known in the community,<sup>\*</sup> we have not found this statement written down explicitly in the literature. More importantly for this work, to the best of our knowledge the resulting recursive structure (which DDs are) has not been exploited in the context of classical simulation before.

Th. 2 shows us that LIMDDs are highly interesting as a classical simulation formalism because of the exponential separation with QMDDs and Matrix Product States it implies. We emphasize that we are not looking for faster simulation algorithms using LIMDDs for stabilizer states only: rather, in this work we formulate simulation algorithms for general circuits.

Finally, we stress that obtaining the LIMs for the Pauli Tower-LIMDD of a stabilizer state is not immediate from the stabilizer generators; specifically, the edge labels in the Pauli-LIMDD are not directly the stabilizers of the state. For example, the state  $|000\rangle + |111\rangle$  is represented by  $\bigotimes \text{---} \bigcirc \xrightarrow{X \otimes X} \bigotimes$  with  $|\varphi\rangle = |00\rangle$  but  $X \otimes X$  is not a stabilizer of  $|00\rangle$ .

### 3.2.2 Succinct LIMDD whose states have exponentially large bond dimension as Matrix Product States

A popular method for simulation of quantum circuits is based on Matrix Product States (MPS), i.e., tensor networks on a chain of nodes [34, 42]. The expressive power of an MPS is determined by the chosen *bond dimension*: the height or width of the largest matrix that is used in the MPS. Informally, the bond dimension of an MPS is always at least as large as than the Schmidt rank of the state it represents. In particular, any quantum state can be represented by an MPS with exponentially large bond dimension. We now give a lemma which gives a well-known result that the  $n \times n$  two-dimensional grid has exponentially-large Schmidt rank.

**Lemma 4.** [44, 45] When represented as Matrix Product State, the cluster state on the  $n \times n$  grid graph requires bond dimension  $2^{\Omega(n)}$ .

*Proof.* Suppose the MPS representing the cluster state has bond dimension  $D$  and that its qubits are ordered as  $q_1, \dots, q_n$ . For  $1 \leq j < n$ , let  $A_j = \{q_1, \dots, q_j\}$  and  $B_j = \{q_{j+1}, \dots, q_n\}$ , so that  $P_j = (A_j, B_j)$  is a bipartition of the qubits. Then, for any  $j$ , the bond dimension  $D$  must be greater than or equal to the Schmidt rank relative to the bipartition  $P_j$ . Van den Nest et al. showed that the maximum Schmidt rank of the cluster state, relative to the bipartition  $P_j$ , where the maximization is over  $j = 1 \dots n-1$ , is at least  $2^s$  with  $s$  the state's *Schmidt rank width*, which is equal to the *rank width* of the corresponding graph [44]. Jelinek showed that the rank width of the  $n \times n$  grid graph is  $n-1$  [45]; therefore, the bond dimension is  $D \geq 2^{n-1}$ .  $\square$

In contrast, Clifford circuits, in particular those which prepare the output cluster states, are efficiently simulatable as Pauli-LIMDD (Th. 2). This shows that any Clifford circuit outputting a cluster state is efficiently simulatable using LIMDDs but not using MPS.

### 3.2.3 A LIMDD-efficient, linear-T-count circuit family

In this section, we consider a circuit family that LIMDDs can efficiently simulate, but which is difficult for the Clifford+ $T$  simulator because the circuit contains many  $T$  gates, assuming the Exponential Time Hypothesis (ETH, a standard complexity-theoretic assumption which is widely believed to be true). This method decomposes a given quantum circuit into a circuit consisting only of Clifford gates and the  $T = \begin{bmatrix} 1 & 0 \\ 0 & e^{i\pi/4} \end{bmatrix}$  gate, as explained in Sec. 2.

---

<sup>\*</sup>Namely, this fact can be observed (excluding global scalars) by executing the original algorithm for simulating single-qubit computational-basis measurement [4] on the first qubit. Similarly, the characterization of Tower-LIMDDs with the simpler case  $G = \langle Z \rangle$ , which represent precisely the graph states, is immediate by defining graph states recursively (see App. C). The case  $G = \langle X \rangle$ , which yields coset states, is less evident and requires a separate proof, which we also give in App. C.

The circuit family, given by McClung [46], maps the input state  $|0\rangle^{\otimes n}$  to the  $n$ -qubit  $W$  state  $|W_n\rangle$ , which is the equal superposition over computational-basis states with Hamming weight 1,

$$|W_n\rangle = \frac{1}{\sqrt{n}} (|100\dots 00\rangle + |010\dots 00\rangle + \dots + |000\dots 01\rangle)$$

Arunachalam et al. showed that, assuming ETH, any circuit which deterministically produces the  $|W_n\rangle$  state in this way requires  $\Omega(n)$   $T$  gates [47]. Consequently, the Clifford +  $T$  simulator cannot efficiently simulate the circuit family, even when one allows for preprocessing with a compilation algorithm aiming to reduce the  $T$ -count of the circuit (such as the ones developed in [48, 49]).

**Theorem 5.** There exists a circuit family  $C_n$  such that  $C_n |0\rangle^{\otimes n} = |W_n\rangle$ , that Pauli-LIMDDs can efficiently simulate. Here simulation means that it constructs representations of all intermediate states, in a way which allows one to, e.g., efficiently simulate any single-qubit computational-basis measurement or compute any computational basis amplitude on any intermediate state and the output state. App. F gives the proof.

We note that we could have obtained a similar result using the simpler scenario where one applies a  $T$  gate to each qubit of the  $(|0\rangle + |1\rangle)^{\otimes n}$  input state. However, our goal is to show that LIMDDs can natively simulate scenarios which are relevant to quantum applications, such as the stabilizer states from the previous section. The  $W$  state is a relevant example, as several quantum communication protocols use the  $W$  state [50–52]. In contrast, the circuit with only  $T$  gates yields a product state, hence it is not relevant unless we consider it as part of a larger circuit which includes multi-qubit operations.

Lastly, it would be interesting to analytically compare LIMDD with general stabilizer rank based simulation (without assuming ETH). However, this would require finding a family of states with provably superpolynomial stabilizer rank, which is a major open problem. Instead, we implemented a heuristic algorithm by Bravyi et al. [12] to empirically find upper bounds on the stabilizer rank and apply it to a superset of the  $W$  states, so-called Dicke states, which can be represented as polynomial-size LIMDD. The  $\mathcal{O}(n^2)$ -size LIMDD can be obtained via a construction by Bryant [17], since the amplitude function of a Dicke state is a symmetric function. The results hint at a possible separation but are inconclusive due to the small number of qubits which the algorithm can feasibly investigate in practice. See App. G for details.

### 3.3 Simulating Quantum Circuits with Pauli-LIMDDs

In this section, we give all algorithms that are necessary to simulate a quantum circuit with Pauli-LIMDDs (referred to simply as LIMDD from now on). We provide algorithms which update the LIMDD after an arbitrary gate or single-qubit measurement in the computational basis. In addition, we give efficient specialized algorithms for applying generators of the Clifford group: a single-qubit Pauli gate, phase gate, controlled-Pauli and Hadamard gate (although the Hadamard and “upward-controlled” Pauli are not always efficient). The  $T$ -gate can be efficiently applied to the top qubit using the algorithms in this section. Central to the speed of many DD algorithms is keeping the diagram canonical throughout the computation, by using a ‘MakeEdge’ routine to convert a node into its canonical counterpart. We provide the subroutine MAKEEDGE in Sec. 4.2 (Alg. 5). Table 1 provides an overview of the LIMDD algorithms and their complexities compared to QMDDs.

Our algorithms will use the notation in Table 2 to easily navigate and construct diagrams. The notation  $\xrightarrow{A} \bigcirc_v$  creates an edge to an existing node  $v$ , labeled with a LIM  $A$ . If  $v_0$  and  $v_1$  are two existing nodes, then the notation  $\bigcirc_{v_0} \xrightarrow{A} \bigcirc \xrightarrow{B} \bigcirc_{v_1}$  creates a new (not-necessarily-reduced)

<sup>†</sup>This complexity holds if the stabilizer groups of all nodes have been computed; this happens during construction of the LIMDD

<sup>‡</sup>The worst-case of QMDDs and LIMDDs is caused by the vector addition introduced by the Hadamard gate [53, Table 2, +BC, +SLDD].

Table 1: Worst-case complexity of currently *best-known algorithms* for applying specific operations, in terms of the size of the input diagram size  $m$  (i.e., the number of nodes in the DD) and the number of qubits  $n$ . Although addition of quantum states is not, strictly speaking, a quantum operation, we include it because it is a subroutine of gate application. Note that several of the LIMDD algorithms invoke MAKEEDGE and therefore inherit its cubic complexity (as a factor).

Operation \ input:	QMDD	LIMDD	Section
Checking state equality	$\mathcal{O}(1)$	$\mathcal{O}(n^3)^\dagger$	<a href="#">Sec. 4.2.2</a>
Single $ 0\rangle /  1\rangle$ -basis measurement	$\mathcal{O}(m)$	$\mathcal{O}(m)$	<a href="#">Sec. 3.3.1</a>
Single Pauli gate	$\mathcal{O}(m)$	$\mathcal{O}(1)$	<a href="#">Sec. 3.3.2</a>
Single Hadamard gate / ADD()	$\mathcal{O}(2^n)$ note <sup>‡</sup>	$\mathcal{O}(n^3 2^n)$ note <sup>‡</sup>	<a href="#">Sec. 3.3.2</a>
Clifford gate on stabilizer state	$\mathcal{O}(2^n)$	$\mathcal{O}(n^4)$	<a href="#">Sec. 3.3.2</a>
Multi-qubit gate	$\mathcal{O}(4^n)$	$\mathcal{O}(n^3 4^n)$	<a href="#">Sec. 3.3.3</a>
MAKEEDGE	$\mathcal{O}(1)$	$\mathcal{O}(n^3)$	<a href="#">Sec. 4.2</a>

Table 2: Notation to navigate and construct LIMDDs.

Type	Notation	Semantics
(New) EDGE $e$	$e \xrightarrow{A} \textcircled{v}$	$ e\rangle =  \xrightarrow{A} \textcircled{v}\rangle \triangleq A v\rangle$
(New) NODE $v$	$\textcircled{v_0} \xleftarrow{A} \textcircled{v} \xrightarrow{B} \textcircled{v_1}$	$ v\rangle \triangleq  0\rangle A v_0\rangle +  1\rangle B v_1\rangle$
NODE $\rightarrow$ EDGE	$B \cdot v$	$\triangleq \xrightarrow{B} \textcircled{v}$
EDGE $\rightarrow$ EDGE	$B \cdot (\xrightarrow{A} \textcircled{v})$	$\triangleq \xrightarrow{BA} \textcircled{v}$
EDGE $\rightarrow$ EDGE	$\text{FOLLOW}_b(\xrightarrow{\lambda X^x \begin{bmatrix} z_1 & 0 \\ 0 & z_2 \end{bmatrix} \otimes P'} \textcircled{v})$	$\triangleq \begin{cases} \xrightarrow{z_1 \lambda P' B_0} \textcircled{v_0} & \text{if } x = b, \text{low}(v) = \xrightarrow{B_0} \textcircled{v_0} \\ \xrightarrow{z_2 \lambda P' B_1} \textcircled{v_1} & \text{if } x \neq b, \text{high}(v) = \xrightarrow{B_1} \textcircled{v_1} \end{cases}$
EDGE $\rightarrow$ EDGE	$\text{FOLLOW}_{b_k \dots b_1}(\xrightarrow{A} \textcircled{v})$	$\triangleq \text{FOLLOW}_{b_1}(\dots \text{FOLLOW}_{b_k}(\xrightarrow{A} \textcircled{v}) \dots)$

node whose left edge is  $\xrightarrow{A} \textcircled{v_0}$  and whose right edge is  $\xrightarrow{B} \textcircled{v_1}$ . LIMs are decomposed using  $A = \lambda_A P_n \otimes P'$ . Here  $\lambda_A \in \mathbb{C}$  is a non-zero scalar, and the matrices satisfy  $P_j \in \{\mathbb{I}, X, Z, Y\}$  for every  $j$ . Finally, the  $\text{FOLLOW}_b(\xrightarrow{\lambda P_n \otimes P'} \textcircled{v})$  notation allows us to *semantically* follow low and high edges, by applying  $P_n$  on qubit  $\text{idx}(v) = n$  and returning either  $\text{low}(v)$  or  $\text{high}(v)$  multiplied by  $\lambda_A P'$ . Specifically, if  $e$  is an edge with  $|e\rangle = |0\rangle |\varphi_0\rangle + |1\rangle |\varphi_1\rangle$ , then  $\text{FOLLOW}_b(e)$  denotes an edge  $f$  satisfying  $|f\rangle = |\varphi_b\rangle$ . For example, the amplitude of basis state  $|1111\rangle$  for the LIMDD root edge  $e$  in [Fig. 3](#) is computed by taking  $|\text{FOLLOW}_{1111}(e)\rangle = |\xrightarrow{-\omega} \textcircled{1}\rangle = -\omega$ .

In line with other existing efficient decision-diagram algorithms, we use dynamic programming in our algorithms to avoid traversing all paths (possibly exponentially many) in the LIMDD. To implement this, we use a cache data structure (a lossy set) storing the parameters and results of the recursive function calls. We treat the subject of dynamic programming in [Sec. 4.3](#), and gloss over these details in this section.

We defer the treatment of the MAKEEDGE subroutine to [Sec. 4.2](#); for now, the reader may assume the trivial implementation below, which does not yet merge LIM-isomorphic nodes and hence does not yield canonical diagrams.

**Algorithm 1** Provisionary algorithm MAKEEDGE for creating a new edge. Given two edges representing states  $A|v\rangle, B|w\rangle$ , returns an edge representing the state  $|0\rangle A|v\rangle + |1\rangle B|w\rangle$ .

---

```

1: procedure MAKEEDGE(EDGE  $\xrightarrow{A} \textcircled{v}$ , EDGE  $\xrightarrow{B} \textcircled{w}$ )
2:    $v := \textcircled{v} \xleftarrow{A} \textcircled{v} \xrightarrow{B} \textcircled{w}$ 
3:   EDGE  $\xrightarrow{\mathbb{I}} \textcircled{v}$ 

```

---

### 3.3.1 Performing a measurement in the computational basis

We provide efficient algorithms for (1) sampling measurement outcomes and (2) computing measurement outcome probabilities for computational-basis measurement of (a) the top qubit (Alg. 2) and of (b) all qubits. We also show how to update the LIMDD after a given measurement outcome. We show (2a) here; see App. E for the other algorithms. This happens in three steps:

1. Use the procedure MEASUREMENTPROBABILITY in Alg. 2 to compute the probability  $p$  of observing the outcome  $|0\rangle$ . If the (non-normalized) quantum state can be written as  $|e\rangle = |0\rangle|e_0\rangle + |1\rangle|e_1\rangle$ , then the probability is  $p = \langle e_0|e_0\rangle / \langle e|e\rangle$ , where we have  $\langle e|e\rangle = \langle e_0|e_0\rangle + \langle e_1|e_1\rangle$ . To this end, we build states  $e_x$  using FOLLOW <sub>$x$</sub> ( $e$ ), and compute their squared norms using the SQUAREDNORM subroutine.
2. Throw a  $p$ -biased coin, obtaining outcome  $m \in \{0, 1\}$ .
3. Use the procedure UPDATEPOSTMEAS to construct the updated LIMDD given  $m$ . This algorithm is straightforward: in order to update the state  $|e\rangle = |0\rangle|e_0\rangle + |1\rangle|e_1\rangle$  after the top qubit is measured to be  $m$ , we simply construct an edge  $|m\rangle|e_m\rangle$  using the MAKEEDGE subroutine.

The runtime of this procedure is dominated by the subroutine SQUAREDNORM, which computes the quantity  $\langle e|e\rangle$  given a LIMDD edge  $e = \frac{\lambda P}{\circlearrowleft} \circ v$ . We have  $\langle e|e\rangle = |\lambda|^2 \langle v|P^\dagger P|v\rangle = |\lambda|^2 \langle v|v\rangle$ , because  $P^\dagger P = \mathbb{I}$  for Pauli matrices. Therefore, to this end, it computes the squared norm of  $|v\rangle$ . Since  $\langle v|v\rangle = \langle v_0|v_0\rangle + \langle v_1|v_1\rangle$ , this is accomplished by recursively computing the squared norm of the node's low and high edges  $v_0$  and  $v_1$ . This subroutine visits any node at most once, because it stores the result of each computation in the cache. In the worst case, this subroutine visits each node, in which case it runs in time  $\mathcal{O}(m)$ , if the diagram has  $m$  nodes.

---

**Algorithm 2** Algorithms MEASUREMENTPROBABILITY and UPDATEPOSTMEAS for respectively computing the probability of observing outcome  $|0\rangle$  when measuring the top qubit of a Pauli LIMDD in the computational basis and converting the LIMDD to the post-measurement state after outcome  $m \in \{0, 1\}$ . The subroutine SQUAREDNORM takes as input a Pauli LIMDD edge  $e$ , and returns  $\langle e|e\rangle$ . It uses a cache to store the value  $s$  of a node  $v$ .

---

```

1: procedure MEASUREMENTPROBABILITY(EDGE  $e$ )
2:    $s_0 := \text{SQUAREDNORM}(\text{FOLLOW}_0(e))$ 
3:    $s_1 := \text{SQUAREDNORM}(\text{FOLLOW}_1(e))$ 
4:   return  $s_0 / (s_0 + s_1)$ 

5: procedure SQUAREDNORM(EDGE  $\frac{\lambda P}{\circlearrowleft} \circ v$ )
6:   if  $n = 0$  then return  $|\lambda|^2$ 
7:    $s := \text{SQUAREDNORM}(\text{FOLLOW}_0(\frac{\mathbb{I}}{\circlearrowleft} \circ v)) + \text{SQUAREDNORM}(\text{FOLLOW}_1(\frac{\mathbb{I}}{\circlearrowleft} \circ v))$ 
8:   return  $|\lambda|^2 s$ 

9: procedure UPDATEPOSTMEAS(EDGE  $e \xrightarrow{\lambda P_n \otimes P'_n} \circ v$ , measurement outcome  $m \in \{0, 1\}$ )
10:  if  $m = 0$  then
11:    return MAKEEDGE(FOLLOW0( $e$ ),  $0 \cdot \text{FOLLOW}_0(e)$ )
12:  else
13:    return MAKEEDGE( $0 \cdot \text{FOLLOW}_0(e)$ , FOLLOW1( $e$ ))

```

---

### 3.3.2 Simple Gates

Before we give the algorithm for arbitrary gates in Sec. 3.3.3, we first show how to apply several simple gates, all of which efficiently except for the Hadamard and CNOT in some cases. Fig. 6 illustrates some of these gates. In the description below, for brevity we omit the calls to MAKEEDGE which make the diagram canonical. In the case of a controlled gate, we distinguish two cases,

depending whether the control or the target qubit comes first; we call these a *downward* and an *upward* controlled gate, respectively.

- Applying a **single-qubit Pauli gate**  $Q$  to qubit  $k$  of a LIMDD can be done in constant time, by updating the diagram's root edge from  $\lambda P_n \otimes \dots \otimes P_1$  to  $\lambda P_n \otimes \dots \otimes P_{k+1} \otimes Q P_k \otimes P_{k-1} \otimes \dots \otimes P_1$ .
- Applying the **phase gate** ( $S = \begin{bmatrix} 1 & 0 \\ 0 & i \end{bmatrix}$ ) to qubit with index  $k$  is also efficient. If  $k = n$  (top qubit), then note  $SB_{\text{root}}|v_{\text{root}}\rangle = (SB_{\text{root}}S^\dagger)S|v_{\text{root}}\rangle$  where  $SB_{\text{root}}S^\dagger$  is an ( $\mathcal{O}(n)$ -computable) Pauli LIM because  $S$  is a Clifford gate. Then, to apply  $S$  to  $v_{\text{root}}$ , we multiply the high edge label with  $i$ . Otherwise, if  $k < n$ , then we note  $S_k(|0\rangle \otimes |v_0\rangle + |1\rangle \otimes B_{\text{high}}|v_1\rangle) = |0\rangle \otimes S_k|v_0\rangle + |1\rangle \otimes (S_k B_{\text{high}} S_k^\dagger) S_k|v_1\rangle$ , where, again  $S_k B_{\text{high}} S_k^\dagger$  is a Pauli LIM. We then call this algorithm recursively to evaluate  $S_k|v_0\rangle$  and  $S_k|v_1\rangle$ , obtaining edges  $e_0, e_1$ . Finally, we can construct the desired node by calling MAKEEDGE on edges  $e_0$  and  $(S_k B_{\text{high}} S_k^\dagger) e_1$ .
- **Downward Controlled-Pauli gate**  $CQ_t^c$  (here  $Q$  is a single-qubit Pauli gate,  $c$  is the control qubit,  $t$  is the target qubit with  $t < c$ ) to a node  $v$ . If  $\text{idx}(v) > c$ , then since  $CQ_t^c$  is a Clifford gate, we may push it through the node's root label, and then apply  $CQ_t^c$  to the children  $v_0$  and  $v_1$ , similar to the  $S$  gate. Otherwise, if  $\text{idx}(v) = c$ , then update  $v$ 's high edge label as  $B_{\text{high}} \mapsto Q_t B_{\text{high}}$ , and do not recurse.
- Applying an **upward Controlled NOT**, i.e.,  $CX_t^c$  with  $t > c$ , is done by noting that  $CX_t^c$  applied to a state  $|0\rangle|\varphi_0\rangle + |1\rangle|\varphi_1\rangle$  equals  $|0\rangle(\Pi_0^c|\varphi_0\rangle + \Pi_1^c|\varphi_1\rangle) + |1\rangle(\Pi_1^c|\varphi_0\rangle + \Pi_0^c|\varphi_1\rangle)$ . Here  $\Pi_j^c$  projects qubit  $c$  to the state  $|j\rangle$ . Therefore, first construct the LIMDDs of the four states  $\Pi_j^c|\varphi_k\rangle$ , projecting qubit  $c$  onto  $|j\rangle$  by a similar method that was used to simulate the measurement outcome  $j$  in [Sec. 3.3.1](#), and then add the resulting states using the ADD procedure ([Alg. 4](#)).
- To apply a **Hadamard gate** ( $H = \frac{1}{\sqrt{2}} \begin{bmatrix} 1 & 1 \\ 1 & -1 \end{bmatrix}$ ) to the first qubit, we first construct edges representing the states  $|a_0\rangle = |\varphi_0\rangle + |\varphi_1\rangle$  and  $|a_1\rangle = |\varphi_0\rangle - |\varphi_1\rangle$ , using the ADD procedure ([Alg. 4](#)). Then we construct an edge representing the state  $|0\rangle|a_0\rangle + |1\rangle|a_1\rangle$  using MAKEEDGE. Lastly, the complex factor on the new edge's root label is multiplied by  $\frac{1}{\sqrt{2}}$ .
- Applying any diagonal or antidiagonal single-qubit gate to the top qubit can be done efficiently using the APPLYGATE from [Sec. 3.3.3](#), such as the  **$T$ -gate to the top qubit**. It propagates the root edge's LIM to the root's two children, and then multiplies the high edge by  $e^{i\pi/4}$ .

It follows that all Clifford gates are polynomial-time, except for the Hadamard gate and upward CNOT. All Clifford gates (including the Hadamard gate and upward CNOT) are polynomial-time when applied to a stabilizer state represented as a LIMDD, as shown by [Th. 20](#) in [Sec. E.2](#), which shows that the specific pointwise additions required to implement Hadamard are all  $\mathcal{O}(n^4)$ . For QMDDs, it was known that applying a Hadamard gate to the top qubit of a state requires exponential time, because of the needed point-wise addition [[53](#), Table 2]. This behavior remains for LIMDDs; however, LIMDDs can be exponentially more succinct than QMDDs as shown in [Sec. 3.2](#).

### 3.3.3 Applying a generic multi-qubit gate to a state

We use a standard approach [[22](#)] to represent quantum gates ( $2^n \times 2^n$  unitary matrices) using LIMDDs. Here a matrix  $U$  is interpreted as a function  $u(r_1, c_1, \dots, r_n, c_n) \triangleq \langle r|U|c \rangle$  on  $2n$  variables, which returns the entry of  $U$  on row  $r$  and column  $c$ . The function  $u$  is then represented using a LIMDD of  $2n$  levels. The bits of  $r$  and  $c$  are interleaved to facilitate recursive descent on the structure. In particular, for  $x, y \in \{0, 1\}$ , the subfunction  $u_{xy}$  represents a quadrant of the matrix, namely the submatrix  $u_{xy}(r_2, c_2, \dots, r_n, c_n) \triangleq u(x, y, r_2, c_2, \dots, r_n, c_n)$ , as follows:

$$u = \overbrace{\begin{bmatrix} u_{00} & u_{01} \\ u_{10} & u_{11} \end{bmatrix}}^{u_{0*}} \bigg\} u_{*1} \quad (3)$$

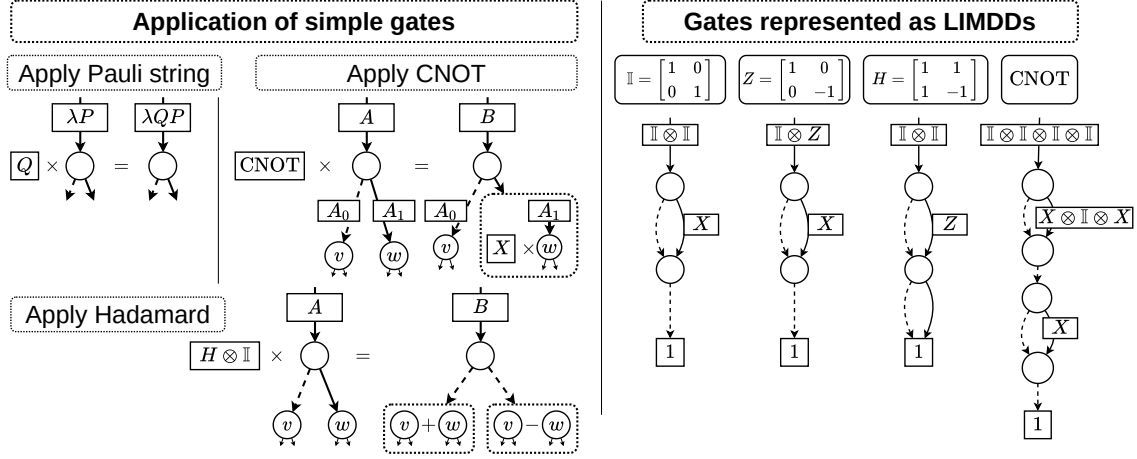


Figure 6: **Left half:** illustration of applying several simple gates (some details are omitted). Leftmost: applying a Pauli string  $Q$  to an edge entails only updating the label on that edge. Right: To apply a CNOT gate to the top qubit, apply  $X \otimes I^{\otimes n-2}$  to the right child; here this operation is represented inside a dotted box. The incoming edge's label changes from  $A$  to  $B = \text{CNOT} \cdot A \cdot \text{CNOT}$ , which is guaranteed to be a Pauli string. Bottom: Applying a Hadamard gate on the top qubit is done by first making nodes representing  $|v\rangle + |w\rangle$  and  $|v\rangle - |w\rangle$ , here shown in dotted boxes, and setting  $B = HAH$ . **Right half:** Examples of four gates, represented as LIMDDs. Left: The identity gate  $I$  is represented by a LIMDD of two levels. The first level indicates the row, and the second level indicates the column. Second from the right: the Hadamard gate; notice that the  $Z$  label produces the  $-1$  value in the matrix' bottom right entry. Rightmost: The CNOT gate. Since this gate is on  $n = 2$  qubits, it has  $2n = 4$  levels. Edges with label  $I$  are drawn without label; edges with label  $0$  are not drawn.

Definition 3 formalizes this idea. Fig. 6 shows a few examples of gates represented as LIMDDs.

**Definition 3** (LIMDDs for gates). A reduced LIMDD edge  $e = \xrightarrow{A} \textcircled{u}$  can represent a (unitary)  $2^n \times 2^n$  matrix  $U$  iff  $\text{idx}(u) = 2n$ . The value of the matrix cell  $U_{r,c}$  is defined as  $\text{FOLLOW}_{r_1 c_1 r_2 c_2 \dots r_n c_n}(\xrightarrow{A} \textcircled{u})$  where  $r, c$  are the row and column index, respectively, with binary representation  $r_1, \dots, r_n$  and  $c_1, \dots, c_n$ . The semantics of a LIMDD edge  $e$  as a matrix is denoted  $[e] \triangleq U$  (as opposed to its semantics  $|e\rangle$  as a vector).

The procedure **APPLYGATE** (Alg. 3) applies a gate  $U$  to a state  $|\varphi\rangle$ , represented by LIMDDs  $e_U$  and  $e_\varphi$ . It outputs a LIMDD edge representing  $U|\varphi\rangle$ . It works as follows (see Fig. 8 for an illustration). Using the  $\text{FOLLOW}_x(e)$  procedure, we write  $|\varphi\rangle$  and  $U$  as

$$|\varphi\rangle = |0\rangle |\varphi_0\rangle + |1\rangle |\varphi_1\rangle \quad (4)$$

$$U = |0\rangle \langle 0| \otimes U_{00} + |0\rangle \langle 1| \otimes U_{01} + |1\rangle \langle 0| \otimes U_{10} + |1\rangle \langle 1| \otimes U_{11} \quad (5)$$

Then, on Line 4, we compute each of the four terms  $U_{rc}|\varphi_c\rangle$  for row/column bits  $r, c \in \{0, 1\}$ . We do this by constructing four LIMDDs  $f_{r,c}$  representing the states  $|f_{r,c}\rangle = U_{r,c}|\varphi_c\rangle$ , using four recursive calls to the **APPLYGATE** algorithm. Next, on lines 5 and 6, the appropriate states are added, using **ADD** (Alg. 4), producing LIMDDs  $e_0$  and  $e_1$  for the states  $|e_0\rangle = U_{00}|\varphi_0\rangle + U_{01}|\varphi_1\rangle$  and for  $|e_1\rangle = U_{10}|\varphi_0\rangle + U_{11}|\varphi_1\rangle$ . The base case of **APPLYGATE** is the case where  $n = 0$ , which means  $U$  and  $|\varphi\rangle$  are simply scalars, in which case both  $e^u$  and  $e^v$  are edges that point to the leaf. We employ dynamic programming to avoid performing duplicate computations, by storing the result of each computation in a cache; we defer this topic to Sec. 4.3.

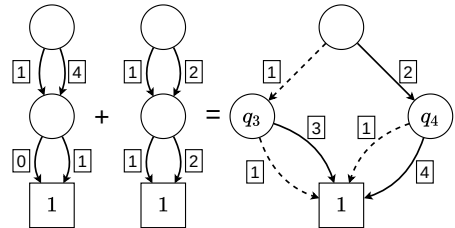


Figure 7: Adding two states  $(0, 1, 0, 4)$  and  $(1, 2, 2, 4)$  as QMDDs can cause an exponentially larger result QMDD  $(1, 3, 2, 8)$  due to the loss of common factors.

**Algorithm 3** Applies the gate  $[e_U]$  to the state  $|e_\varphi\rangle$ . Here  $e_U$  and  $e_\varphi$  are LIMDD edges. The output is a LIMDD edge  $\psi$  satisfying  $|\psi\rangle = [e_U]|e_\varphi\rangle$ . It assumes that  $2\text{idx}(v) = \text{idx}(u)$ . This algorithm employs dynamic programming by looking up and storing its results in the cache; for sake of simplicity, we omit these calls here; [Sec. 4.3](#) details how this is done.

---

```

1: procedure APPLYGATE(EDGE  $e_U \xrightarrow{A} \textcircled{u}$ , EDGE  $e_\varphi \xrightarrow{B} \textcircled{v}$ )
2:   if  $n = 0$  then return  $\xrightarrow{A \cdot B} \textcircled{1}$ 
3:   for  $r, c \in \{0, 1\}$  do
4:     | EDGE  $f_{r,c} := \text{APPLYGATE}(\text{FOLLOW}_{rc}(e_U), \text{FOLLOW}_c(e_\varphi))$ 
5:   EDGE  $e_0 := \text{ADD}(f_{0,0}, f_{0,1})$ 
6:   EDGE  $e_1 := \text{ADD}(f_{1,0}, f_{1,1})$ 
7:   return  $\psi$ 

```

---

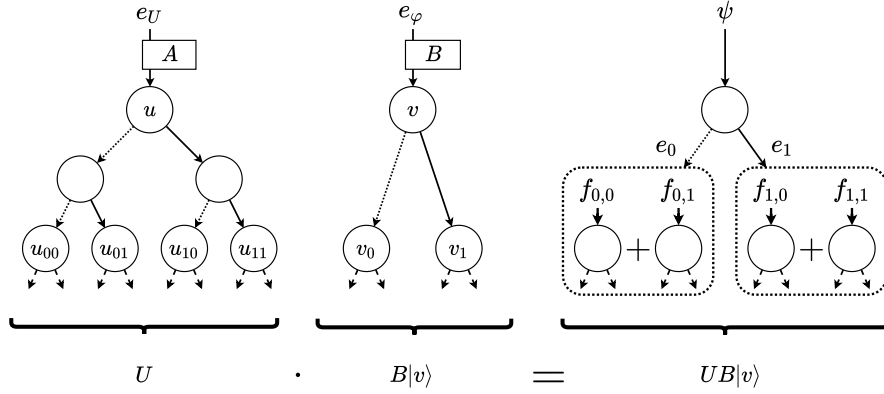


Figure 8: An illustration of `APPLYGATE` ([Alg. 3](#)), where matrix  $U$  is applied to state  $B|v\rangle$ , both represented as Pauli-LIMDDs. The edges  $f_{0,0}$ ,  $f_{0,1}$ , etc. are the edges made on [Line 4](#). The dotted box indicates that these states are added, using `ADD` ([Alg. 4](#)), before they are passed to `MAKEEDGE`, producing edges  $e_0$  and  $e_1$ . For readability, not all edge labels are shown.

The subroutine `ADD` ([Alg. 4](#)) adds two quantum states, i.e., given two LIMDDs representing  $|e\rangle$  and  $|f\rangle$ , it returns a LIMDD representing  $|e\rangle + |f\rangle$ . It proceeds by simple recursive descent on its children. The base case is when both edges point to the diagram's Leaf. In this case, these edges are labeled with scalars  $A, B \in \mathbb{C}$ , so we return the edge  $\xrightarrow{A+B} \textcircled{1}$ . Again, we defer the treatment of dynamic programming and caching to [Sec. 4.3](#).

---

**Algorithm 4** Given two  $n$ -LIMDD edges  $e, f$ , constructs a new LIMDD edge  $a$  with  $|a\rangle = |e\rangle + |f\rangle$ . For sake of simplicity, we omit the calls to the cache, choosing to postpone the treatment of dynamic programming to [Sec. 4.3](#).

---

```

1: procedure ADD(EDGE  $e \xrightarrow{A} \textcircled{v}$ , EDGE  $f \xrightarrow{B} \textcircled{w}$  with  $\text{idx}(v) = \text{idx}(w)$ )
2:   if  $n = 0$  then return  $\xrightarrow{A+B} \textcircled{1}$   $\triangleright A, B \in \mathbb{C}$ 
3:   EDGE  $a_0 := \text{ADD}(\text{FOLLOW}_0(e), \text{FOLLOW}_0(f))$ 
4:   EDGE  $a_1 := \text{ADD}(\text{FOLLOW}_1(e), \text{FOLLOW}_1(f))$ 
5:   return  $a$ 

```

---

The worst-case running time of `ADD` is  $\mathcal{O}(n^3 2^n)$ , if  $n$  is the number of qubits. This happens when the resulting LIMDD is exponential in the input sizes (bounded by  $2^n$ ). This exponential-size behavior was identified for QMDDs in [\[53, Table 2\]](#) and happens here for the same reason: addition may remove any common factors, as illustrated in [Fig. 7](#). However, the `ADD` algorithm is polynomial-time when  $v = w$  and  $v$  is a stabilizer state ([Lemma 21](#)).

## 4 Canonicity: how to keep a LIMDD fully reduced during simulation

In general, there are many different LIMDDs which represent a given quantum state. However, by imposing a small number of constraints on the diagram, listed in [Definition 4](#) and visualized in [Fig. 9](#), we ensure that every quantum state is represented by a unique ‘*reduced*’ LIMDD. Unique representation, or canonicity, is a crucial property for the efficiency and effectiveness of decision diagrams. In the first place, it allows for circuit analysis and simplification [18, 24], by facilitating efficient manipulation operations. Namely, canonicity enables us to cache the result of intermediate computations in such a way that we can retrieve them when the algorithm is later called with parameters that represent the same quantum state. In the second place, a reduced diagram is smaller than an unreduced diagram because it merges nodes with the same semantics. For instance, Pauli-LIMDDs allow all states in the same  $\simeq_{\text{Pauli}}$  equivalence class to be merged. In our case, the nodes are brought into canonical form, and are then merged, in the MAKEEDGE algorithm ([Alg. 5](#) in [Sec. 4.2](#)). The algorithms for quantum circuit simulation in [Sec. 3.3](#) ensure that all intermediate LIMDDs are reduced by creating nodes exclusively through this subroutine.

### 4.1 LIMDD canonical form

While the definition of a reduced LIMDD ([Definition 4](#)) may appear complex, it can be derived from two simple guiding principles. First, we wish to merge two nodes whenever their states are  $G$ -isomorphic, so that the diagram contains only one node per isomorphism class. This is accomplished rather straightforwardly by the Merge rule. As a consequence, this fixes the topology of the diagram. Second, to make the diagram *canonical*, we must make a deterministic choice between nodes representing the same states, which is accomplished by the other four rules, which are illustrated in [Fig. 9](#). The high determinism rule requires a deterministic function to choose LIMs, which we give in [Sec. 4.2](#).

**Definition 4** (Reduced LIMDD). A PAULI-LIMDD is *reduced* when it satisfies the following constraints. It is *semi-reduced* if it satisfies all constraints except high determinism.

1. **Merge:** No two nodes are identical: We say two nodes  $v, w$  are identical if  $\text{low}(v) = \text{low}(w)$ ,  $\text{high}(v) = \text{high}(w)$ ,  $\text{label}(\text{low}(v)) = \text{label}(\text{low}(w))$ ,  $\text{label}(\text{high}(v)) = \text{label}(\text{high}(w))$ .
2. **(Zero) Edge:** Any edge  $(v, w) \in \text{high} \cup \text{low}$  has  $\text{idx}(v) = \text{idx}(w) + 1$ , and if  $\text{label}(v, w) = 0$ , then both edges outgoing from  $v$  point to the same node, i.e.,  $\text{high}(v) = \text{low}(v) = w$ .
3. **Low Precedence:** Each node  $v$  has  $\text{low}(v) \preceq \text{high}(v)$ , where  $\preceq$  is a total order on nodes.
4. **Low Factoring:** The label on every low edge to a node  $v$  is the identity  $\mathbb{I}_2^{\otimes \text{idx}(v)}$ .
5. **High Determinism:** The label on the high edge of any node  $v$  is  $B_{\text{high}} = \text{HighLabel}(v)$ , where  $\text{HighLabel}$  is a function that takes as input a semi-reduced  $n$ -PAULI-LIMDD node  $v$ , and outputs an  $(n - 1)$ -PAULI-LIM  $B_{\text{high}}$  satisfying  $|v\rangle \simeq_{\text{PAULI}} |0\rangle |\text{low}(v)\rangle + |1\rangle \otimes B_{\text{high}} |\text{high}(v)\rangle$ . Moreover, for any other semi-reduced node  $w$  with  $|v\rangle \simeq_{\text{PAULI}} |w\rangle$ , it returns  $\text{HighLabel}(w) = B_{\text{high}}$ . In other words,  $\text{HighLabel}$  is constant within an isomorphism class.

We make several observations about reduced LIMDDs. First, let us apply this definition to a state  $|0\rangle \otimes |\varphi\rangle$ . There is a choice between representing this state as either  $\textcircled{\varphi} \xrightarrow{\mathbb{I}} \textcircled{0} \xrightarrow{\varphi}$  or  $\textcircled{\varphi} \xrightarrow{0} \textcircled{1} \xrightarrow{\varphi}$ , which denote the states  $|0\rangle \otimes |\varphi\rangle$  and  $|1\rangle \otimes |\varphi\rangle$ , as these are related by the isomorphism  $X \otimes \mathbb{I}$ . In this case, the low factoring rule forces us to take the  $\mathbb{I}$  label on the low edge, so this gives a node of the form  $|0\rangle \otimes |\varphi\rangle$ . Consequently, the high edge must be labeled with 0. Notice that there is no reduced LIMDD for the 0-vector, because any low edge must be labeled with  $\mathbb{I}_2^{\otimes n}$ . This is not a problem for us, since the 0-vector is not a quantum state.

If  $G$  is a group without the element  $X \notin G$ , the reduced  $G$ -LIMDD is not universal (does not represent all quantum states), because the low precedence rule cannot always be satisfied, since it

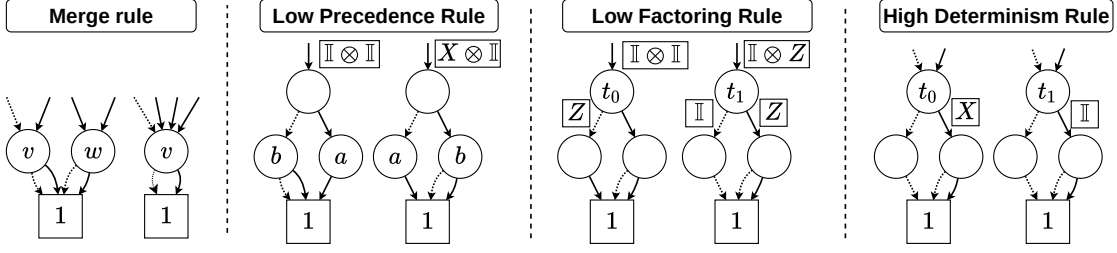


Figure 9: Illustration of the reduction rules in Definition 4. In each case, the left and right LIMDDs represent the same state, but the left LIMDD violates a reduction rule, while the right LIMDD satisfies it. The Merge rule regards the merging of two identical nodes  $v$  and  $w$ . Low Precedence determines which child is the low child, and which is the high child according to  $\preccurlyeq$ ; in this case, the intended meaning is that  $a \prec b$  in the total order. Low Factoring ensures that the low edge is always labeled with  $\mathbb{I}$ . High Determinism ensures that the label on a high edge is chosen canonically. In this case,  $|t_0\rangle \simeq |t_1\rangle$ , and label  $I$  is preferable to label  $X$  because  $\mathbb{I} \prec X$  according to the lexicographic order defined in App. A.

requires that  $v_0 \preccurlyeq v_1$  for every node. Hence, in this case, reduced  $G$ -LIMDD cannot represent a state  $|0\rangle|v_0\rangle + |1\rangle|v_1\rangle$  when  $v_1 \prec v_0$ .

Lastly, while the literature on other decision diagrams [16, 17, 54] often considers a “redundant test” rule that allows edges to skip multiple levels, we omit this reduction rule for the sake of simplicity, because it offers only linear improvements in the best case and complicates correctness proofs (see, e.g., [55, Lemma 1]). However, such a deletion rule can be added in a straightforward way.

We now give a proof of Lemma 6, which states that LIMDDs are canonical.

**Lemma 6** (Node canonicity). For each  $n$ -qubit state vector  $|\varphi\rangle$ , there exists a unique reduced Pauli-LIMDD  $L$  with root node  $v_L$  such that  $|v_L\rangle \simeq |\varphi\rangle$ .

*Proof.* We use induction on the number of qubits  $n$  to show universality (the existence of an isomorphic LIMDD node) and uniqueness (canonicity).

**Base case.** If  $n = 0$ , then  $|\varphi\rangle$  is a complex number  $\lambda$ . A reduced Pauli-LIMDD for this state is the leaf node representing the scalar 1. To show it is unique, consider that nodes  $v$  other than the leaf have an  $\text{idx}(v) > 0$ , by the edges rule, and hence represent multi-qubit states. Since the leaf node itself is defined to be unique, the merge rule is not needed and canonicity follows. Finally,  $|\varphi\rangle$  is represented by root edge  $\xrightarrow{\lambda} \textcircled{1}$ .

**Inductive case.** Suppose  $n > 0$ . We first show existence, and then show uniqueness.

We use the unique expansion of  $|\varphi\rangle$  as  $|\varphi\rangle = |0\rangle \otimes |\varphi_0\rangle + |1\rangle \otimes |\varphi_1\rangle$  where  $|\varphi_0\rangle$  and  $|\varphi_1\rangle$  are either  $(n-1)$ -qubit state vectors, or the all-zero vector. We distinguish three cases based on whether  $|\varphi_0\rangle, |\varphi_1\rangle = 0$ .

**Case  $|\varphi_0\rangle, |\varphi_1\rangle = 0$ :** This case is ruled out because  $|\varphi\rangle \neq 0$ .

**Case  $|\varphi_0\rangle = 0$  or  $|\varphi_1\rangle = 0$ :** In case  $|\varphi_0\rangle \neq 0$ , by the induction hypothesis, there exists a Pauli-LIMDD with root node  $w$  satisfying  $|w\rangle \simeq |\varphi_0\rangle$ . By definition of  $\simeq$ , there exists an  $n$ -qubit Pauli isomorphism  $A$  such that  $|\varphi_0\rangle = A|w\rangle$ . We construct the following reduced Pauli-LIMDD for  $|\varphi\rangle$ :

$\textcircled{w} \xrightarrow{X \cdot I} \textcircled{v} \xrightarrow{0} \textcircled{w}$ . In case  $|\varphi_1\rangle \neq 0$ , we do the same for root  $|w\rangle \simeq |\varphi_1\rangle = A|w\rangle$ . In both cases, it is easy to check that the root node is reduced. Also in both cases, we have  $|\varphi\rangle \simeq |v\rangle$  because either  $|\varphi\rangle = \mathbb{I}_2 \otimes A|v\rangle$  or  $|\varphi\rangle = X \otimes A|v\rangle$  as illustrated in Fig. 10 (left).

**Case  $|\varphi_0\rangle, |\varphi_1\rangle \neq 0$ :** By the induction hypothesis, there exist PAULI-LIMDDs  $L$  and  $R$  with root nodes  $|v_L\rangle \simeq |\varphi_0\rangle$  and  $|v_R\rangle \simeq |\varphi_1\rangle$ .<sup>§</sup> By definition of  $\simeq$ , there exist  $n$ -qubit Pauli isomorphisms  $A$  and  $B$  such that  $|\varphi_0\rangle = A|v_L\rangle$  and  $|\varphi_1\rangle = B|v_R\rangle$ . In case  $v_L \preccurlyeq v_R$ , we construct the following

<sup>§</sup>Note that the induction hypothesis implies a ‘local’ reduction of LIMDDs  $L$  and  $R$ , but not automatically a reduction of their union. For instance,  $L$  might contain a node  $w$  and  $R$  a node  $w$  such that  $v \simeq w$ . While the other

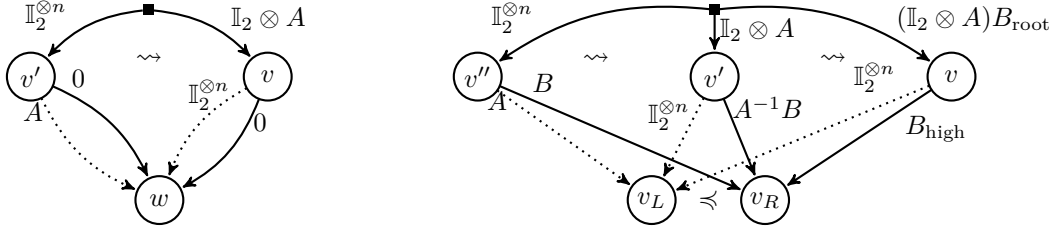


Figure 10: Reduced node construction in case  $|\varphi_1\rangle = 0$  (left), and  $|\varphi_0\rangle, |\varphi_0\rangle \neq 0$  and  $v_L \preceq v_R$  (right). For cases  $|\varphi_0\rangle = 0$  and  $v_R \preceq v_L$ , we take instead root edge  $X \otimes A$  and swap low/high edges. The black square (■) signifies a unique quantum state (all root edge represent this one state).

reduced Pauli-LIMDD for  $|\varphi\rangle$ : the root node is  $\textcircled{v_L} \xrightarrow{\mathbb{I}} \textcircled{v} \xrightarrow{E} \textcircled{v_R}$ , where  $E$  is the LIM computed by  $\text{HighLabel}(\textcircled{v_L} \xrightarrow{\mathbb{I}} \textcircled{v} \xrightarrow{A^{-1}B} \textcircled{v_R})$ . Otherwise, if  $v_R \preceq v_L$ , then we construct the following reduced Pauli-LIMDD for  $|\varphi\rangle$ : the root node is  $\textcircled{v_R} \xrightarrow{\mathbb{I}} \textcircled{v} \xrightarrow{F} \textcircled{v_L}$ , where  $F = \text{HighLabel}(\textcircled{v_L} \xrightarrow{\mathbb{I}} \textcircled{v} \xrightarrow{B^{-1}A} \textcircled{v_R})$ . It is straightforward to check that, in both cases, this Pauli-LIMDD is reduced. Moreover,  $|v\rangle$  is isomorphic to  $|\varphi\rangle$  as illustrated in Fig. 10 (right).

To show uniqueness, let  $L$  and  $M$  be reduced LIMDDs (root nodes  $v_L, v_M$ ) such that  $|v_L\rangle \simeq |\varphi\rangle \simeq |v_M\rangle$ . Expanding the semantics of  $v_L$  and  $v_M$ , this implies there exists a Pauli isomorphism  $\lambda P_{\text{top}} \otimes P_{\text{rest}} \neq 0$ , where  $P_{\text{top}}$  is a single-qubit Pauli and  $P_{\text{rest}}$  an  $(n-1)$ -qubit Pauli isomorphism, such that

$$\lambda P_{\text{top}} \otimes P_{\text{rest}}(|0\rangle \otimes A_L |v_L^0\rangle + |1\rangle \otimes B_L |v_L^1\rangle) = |0\rangle \otimes A_M |v_M^0\rangle + |1\rangle \otimes B_M |v_M^1\rangle. \quad (6)$$

We distinguish two cases from here on: where  $P_{\text{top}} \in \{\mathbb{I}, Z\}$  or  $P_{\text{top}} \in \{X, Y\}$ .

**Case  $P_{\text{top}} = I, Z$ .** If  $P_{\text{top}} = \begin{bmatrix} 1 & 0 \\ 0 & z \end{bmatrix}$  for  $z \in \{1, -1\}$ , then Eq. 6 gives:

$$\lambda P_{\text{rest}} A_L |v_L^0\rangle = A_M |v_M^0\rangle \quad \text{and} \quad z \lambda P_{\text{rest}} B_L |v_L^1\rangle = B_M |v_M^1\rangle \quad (7)$$

By low factoring, we have  $A_L = A_M = \mathbb{I}$ , so we obtain  $\lambda P_{\text{rest}} |v_L^0\rangle = |v_M^0\rangle$ . Hence  $|v_L^0\rangle$  is isomorphic with  $|v_M^0\rangle$ , so by the induction hypothesis, we have  $v_L^0 = v_M^0$ . We now show that also  $v_L = v_M$  by considering two cases.

**$B_L \neq 0$  and  $B_M \neq 0$ :** then  $z \lambda P_{\text{rest}} B_L |v_L^1\rangle = B_M |v_M^1\rangle$ , so the nodes  $v_L^1$  and  $v_M^1$  represent isomorphic states, so by the induction hypothesis we have  $v_L^1 = v_M^1$ . We already noticed by the low factoring rule that  $v_L$  and  $v_M$  have  $\mathbb{I}$  as low edge label. By the high edge rule, their high edge labels are  $\text{HighLabel}(v_L)$  and  $\text{HighLabel}(v_M)$ , and since the reduced LIMDDs  $L$  and  $M$  also satisfy low precedence and edge rules and  $|v_L\rangle \simeq |v_M\rangle$ , we have  $\text{HighLabel}(v_M) = \text{HighLabel}(v_L)$  by definition of  $\text{HighLabel}$ .

**$B_L = 0$  or  $B_M = 0$ :** In case  $B_L = 0$ , we see from Eq. 7 that  $0 = B_M |v_M^1\rangle$ . Since the state vector  $|v_M^1\rangle \neq 0$  by the observation that a reduced node does not represent the zero vector, it follows that  $B_M = 0$ . Otherwise, if  $B_M = 0$ , then Eq. 7 yields  $z \lambda P_{\text{rest}} B_L |v_L^1\rangle = 0$ . We have  $z \lambda \neq 0$ ,  $P_{\text{rest}} \neq 0$  by definition, and we observed  $|v_L^1\rangle \neq 0$  above. Therefore  $B_L = 0$ . In both cases,  $B_L = B_M$ .

We conclude that in both cases  $v_L$  and  $v_M$  have the same children and the same edge labels, so they are identical by the merge rule.

**Case  $P_{\text{top}} = X, Y$ .** If  $P_{\text{top}} = \begin{bmatrix} 0 & z^* \\ z & 0 \end{bmatrix}$  for  $z \in \{1, i\}$ , then Eq. 6 gives:

$$\lambda z P_{\text{rest}} A_L |v_L^0\rangle = B_M |v_M^1\rangle \quad \text{and} \quad \lambda z^* P_{\text{rest}} B_L |v_L^1\rangle = A_M |v_M^0\rangle.$$

reduction rules ensure that  $v$  and  $w$  will be structurally the same, the induction hypothesis only applies the merge rule  $L$  and  $M$  in isolation, leaving two separate identical nodes  $v, w$ . We can solve this by applying merge on the union of nodes in  $L$  and  $M$ , to merge any equivalent nodes.

By low factoring,  $A_L = A_M = \mathbb{I}$ , so we obtain  $z\lambda P_{\text{rest}} |v_L^0\rangle = B_M |v_M^1\rangle$  and  $\lambda z^* P_{\text{rest}} B_L |v_L^1\rangle = |v_M^0\rangle$ . To show that  $v_L = v_M$ , we consider two cases.

**$B_L \neq 0$  and  $B_M \neq 0$ :** we find  $|v_L^0\rangle \simeq |v_M^1\rangle$  and  $|v_L^1\rangle \simeq |v_M^0\rangle$ , so by the induction hypothesis,  $v_L^0 = v_M^1$  and  $v_L^1 = v_M^0$ . By low precedence, it must be that  $v_L^1 = v_M^1 = v_L^0 = v_M^0$ . Now use high determinism to infer that  $B_L = B_M$  as in the  $P_{\text{top}} = I, Z$  case.

**$B_L = 0$  or  $B_M = 0$ :** This case leads to a contradiction and thus cannot occur.  $B_L$  cannot be zero, because then  $|v_M^0\rangle$  is the all-zero vector, which we excluded. The other case:  $B_M = 0$ , then it must be that  $P_{\text{rest}}$  is zero, hence  $|v_M^0\rangle$  is the all-zero vector, which is again excluded.

We conclude that  $v_L$  and  $v_M$  have the same children and the same edge labels for all choices of  $P_{\text{top}}$ , so they are identical by the merge rule.  $\square$

## 4.2 The MAKEEDGE subroutine: Maintaining canonicity during simulation

To construct new nodes and edges, our algorithms use the MAKEEDGE subroutine (Alg. 5), as discussed above. MAKEEDGE produces a reduced parent node given two reduced children, so that the LIMDD representation becomes canonical. Here we give the algorithm for MAKEEDGE and show that it runs in time  $O(n^3)$  (assuming the input nodes are reduced).

The MAKEEDGE subroutine distinguishes two cases, depending on whether both children are non-zero vectors. It works as follows:

- First it ensures low precedence, switching  $e_0$  and  $e_1$  if necessary at Line 3. This is also done if  $e_0$ 's label  $A$  is 0 to allow for low factoring (avoiding divide by zero).
- Low factoring, i.e., dividing out the LIM  $A$ , placing it on the root node, is visualized in Fig. 10 for the cases  $e_1 = 0/e_1 \neq 0$ , and done in the algorithm at Line 6,7 / 9,11.
- The zero edges rule is enforced in the  $B = 0$  branch by taking  $v_1 := v_0$ .
- The canonical high label  $B_{\text{high}}$  is computed by GETLABELS, discussed below, for the semi-reduced node  $\textcircled{v_0} \xrightarrow{\mathbb{I}} \textcircled{w} \xrightarrow{\hat{A}} \textcircled{v_1}$ . With the resulting high label, it now satisfies the high determinism rule of Definition 4 with  $\text{HighLabel}(w) = B_{\text{high}}$ .
- Finally, we merge nodes by creating an entry  $(v_0, B_{\text{high}}, v_1)$  in a table called the *unique table* [56] at Line 13.

All steps except for GETLABELS have complexity  $O(1)$  or  $O(n)$  (for checking low precedence, we use the nodes' order in the unique table). The algorithm GETLABELS, which we sketch below in Sec. 4.2.1 and fully detail in App. D, has runtime  $O(n^3)$  if both input nodes are reduced, yielding an overall complexity  $O(n^3)$ .

### 4.2.1 Choosing a canonical high-edge label

In order to choose the canonical high edge label of node  $v$ , the MAKEEDGE algorithm calls GETLABELS (Line 10 of Alg. 5). The function GETLABELS returns a uniquely chosen LIM  $B_{\text{high}}$  among all possible high-edge labels which yield LIMDDs representing states that are Pauli-isomorphic to  $|v\rangle$ . We sketch the algorithm for GETLABELS here and provide the algorithm in full detail in App. D. First, we characterize the eligible high-edge labels. That is, given a semi-reduced node  $\textcircled{v_0} \xrightarrow{\mathbb{I}} \textcircled{v} \xrightarrow{\hat{A}} \textcircled{v_1}$ , we characterize all  $C$  such that the node  $\textcircled{v_0} \xrightarrow{\mathbb{I}} \textcircled{v} \xrightarrow{C} \textcircled{v_1}$  is isomorphic to  $\textcircled{v_0} \xrightarrow{\mathbb{I}} \textcircled{v} \xrightarrow{\hat{A}} \textcircled{v_1}$ . Our characterization shows that, modulo some complex factor, the eligible labels  $C$  are of the form

$$C \propto g_0 \cdot \hat{A} \cdot g_1, \quad \text{for } g_0 \in \text{Stab}(|v_0\rangle), g_1 \in \text{Stab}(|v_1\rangle) \quad (8)$$

**Algorithm 5** Algorithm MAKEEDGE takes two root edges to (already reduced) nodes  $v_0, v_1$ , the children of a new node, and returns a reduced node with root edge. It assumes that  $\text{idx}(v_0) = \text{idx}(v_1) = n$ . We indicate which lines of code are responsible for which reduction rule in [Definition 4](#).

---

```

1: procedure MAKEEDGE(EDGE  $e_0 \xrightarrow{A} \bigcirc_{v_0}$ , EDGE  $e_1 \xrightarrow{B} \bigcirc_{v_1}$ , where  $v_0, v_1$  reduced, with  $A \neq 0$ 
   or  $B \neq 0$ )
2:   if  $v_0 \not\sim v_1$  or  $A = 0$  then                                      $\triangleright$  Enforce low precedence and enable factoring
3:     return  $(X \otimes \mathbb{I}_2^{\otimes n}) \cdot \text{MakeEdge}(e_1, e_0)$ 
4:   if  $B = 0$  then
5:      $v_1 := v_0$                                                           $\triangleright$  Enforce zero edges
6:    $v := \bigcirc_{v_0} \xrightarrow{\mathbb{I}_2^{\otimes n}} \bigcirc \xrightarrow{0} \bigcirc_{v_0}$                                 $\triangleright$  Enforce low factoring
7:    $B_{\text{root}} := \mathbb{I}_2 \otimes A$                                             $\triangleright B_{\text{root}} |v\rangle = |0\rangle \otimes A |v_0\rangle + |1\rangle \otimes B |v_1\rangle$ 
8:   else
9:      $\hat{A} := A^{-1}B$                                                     $\triangleright$  Enforce low factoring
10:     $B_{\text{high}}, B_{\text{root}} := \text{GETLABELS}(\hat{A}, v_0, v_1)$                   $\triangleright$  Enforce high determinism
11:     $v := \bigcirc_{v_0} \xrightarrow{\mathbb{I}_2^{\otimes n}} \bigcirc \xrightarrow{B_{\text{high}}} \bigcirc_{v_1}$                     $\triangleright B_{\text{root}} |v\rangle = |0\rangle \otimes |v_0\rangle + |1\rangle \otimes A^{-1}B |v_1\rangle$ 
12:     $B_{\text{root}} := (\mathbb{I}_2 \otimes A)B_{\text{root}}$                                     $\triangleright (\mathbb{I}_2 \otimes A)B_{\text{root}} |v\rangle = |0\rangle \otimes A |v_0\rangle + |1\rangle \otimes B |v_1\rangle$ 
13:     $v_{\text{root}} := \text{Find or create unique table entry } \text{UNIQUE}[v] = (v_0, B_{\text{high}}, v_1)$   $\triangleright$  Enforce merge
14:  return  $\xrightarrow{B_{\text{root}}} \bigcirc_{v^*}$ 

```

---

where  $\text{Stab}(|v_0\rangle)$  and  $\text{Stab}(|v_1\rangle)$  are the stabilizer subgroups of  $|v_0\rangle$  and  $|v_1\rangle$ , i.e., the already reduced children of our input node  $v$ . Note that the set of eligible high-edge labels might be exponentially large in the number of qubits. Fortunately, eq. (8) shows that this set has a polynomial-size description by storing only the generators of the stabilizer subgroups.

Our algorithm chooses the lexicographically smallest eligible label, i.e., the smallest  $C$  of the form  $C \propto g_0 \hat{A} g_1$  (the definition of ‘lexicographically smallest’ is given in [App. A](#)). To this end, we use two subroutines: (1) an algorithm which finds (a generating set of) the stabilizer group  $\text{Stab}(|v\rangle)$  of a LIMDD node  $v$ ; and (2) an algorithm that uses these stabilizer subgroups of the children nodes to choose a unique representative of the eligible-high-label set from eq. (8).

For (1), we use an algorithm which recurses on the children nodes. First, we note that, if the Pauli LIM  $A$  stabilizes both children, then  $\mathbb{I} \otimes A$  stabilizes the parent node. Therefore, we compute (a generating set for) the intersection of the children’s stabilizer groups. Second, our method finds out whether the parent node has stabilizers of the form  $P_n \otimes A$  for  $P_n \in \{X, Y, Z\}$ . This requires us to decide whether certain cosets of the children’s stabilizer groups are empty. These groups are relatively simple, since, modulo phase, they are isomorphic to a binary vector space, and cosets are hyperplanes. We can therefore rely in large part on existing algorithms for linear algebra in vector spaces. The difficult part lies in dealing with the non-abelian aspects of the Pauli group. We provide the full algorithm, which is efficient, also in [App. D](#).

Our algorithm for (2) applies a variant of Gauss-Jordan elimination to the generating sets of  $\text{Stab}(|v_0\rangle)$  and  $\text{Stab}(|v_1\rangle)$  to choose  $g_0$  and  $g_1$  in eq. (8) which, when multiplied with  $\hat{A}$  as in eq. (8), yield the smallest possible high label  $C$ . (We recall that Gauss-Jordan elimination, a standard linear-algebra technique, is applicable here because the stabilizer groups are group isomorphic to binary vector spaces, see also [App. A](#)). We explain the full algorithm in [App. D](#).

#### 4.2.2 Checking whether two LIMDDs are Pauli-equivalent

To check whether two states represented as LIMDDs are Pauli-equivalent, it suffices to check whether they have the same root node. Namely, due to canonicity, and in particular the Merge rule (in [Definition 4](#)), there is a unique LIMDD representing a quantum state up to phase and local Pauli operators.

### 4.3 Dynamic programming in the APPLYGATE algorithm

A naive implementation of APPLYGATE and ADD, as given in Alg. 3 and Alg. 4 (in Sec. 3.3.3) would lead to exponential running times by exploring every path in the diagram. In order to make the algorithms efficient in many cases, including stabilizer states, dynamic programming is necessary: we store all results of recursive calls to these subroutines in a cache, so that no computation needs to be performed twice, but can instead be retrieved from the cache (i.e., the results are *memoized*). In this section, we detail how to implement the cache in such a way to achieve polynomial-time simulation of Clifford circuits; then App. E proves that polynomial-time simulation is indeed achieved.

A straightforward way to implement dynamic programming is to simply store all results of ApplyGate and Add in the cache, i.e., when APPLYGATE( $\frac{A}{\rightarrow}u, \frac{B}{\rightarrow}v$ ) is called, store an entry with key  $(A, u, B, v)$  in the cache. This allows us to retrieve the value the next time APPLYGATE is called with the same parameters. However, we can do much better, in such a way that we can retrieve the result from the cache also when the procedure is called with parameters APPLYGATE( $\frac{C}{\rightarrow}x, \frac{D}{\rightarrow}y$ ) satisfying  $[\frac{A}{\rightarrow}u] = [\frac{C}{\rightarrow}x]$  and  $[\frac{B}{\rightarrow}v] = [\frac{D}{\rightarrow}y]$ . This can happen even when  $A \neq C$  or  $B \neq D$ ; therefore, this technique makes the cache more compact.

To this end, we store not just an edge-edge tuple as above, but a *canonical* edge-edge tuple. To obtain canonical edge labels, our algorithms use the function RootLabel. This function returns a *canonically chosen* LIM, i.e., it holds that  $\text{RootLabel}(\frac{A}{\rightarrow}v) = \text{RootLabel}(\frac{B}{\rightarrow}v)$  whenever  $A|v\rangle = B|v\rangle$ . A specific choice for RootLabel is the lexicographic minimum of all possible root labels, following a similar choice for making a canonical choice for the high edge label of a node in Sec. 4.2. In Alg. 12, we give an  $O(n^3)$ -time algorithm for computing the lexicographically minimal root label.

---

**Algorithm 6** Subroutines which store and retrieve the results of APPLYGATE and ADD computations in the cache, facilitating dynamic programming in these algorithms.

---

```

1: procedure APPLYCACHELOOKUP(EDGE  $\frac{\lambda_A P}{\rightarrow}u$ , EDGE  $\frac{\lambda_B Q}{\rightarrow}v$ )
2:   |  $P', Q' := \text{RootLabel}(\frac{P}{\rightarrow}u), \text{RootLabel}(\frac{Q}{\rightarrow}v)$  ▷ Get canonical root labels
3:   | if  $(\frac{P'}{\rightarrow}u, \frac{Q'}{\rightarrow}v) \in \text{APPLY-CACHE}$  then return  $\lambda_A \lambda_B \cdot \text{APPLY-CACHE}[\frac{P'}{\rightarrow}u, \frac{Q'}{\rightarrow}v]$ 
4:   | else return “Not found”
5: procedure APPLYCACHESTORE(EDGE  $\frac{\lambda_A P}{\rightarrow}u$ , EDGE  $\frac{\lambda_B Q}{\rightarrow}v$ , EDGE  $e$ )
6:   |  $P', Q' := \text{RootLabel}(\frac{P}{\rightarrow}u), \text{RootLabel}(\frac{Q}{\rightarrow}v)$  ▷ Get canonical root labels
7:   |  $\text{APPLY-CACHE}[\frac{P'}{\rightarrow}u, \frac{Q'}{\rightarrow}v] := e$ 
8: procedure ADDCACHELOOKUP(EDGE  $\frac{A}{\rightarrow}v$ , EDGE  $\frac{B}{\rightarrow}w$ )
9:   | if  $v \not\approx w$  then return  $\text{ADDCACHELOOKUP}(\frac{B}{\rightarrow}w, \frac{A}{\rightarrow}v)$ 
10:  |  $C := \text{RootLabel}(\frac{A^{-1}B}{\rightarrow}w)$ 
11:  | if  $(v, \frac{C}{\rightarrow}w) \in \text{ADD-CACHE}$  then return  $A \cdot \text{ADD-CACHE}[v, \frac{C}{\rightarrow}w]$ 
12:  | else return “Not found”
13: procedure ADDCACHESTORE(EDGE  $\frac{A}{\rightarrow}v$ , EDGE  $\frac{B}{\rightarrow}w$ , EDGE  $a$ )
14:  | if  $v \not\approx w$  then  $\text{ADDCACHESTORE}(\frac{B}{\rightarrow}w, \frac{A}{\rightarrow}v)$ 
15:  |  $C := \text{RootLabel}(\frac{A^{-1}B}{\rightarrow}w)$ 
16:  |  $\text{ADD-CACHE}[v, \frac{C}{\rightarrow}w] := A^{-1}a$ 

```

---

**Cache of ApplyGate.** In APPLYCACHESTORE in Alg. 6, when APPLYGATE is called with parameters APPLYGATE( $\frac{\lambda_A P}{\rightarrow}u, \frac{\lambda_B Q}{\rightarrow}v$ ), we store a canonically chosen edge-edge tuple  $(P', u, Q', v)$  in the cache. Here  $P' = \text{RootLabel}(\frac{P}{\rightarrow}u)$  and  $Q' = \text{RootLabel}(\frac{Q}{\rightarrow}v)$  are canonically cho-

sen LIMs. Consequently, we will retrieve this result whenever `APPLYGATE` is called with inputs  $(\frac{\lambda'_A P''}{\rightarrow \textcircled{u}}, \frac{\lambda'_B Q''}{\rightarrow \textcircled{v}})$ , whenever  $Q''|v\rangle = Q|v\rangle$ , even if  $Q'' \neq Q$ .

As a further optimization, we opt to not store the scalars  $\lambda_A, \lambda_B$  in the cache (they are “factored out”), so that we can retrieve this result also when `APPLYGATE` is called with inputs that are equal up to a complex phase. The scalars are then factored back in on [Line 3](#).

**Cache of Add.** A straightforward way to implement the Add cache is to store a tuple with key  $(A, v, B, w)$  in the call `ADD`( $\frac{A}{\rightarrow \textcircled{v}}, \frac{B}{\rightarrow \textcircled{w}}$ ). However, we can do much better; namely, we remark that we are looking to construct the state  $A|v\rangle + B|w\rangle$ , and that this is equal to  $A \cdot (|v\rangle + A^{-1}B|w\rangle)$ . This gives us the opportunity to “factor out” the LIM  $A$ , and only store the tuple  $(v, A^{-1}B, w)$ .

We can do even better by finding a canonically chosen LIM  $C = \text{RootLabel}(\frac{A^{-1}B}{\rightarrow \textcircled{v}})$  and storing  $(v, C, w)$ . This way, we get a cache hit upon the call `ADD`( $\frac{D}{\rightarrow \textcircled{v}}, \frac{E}{\rightarrow \textcircled{w}}$ ) whenever  $A^{-1}B|w\rangle = C^{-1}D|w\rangle$ . This happens of course in particular when  $(A, v, B, w) = (D, v, E, w)$ , but can happen in exponentially more cases; therefore, this technique works at least as well as the “straightforward” way outlined above.

Finally, on lines [Line 9](#) and [Line 14](#), we take advantage of the fact that addition is commutative; therefore it allows us to pick a preferred order in which we store the nodes, thus reducing the size of the cache by a factor 2.

## 5 Related work

We mention related work on classical simulation formalisms and decision diagrams other than QMDDs.

The Affine Algebraic Decision Diagram, introduced by Tafertshofer and Peadar [\[57\]](#), and by Sanner and McAllister [\[26\]](#), is akin to a QMDD except that its edges are labeled with a pair of real numbers  $(a, b)$ , so that an edge  $\frac{(a, b)}{\rightarrow \textcircled{v}}$  represents the state vector  $a|v\rangle + b$ . To the best of our knowledge, this diagram has not been applied to quantum computing.

Günther and Drechsler introduced a BDD variant [\[58\]](#) which, in LIMDD terminology, has a label on the root node only. To be precise, this diagram’s root edge is labeled with an invertible matrix  $A \in \mathbb{F}_2^{n \times n}$ . If the root node represents the function  $r$ , then the diagram represents the function  $f(\vec{x}) = r(A \cdot \vec{x})$ . In contrast, LIMDDs allow a label on every edge in the diagram, not only the root edge.

A multilinear arithmetic formula is a formula over  $+, \times$  which computes a polynomial in which no variable appears raised to a higher power than 1. Aaronson showed that some stabilizer states require superpolynomial-size multilinear arithmetic formulas [\[31, 59\]](#).

## 6 Discussion

We have introduced LIMDD, a novel decision diagram-based method to simulate quantum circuits, which enables polynomial-size representation of a strict superset of stabilizer states and the states represented by polynomially large QMDDs. To prove this strict inclusion, we have shown the first lower bounds on the size of QMDDs for stabilizer states: they require exponential size for certain families of stabilizer states. Our results show that these states are thus hard for QMDDs. We also give the first analytical comparison between decision diagrams, Matrix Product States, and the Clifford+ $T$  simulator.

LIMDDs achieve a more succinct representation than QMDDs by representing states up to local

invertible maps which uses single-qubit (i.e., local) operations from a group  $G$ . We have investigated the choices  $G = \text{PAULI}$ ,  $G = \langle Z \rangle$  and  $G = \langle X \rangle$ , and found that any choice suffices for an exponential advantage over QMDDs; notably, the choice  $G = \text{PAULI}$  allows us to succinctly represent any stabilizer state. Furthermore, we showed how to simulate arbitrary quantum circuits, encoded as Pauli-LIMDDs. The resulting algorithms for simulating quantum circuits are exponentially faster than for QMDDs in the best case, and never more than a polynomial factor slower. In the case of Clifford circuits, the simulation by LIMDDs is in polynomial time (in contrast to QMDDs).

We have shown that Pauli-LIMDDs can efficiently simulate a circuit family outputting the  $W$  states, in contrast to the Clifford + T simulator which requires exponential time to do so (assuming the widely believed ETH), even when allowing for preprocessing of the circuit with a  $T$ -count optimizer.

Since we know from experience that implementing a decision diagram framework is a major endeavor, we leave an implementation of the Pauli-LIMDD, in order to observe its runtimes in practice on relevant quantum circuits, to future work. We emphasize that from the perspective of algorithm design, we have laid all the groundwork for such an implementation, including the key ingredient for the efficiency of many operations for existing decision diagrams: the existence of a unique canonical representative of the represented function, combined with a tractable MakeEdge algorithm to find it.

Regarding extensions of the LIMDD data structure, an obvious next step is to investigate other choices of  $G$ . Of interest are both the representational capabilities of such diagrams (do they represent interesting states?), and the algorithmic capabilities (can we still find efficient algorithms which make use of these diagrams?). In this vein, an important question is what the relationship is between  $G$ -LIMDDs (for various choices of  $G$ ) and existing formalisms for the classical simulation of quantum circuits, such as those based on match gates [60–62] and tensor networks [27, 63]. It would also be interesting to compare LIMDDs to graphical calculi such as the ZX calculus [64], following similar work for QMDDs [65].

Lastly, we note that the current definition of LIMDD imposes a strict total order over the qubits along every path from root to leaf. It is known that the chosen order can greatly influence the size of the DD [66, 67], making it interesting to investigate variants of LIMDDs with a flexible ordering, for example taking inspiration from the Sentential Decision Diagram [68, 69].

## 7 Acknowledgements

We thank Dan Browne for help with establishing stabilizer ranks. We thank Marie Anastacio, Jonas Helsen, Yash Patel and Matthijs Rijlaarsdam for their feedback on early versions of the manuscript, and we thank Kenneth Goodenough for useful discussions. The second author acknowledges the QIA project (funded by European Union’s Horizon 2020, Grant Agreement No. 820445). The third and fourth author are funded by the Netherlands Organization for Scientific Research (NWO/OCW), as part of the Quantum Software Consortium program (Project No. 024.003.037/3368). The last author is funded by the research program VENI with project number 639.021.649 of the Netherlands Organization for Scientific Research (NWO).

## References

- [1] Alwin Zulehner and Robert Wille. “One-pass design of reversible circuits: Combining embedding and synthesis for reversible logic”. *IEEE Transactions on Computer-Aided Design of Integrated Circuits and Systems* **37**, 996–1008 (2017).
- [2] Lukas Burgholzer and Robert Wille. “Improved dd-based equivalence checking of quantum circuits”. In *2020 25th Asia and South Pacific Design Automation Conference (ASP-DAC)*. Pages 127–132. IEEE (2020).
- [3] John Preskill. “Quantum Computing in the NISQ era and beyond”. *Quantum* **2**, 79 (2018).
- [4] Daniel Gottesman. “The Heisenberg representation of quantum computers” (1998).

- [5] Scott Aaronson and Daniel Gottesman. “Improved simulation of stabilizer circuits”. *Physical Review A* **70** (2004).
- [6] Daniel Gottesman. “Stabilizer codes and quantum error correction” (1997).
- [7] Maarten Van den Nest, Jeroen Dehaene, and Bart De Moor. “Local unitary versus local clifford equivalence of stabilizer states”. *Phys. Rev. A* **71**, 062323 (2005).
- [8] Matthias Englbrecht and Barbara Kraus. “Symmetries and entanglement of stabilizer states”. *Phys. Rev. A* **101**, 062302 (2020).
- [9] Robert Raussendorf and Hans J. Briegel. “A one-way quantum computer”. *Phys. Rev. Lett.* **86**, 5188–5191 (2001).
- [10] Sergey Bravyi, Graeme Smith, and John A. Smolin. “Trading classical and quantum computational resources”. *Phys. Rev. X* **6**, 021043 (2016).
- [11] Sergey Bravyi and David Gosset. “Improved classical simulation of quantum circuits dominated by clifford gates”. *Phys. Rev. Lett.* **116**, 250501 (2016).
- [12] Sergey Bravyi, Dan Browne, Padraic Calpin, Earl Campbell, David Gosset, and Mark Howard. “Simulation of quantum circuits by low-rank stabilizer decompositions”. *Quantum* **3**, 181 (2019).
- [13] Yifei Huang and Peter Love. “Approximate stabilizer rank and improved weak simulation of clifford-dominated circuits for qudits”. *Phys. Rev. A* **99**, 052307 (2019).
- [14] Lucas Kocia and Peter Love. “Stationary phase method in discrete wigner functions and classical simulation of quantum circuits” (2018).
- [15] Lucas Kocia and Mohan Sarovar. “Improved simulation of quantum circuits by fewer gaussian eliminations” (2020).
- [16] Sheldon B. Akers. “Binary decision diagrams”. *IEEE Computer Architecture Letters* **27**, 509–516 (1978).
- [17] Randal E. Bryant. “Graph-based algorithms for Boolean function manipulation”. *IEEE Trans. Computers* **35**, 677–691 (1986).
- [18] Yirng-An Chen Randal E Bryant. “Verification of arithmetic circuits with binary moment diagrams”. In 32nd Design Automation Conference. Pages 535–541. IEEE (1995).
- [19] George F Viamontes, Igor L Markov, and John P Hayes. “High-performance quidd-based simulation of quantum circuits”. In Proceedings Design, Automation and Test in Europe Conference and Exhibition. Volume 2, pages 1354–1355. IEEE (2004).
- [20] R. I. Bahar, E. A. Frohm, C. M. Gaona, G. D. Hachtel, E. Macii, A. Pardo, and F. Somenzi. “Algebraic decision diagrams and their applications”. In Proceedings of 1993 International Conference on Computer Aided Design (ICCAD). Pages 188–191. (1993).
- [21] George F Viamontes, Igor L Markov, and John P Hayes. “Improving gate-level simulation of quantum circuits”. *Quantum Information Processing* **2**, 347–380 (2003).
- [22] Masahiro Fujita, Patrick C. McGeer, and JC-Y Yang. “Multi-terminal binary decision diagrams: An efficient data structure for matrix representation”. *Formal methods in system design* **10**, 149–169 (1997).
- [23] E. M. Clarke, K. L. McMillan, X Zhao, M. Fujita, and J. Yang. “Spectral transforms for large boolean functions with applications to technology mapping”. In Proceedings of the 30th International Design Automation Conference. Pages 54–60. DAC ’93New York, NY, USA (1993). Association for Computing Machinery.
- [24] D Michael Miller and Mitchell A Thornton. “QMDD: A decision diagram structure for reversible and quantum circuits”. In 36th International Symposium on Multiple-Valued Logic (ISMVL’06). Pages 30–30. IEEE (2006).
- [25] Alwin Zulehner and Robert Wille. “Advanced simulation of quantum computations”. *IEEE Transactions on Computer-Aided Design of Integrated Circuits and Systems* **38**, 848–859 (2018).
- [26] Scott Sanner and David McAllester. “Affine algebraic decision diagrams (aadds) and their application to structured probabilistic inference”. In Proceedings of the 19th International Joint Conference on Artificial Intelligence. Pages 1384–1390. IJCAI’05San Francisco, CA, USA (2005). Morgan Kaufmann Publishers Inc.
- [27] Xin Hong, Xiangzhen Zhou, Sanjiang Li, Yuan Feng, and Mingsheng Ying. “A tensor network based decision diagram for representation of quantum circuits” (2020).

- [28] Stefan Hillmich, Richard Kueng, Igor L. Markov, and Robert Wille. “As accurate as needed, as efficient as possible: Approximations in dd-based quantum circuit simulation”. In Design, Automation & Test in Europe Conference & Exhibition, DATE 2021, Grenoble, France, February 1-5, 2021. **Pages 188–193**. IEEE (2021).
- [29] George F Viamontes, Igor L Markov, and John P Hayes. “Quantum circuit simulation”. Springer Science & Business Media. (2009).
- [30] Xin Hong, Mingsheng Ying, Yuan Feng, Xiangzhen Zhou, and anjiang Li. “Approximate equivalence checking of noisy quantum circuits” (2021).
- [31] Hans J. Briegel and Robert Raussendorf. “Persistent entanglement in arrays of interacting particles”. **Phys. Rev. Lett.** **86**, 910–913 (2001).
- [32] Wolfgang Dür, Guifre Vidal, and J Ignacio Cirac. “Three qubits can be entangled in two inequivalent ways”. *Physical Review A* **62**, 062314 (2000).
- [33] Eric Chitambar, Debbie Leung, Laura Mančinska, Maris Ozols, and Andreas Winter. “Everything you always wanted to know about locc (but were afraid to ask)”. *Communications in Mathematical Physics* **328**, 303–326 (2014).
- [34] Steven R White. “Density matrix formulation for quantum renormalization groups”. *Physical review letters* **69**, 2863 (1992).
- [35] J Ignacio Cirac, David Perez-Garcia, Norbert Schuch, and Frank Verstraete. “Matrix product states and projected entangled pair states: Concepts, symmetries, theorems”. *Reviews of Modern Physics* **93**, 045003 (2021).
- [36] Russell Impagliazzo and Ramamohan Paturi. “On the complexity of k-sat”. *Journal of Computer and System Sciences* **62**, 367–375 (2001).
- [37] Adnan Darwiche and Pierre Marquis. “A knowledge compilation map”. *Journal of Artificial Intelligence Research* **17**, 229–264 (2002).
- [38] Marc Hein, Wolfgang Dür, Jens Eisert, Robert Raussendorf, M Nest, and H-J Briegel. “Entanglement in graph states and its applications” (2006).
- [39] Koenraad M R Audenaert and Martin B Plenio. “Entanglement on mixed stabilizer states: normal forms and reduction procedures”. *New Journal of Physics* **7**, 170 (2005). url: <http://stacks.iop.org/1367-2630/7/i=1/a=170>.
- [40] Sergey Bravyi and Alexei Kitaev. “Universal quantum computation with ideal clifford gates and noisy ancillas”. **Phys. Rev. A** **71**, 022316 (2005).
- [41] Charles H Bennett, Herbert J Bernstein, Sandu Popescu, and Benjamin Schumacher. “Concentrating partial entanglement by local operations”. *Physical Review A* **53**, 2046 (1996).
- [42] David Perez-Garcia, Frank Verstraete, Michael M Wolf, and J Ignacio Cirac. “Matrix product state representations” (2006).
- [43] Richard J Lipton, Donald J Rose, and Robert Endre Tarjan. “Generalized nested dissection”. *SIAM journal on numerical analysis* **16**, 346–358 (1979).
- [44] M. Van den Nest, W. Dür, G. Vidal, and H. J. Briegel. “Classical simulation versus universality in measurement-based quantum computation”. **Phys. Rev. A** **75**, 012337 (2007).
- [45] Vít Jelínek. “The rank-width of the square grid”. *Discrete Applied Mathematics* **158**, 841–850 (2010).
- [46] James McClung. “Constructions and applications of w-states”. PhD thesis. Worcester Polytechnic Institute. (2020).
- [47] Srinivasan Arunachalam, Sergey Bravyi, Chinmay Nirkhe, and Bryan O’Gorman. “The parameterized complexity of quantum verification” (2022).
- [48] Aleks Kissinger and John van de Wetering. “Reducing t-count with the zx-calculus” (2019).
- [49] Himanshu Thapliyal, Edgard Munoz-Coreas, TSS Varun, and Travis S Humble. “Quantum circuit designs of integer division optimizing t-count and t-depth”. *IEEE Transactions on Emerging Topics in Computing* **9**, 1045–1056 (2019).
- [50] Wang Jian, Zhang Quan, and Tang Chao-Jing. “Quantum secure communication scheme with w state”. *Communications in Theoretical Physics* **48**, 637 (2007).
- [51] Wen Liu, Yong-Bin Wang, and Zheng-Tao Jiang. “An efficient protocol for the quantum private comparison of equality with w state”. *Optics Communications* **284**, 3160–3163 (2011).
- [52] Victoria Lipinska, Gláucia Murta, and Stephanie Wehner. “Anonymous transmission in a noisy quantum network using the  $W$  state”. **Phys. Rev. A** **98**, 052320 (2018).

- [53] H  lene Fargier, Pierre Marquis, Alexandre Niveau, and Nicolas Schmidt. “A knowledge compilation map for ordered real-valued decision diagrams”. In Proceedings of the AAAI Conference on Artificial Intelligence. Volume 28. (2014).
- [54] David Y Feinstein and Mitchell A Thornton. “On the skipped variables of quantum multiple-valued decision diagrams”. In 2011 41st IEEE International Symposium on Multiple-Valued Logic. Pages 164–169. IEEE (2011).
- [55] Henrik Reif Andersen. “An introduction to binary decision diagrams”. Lecture notes, available online, IT University of CopenhagenPage 5 (1997).
- [56] Karl S Brace, Richard L Rudell, and Randal E Bryant. “Efficient implementation of a bdd package”. In 27th ACM/IEEE design automation conference. Pages 40–45. IEEE (1990).
- [57] Paul Tafertshofer and Massoud Pedram. “Factored edge-valued binary decision diagrams”. Formal Methods in System Design **10**, 243–270 (1997).
- [58] Wolfgang G  nther and Rolf Drechsler. “Bdd minimization by linear transformations”. In In Advanced Computer Systems. Citeseer (1998).
- [59] Scott Aaronson. “Multilinear formulas and skepticism of quantum computing”. In Proceedings of the Thirty-Sixth Annual ACM Symposium on Theory of Computing. Page 118–127. STOC ’04New York, NY, USA (2004). Association for Computing Machinery.
- [60] Barbara M. Terhal and David P. DiVincenzo. “Classical simulation of noninteracting-fermion quantum circuits”. *Phys. Rev. A* **65**, 032325 (2002).
- [61] Richard Jozsa and Akimasa Miyake. “Matchgates and classical simulation of quantum circuits”. Proceedings: Mathematical, Physical and Engineering SciencesPages 3089–3106 (2008).
- [62] Martin Hebenstreit, Richard Jozsa, Barbara Kraus, and Sergii Strelchuk. “Computational power of matchgates with supplementary resources”. Physical Review A **102**, 052604 (2020).
- [63] Rom  n Or  s. “A practical introduction to tensor networks: Matrix product states and projected entangled pair states”. *Annals of Physics* **349**, 117–158 (2014).
- [64] Bob Coecke and Ross Duncan. “Interacting quantum observables: categorical algebra and diagrammatics”. New Journal of Physics **13**, 043016 (2011).
- [65] Renaud Vilmart. “Quantum multiple-valued decision diagrams in graphical calculi” (2021).
- [66] Richard Rudell. “Dynamic variable ordering for ordered binary decision diagrams”. In Proceedings of 1993 International Conference on Computer Aided Design (ICCAD). Pages 42–47. IEEE (1993).
- [67] Ingo Wegener. “Branching programs and binary decision diagrams: theory and applications”. SIAM. (2000).
- [68] Adnan Darwiche. “Sdd: a new canonical representation of propositional knowledge bases”. In Proceedings of the Twenty-Second international joint conference on Artificial Intelligence-Volume Volume Two. Pages 819–826. AAAI Press (2011).
- [69] Doga Kisa, Guy Van den Broeck, Arthur Choi, and Adnan Darwiche. “Probabilistic sentential decision diagrams”. In Fourteenth International Conference on the Principles of Knowledge Representation and Reasoning. (2014).
- [70] Ewout van den Berg and Kristan Temme. “Circuit optimization of hamiltonian simulation by simultaneous diagonalization of pauli clusters”. Quantum **4**, 322 (2020).
- [71] Eugene M Luks, Ferenc R  k  czi, and Charles RB Wright. “Some algorithms for nilpotent permutation groups”. *Journal of Symbolic Computation* **23**, 335–354 (1997).
- [72] Pavol D  ri  , Juraj Hromkovi  , Stasys Jukna, Martin Sauerhoff, and Georg Schnitger. “On multi-partition communication complexity”. Information and computation **194**, 49–75 (2004).
- [73] Hector J Garcia, Igor L Markov, and Andrew W Cross. “Efficient inner-product algorithm for stabilizer states” (2012).
- [74] “Stabranksearcher: code for finding (upper bounds to) the stabilizer rank of a quantum state”. <https://github.com/timcp/StabRankSearcher> (2021).
- [75] Padraic Calpin. “Exploring quantum computation through the lens of classical simulation”. PhD thesis. UCL (University College London). (2020).

## A Efficient linear-algebra algorithms for stabilizer subgroups

In [Sec. 2](#), we defined a stabilizer subgroup for an  $n$ -qubit state  $|\varphi\rangle$  as the group of Pauli operators  $A \in \text{PAULI}_n$  which stabilize  $|\varphi\rangle$ , i.e.  $A|\varphi\rangle = |\varphi\rangle$ . Here, we explain existing efficient algorithms for solving various tasks regarding stabilizer subgroups (whose elements commute with each other). We will also outline how the algorithms can be extended and altered to work for general PAULILIMs, which do not necessarily commute.

Any  $n$ -qubit Pauli string can (modulo factor  $\in \{\pm 1, \pm i\}$ ) be written as  $(X^{x_n} Z^{z_n}) \otimes \dots \otimes (X^{x_1} Z^{z_1})$  for bits  $x_j, z_j, 1 \leq j \leq n$ . We can therefore write an  $n$ -qubit Pauli string  $P$  as length- $2n$  binary vector

$$\underbrace{(x_n, x_{n-1}, \dots, x_1)}_{\text{X block}} \mid \underbrace{(z_n, z_{n-1}, \dots, z_1)}_{\text{Z block}},$$

where we added the horizontal bar ( $\mid$ ) only to guide the eye. We will refer to such vectors as *check vectors*. For example  $X \sim (1, 0)$  and  $Z \otimes Y \sim (0, 1 \mid 1, 1)$  [\[5\]](#). A set of  $k$  Pauli strings thus can be written as  $2n \times k$  binary matrix, often called *check matrix*, e.g.

$$\begin{pmatrix} X & \otimes & X & \otimes & X \\ \mathbb{I}_2 & \otimes & Z & \otimes & Y \end{pmatrix} \sim \left( \begin{array}{ccc|ccc} 1 & 1 & 1 & 0 & 0 & 0 \\ 0 & 0 & 1 & 0 & 1 & 1 \end{array} \right).$$

This equivalence induces an ordering on Pauli strings following the lexicographic ordering on bit strings. For example,  $X < Y$  because  $(1|0) < (1|1)$  and  $Z \otimes \mathbb{I}_2 < Z \otimes X$  because  $(00|10) < (01|10)$ . Furthermore, if  $P, Q$  are Pauli strings corresponding to binary vectors  $\vec{x}^P, \vec{z}^P$  and  $\vec{x}^Q, \vec{z}^Q$ , then

$$P \cdot Q \propto \bigotimes_{j=1}^n \left( X^{x_j^P} Z^{z_j^P} \right) \left( X^{x_j^Q} Z^{z_j^Q} \right) = \bigotimes_{j=1}^n \left( X^{x_j^P \oplus x_j^Q} Z^{z_j^P \oplus z_j^Q} \right)$$

and therefore the group of  $n$ -qubit Pauli strings with multiplication (disregarding factors) is group isomorphic to the vector space  $\{0, 1\}^{2n}$  with bitwise addition (i.e., exclusive or; ‘xor’). Consequently, many efficient algorithms for linear-algebra problems carry over to sets of Pauli strings. In particular, if  $G = \{g_1, \dots, g_k\}$  are length- $2n$  binary vectors ( $/$   $n$ -qubit Pauli strings) with  $k \leq n$ , then we can efficiently perform the following operations.

**RREF:** bring  $G$  into a reduced-row echelon form (RREF) using Gauss-Jordan elimination (both standard linear algebra notions) where each row (in check matrix form) has strictly more leading zeroes than the row above. The RREF is achievable by  $O(k^2)$  row additions ( $/$  multiplications modulo factor) and thus  $O(k^2 \cdot n)$  time (see [\[70\]](#) for a similar algorithm). In the RREF, the first 1 after the leading zeroes in a row is called a ‘pivot’.

**Independent Set** convert  $G$  to a (potentially smaller) independent set by performing the RREF procedure and discarding resulting all-zero rows.

**Membership:** determining whether a given a vector ( $/$  Pauli string)  $h$  has a decomposition in elements of  $G$ . This task can be reduced to independence by first getting  $G^{\text{RREF}}$  by applying RREF, followed by adding  $h$  to  $G$  and performing the Independent-Set procedure. The result has  $|G^{\text{RREF}}|$  rows if  $h \in \langle G \rangle$ , and  $|G^{\text{RREF}}| + 1$  rows otherwise.

**Intersection:** determine all Pauli strings which, modulo a factor, are contained in both  $G_A$  and  $G_B$ , where  $G_A, G_B$  are generator sets for  $n$ -qubit stabilizer subgroups. This can be achieved using the Zassenhaus algorithm [\[71\]](#) in time  $O(n^3)$ .

**Division remainder:** given a vector  $h$  ( $/$  Pauli string  $h$ ), determine  $h^{\text{rem}} := \min_{g \in \langle G \rangle} \{gh\}$  (minimum in the lexicographic ordering) where  $\oplus$  denotes bitwise XOR ( $/$  factor-discarding multiplication). We do so in the check matrix picture by bringing  $G$  into RREF, and then making the check vector of  $h$  contain as many zeroes as possible by adding rows from  $G$ :

- 1: **for** column index  $j = 1$  to  $2n$  **do**
- 2:    **if**  $h_j = 1$  and  $G$  has a row  $g_i$  with its pivot at position  $j$  **then**  $h := h \oplus g_i$

The resulting  $h$  is  $h^{\text{rem}}$ . This algorithm's runtime is dominated by the RREF step;  $O(n^3)$ .

Since each stabilizer  $\lambda P \in \text{PAULILIM}_n$  has factor  $\lambda = \pm 1$  (follows from  $(\lambda P)|\varphi\rangle = (\lambda P)^2|\varphi\rangle = \lambda^2 \mathbb{I}|\varphi\rangle = |\varphi\rangle$ , hence  $\lambda^2 = 1$ ), the stabilizer subgroups in  $\text{PAULILIM}_n$  are the same as in  $\text{PAULI}_n$ . As extension of the check matrix form to  $A \in \text{PAULILIM}_n$ , we write  $A = r \cdot e^{i\theta} \cdot P_n \otimes \dots \otimes P_1$ , for  $r \in \mathbb{R}_{>0}$  and  $\theta \in [0, 2\pi)$  and represent  $A$  by a length- $(2n+2)$  vector where the last entries store  $r$  and  $\theta$ , e.g.:

$$\begin{pmatrix} 3X & \otimes & X & \otimes & X \\ -\frac{1}{2}i\mathbb{I}_2 & \otimes & Z & \otimes & Y \end{pmatrix} \sim \left( \begin{array}{ccc|ccc|cc} 1 & 1 & 1 & 0 & 0 & 0 & 3 & 0 \\ 0 & 0 & 1 & 0 & 1 & 1 & \frac{1}{2} & \frac{3\pi}{2} \end{array} \right)$$

where we used  $3 = 3 \cdot e^{i \cdot 0}$  and  $-\frac{1}{2}i = \frac{1}{2} \cdot e^{3\pi i/2}$ . The ordering on real numbers induces a lexicographic ordering (from left to right) on such extended check vectors, for example  $(1, 1, |0, 0|3, \frac{1}{2}) < (1, 1|1, 0|2, 0)$ . Let us stress that the factor encoding  $(r, \theta)$  is less significant than the Pauli string encoding  $(x_n, \dots, x_1|z_n, \dots, z_1)$ . As a consequence, we can greedily determine the minimum of two Pauli operators.

Finally, we emphasize that the algorithms above rely on row addition, which is a commutative operation. Since conventional (i.e., factor-respecting) multiplication of Pauli operators is not commutative, the algorithms above are not straightforwardly applicable to (nonabelian subgroups of)  $\text{PAULILIM}_n$ . (For abelian subgroups of  $\text{PAULILIM}_n$ , such as stabilizer subgroups [5], the algorithms still do work.) Fortunately, since Pauli strings either commute or anti-commute, row addition may only yield an factors up to the  $\pm$  sign, not the resulting Pauli strings. This feature, combined with the stipulated order assigning least significance to the factor, enables us to invoke the algorithms above as subroutine, with postprocessing to obtain the correct factor. We will do so in [Sec. 4.2.1–D.1](#).

## B Proof that cluster states and coset states need exponentially-large QMDDs

In this appendix, we formally prove that cluster and coset states have exponential size in QMDDs ([Lemma 3](#) and [Corollary 9.1](#)). In both cases, we first fix notation and definitions, after which we prove the theorem using several lemmas.

**Cluster as QMDD.** Let  $G$  be an undirected graph with vertices  $V_G = \{v_1, \dots, v_n\}$  and edge set  $E_G \subseteq V_G \times V_G$ . For a subset of vertices  $S \subseteq V_G$ , the  $S$ -induced subgraph of  $G$  has vertices  $S$  and edge set  $(S \times S) \cap E$ . Given  $G$ , its graph state  $|G\rangle$  is expressed as

$$|G\rangle = \sum_{\vec{x} \in \{0,1\}^n} (-1)^{f_G(\vec{x})} |\vec{x}\rangle \quad (9)$$

where  $f_G(\vec{x})$  is the number of edges in the  $S$ -induced subgraph of  $G$ .

For a function  $f : \{0,1\}^n \rightarrow \mathbb{C}$  and bit string  $\vec{a} = a_1 \dots a_k \in \{0,1\}^k$ , we denote by  $f_{\vec{a}}$  the subfunction of  $f$  restricted to  $\vec{a}$ :

$$f_{\vec{a}}(x_{k+1}, \dots, x_n) := f(a_1, \dots, a_k, x_{k+1}, \dots, x_n) \quad (10)$$

We also say that  $f_{\vec{a}}$  is a subfunction of  $f$  of order  $|\vec{a}| = k$ .

We will also need the notions of boundary and strong matching.

**Definition 5** (Boundary). For a set  $S \subseteq V_G$  of vertices in  $G$ , the *boundary* of  $S$  is the set of vertices in  $S$  adjacent to a vertex outside of  $S$ .

**Definition 6** (Strong Matching). Let  $G = (V, E)$  be an undirected graph. A *strong matching* is a subset of edges  $M \subseteq E$  that do not share any vertices (i.e., it is a matching) and no two edges

of  $M$  are incident to the same edge of  $G$ , i.e., an edge in  $E \setminus M$ . Alternatively, a strong matching is a matching  $M$  s.t.  $G[V(M)] = M$ . We say that  $M$  is an  $(S, T)$ -strong matching for two sets of vertices  $S, T \subset V$  if  $M \subseteq S \times T$ . For a strong matching  $M$  and a vertex  $v \in V(M)$ , we let  $M(v)$  denote the unique vertex to which  $v$  is matched by  $M$ .

Using these definitions and notation, we prove [Lemma 3](#).

*Proof of Lemma 3.* To define a cluster state, let  $G = \text{lattice}(n, n)$  be the undirected graph of the  $n \times n$  lattice, with vertex set  $V = \{v_1, \dots, v_{n^2}\}$ . Let  $\sigma = v_1 v_2 \dots v_{n^2}$  be a variable order, and let  $S = \{v_1, v_2, \dots, v_{\frac{1}{2}n^2}\} \subset V$  be the first  $\frac{1}{2}n^2$  vertices in this order.

The proof proceeds broadly as follows. First, in [Lemma 7](#), we show that any  $(S, \bar{S})$ -strong matching  $M$  effects  $2^{|M|}$  different subfunctions of  $f_G$ . Second, [Lemma 8](#) shows that the lattice contains a large  $(S, \bar{S})$ -strong matching for any choice of  $S$ . Put together, this will prove the lower bound on the number of QMDD nodes as in [Lemma 3](#) by the fact that a QMDD for the cluster state  $G$  has a node per unique subfunction of the function  $f_G$ . Figure 11 illustrates this setup for the  $5 \times 5$  lattice.

**Lemma 7.** Let  $M$  be a non-empty  $(S, \bar{S})$ -strong matching for the vertex set  $S$  chosen above. If  $\sigma = v_1 v_2 \dots v_{n^2}$  is a variable order where all vertices in  $S$  appear before all vertices in  $\bar{S}$ , then  $f_G(x_1, \dots, x_{n^2})$  has  $2^{|M|}$  different subfunctions of order  $|S|$ .

*Proof.* Let  $S_M := S \cap V(M)$  and  $\bar{S}_M := \bar{S} \cap M$  be the sets of vertices that are involved in the strong matching. Write  $\chi(x_1, \dots, x_n)$  for the indicator function for vertices:  $\chi(x_1, \dots, x_n) := \{v_i \mid x_i = 1, i \in [n]\}$ . Choose two different subsets  $A, B \subseteq S_M$  and let  $\vec{a} = \chi^{-1}(A)$  and  $\vec{b} = \chi^{-1}(B)$  be the corresponding length- $|S|$  bit strings. These two strings induce the two subfunctions  $f_{G, \vec{a}}$  and  $f_{G, \vec{b}}$ . We will show that these subfunctions differ in at least one point.

First, if  $f_{G, \vec{a}}(0, \dots, 0) \neq f_{G, \vec{b}}(0, \dots, 0)$ , then we are done. Otherwise, take a vertex  $s \in A \oplus B$  and say w.l.o.g. that  $s \in A \setminus B$ . Let  $t = M(s)$  be its partner in the strong matching. Then we have,  $|E[A \cup \{t\}]| = |E[A]| + 1$  but  $|E[B \cup \{t\}]| = |E[B]|$ . Therefore we have

$$f_{G, \vec{a}}(0, \dots, 0, x_t = 0, 0, \dots, 0) \neq f_{G, \vec{a}}(0, \dots, 0, x_t = 1, 0, \dots, 0) \quad (11)$$

$$f_{G, \vec{b}}(0, \dots, 0, x_t = 0, 0, \dots, 0) = f_{G, \vec{b}}(0, \dots, 0, x_t = 1, 0, \dots, 0) \quad (12)$$

We see that each subset of  $S_M$  corresponds to a different subfunction of  $f_G$ . Since there are  $2^{|M|}$  subsets of  $M$ ,  $f_G$  has at least that many subfunctions.  $\square$

We now show that the  $n \times n$  lattice contains a large enough strong matching.

**Lemma 8.** Let  $S = \{v_1, \dots, v_{\frac{1}{2}n^2}\}$  be a set of  $\frac{1}{2}n^2$  vertices of the  $n \times n$  lattice, as above. Then the graph contains a  $(S, \bar{S})$ -strong matching of size at least  $\lfloor \frac{1}{12}n \rfloor$ .

*Proof.* Consider the boundary  $B_S$  of  $S$ . This set contains at least  $n/3$  vertices, by Theorem 11 in [43]. Each vertex of the boundary of  $S$  has degree at most 4. It follows that there is a set of  $\lfloor \frac{1}{4}|B_S| \rfloor$  vertices which share no neighbors. In particular, there is a set of  $\lfloor \frac{1}{4}|B_S| \rfloor \geq \lfloor \frac{1}{12}n \rfloor$  vertices in  $B_S$  which share no neighbors in  $\bar{S}$ .  $\square$

Put together, every choice of half the vertices in the lattice yields a set with a boundary of at least  $n/3$  nodes, which yields a strong matching of at least  $\lfloor \frac{1}{12}n \rfloor$  edges, which shows that  $f_G$  has at least  $2^{\lfloor \frac{1}{12}n \rfloor}$  subfunctions of order  $\frac{1}{2}n^2$ .  $\square$

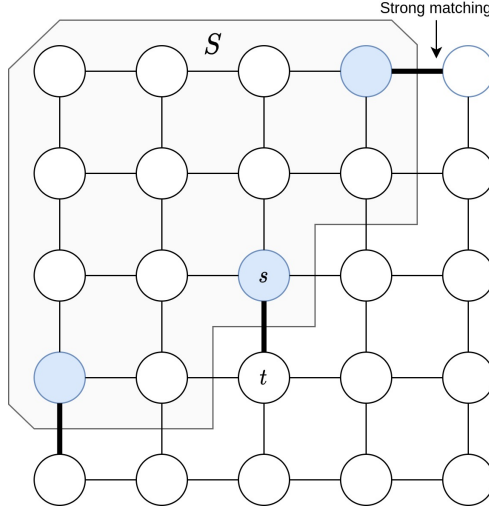


Figure 11: The  $5 \times 5$  lattice, partitioned in a vertex set  $S$  and its complement  $\bar{S}$ . A strong matching between  $S$  and  $\bar{S}$  is indicated by black edges.

**Coset States as QMDD.** We now show that QMDDs which represent so-called coset states are exponentially large in the worst case. On the other hand, in App. C, we will show that these states can be represented using only  $\mathcal{O}(n)$  nodes by  $\langle X \rangle$ -LIMDDs, showing that they are exponentially more succinct than QMDDs. Aaronson [59] defines coset states as uniform superpositions over the elements of a coset of the group  $\{0, 1\}^n$ , as follows.

**Definition 7** (Coset state). Let  $V \subseteq \{0, 1\}^n$  be a coset in the group of bit-strings of length  $n$  (in this group, addition corresponds to bit-wise XOR). Then the coset state  $|V\rangle$  is the uniform superposition over the elements of  $V$ , i.e.,

$$|V\rangle = \frac{1}{\sqrt{|V|}} \sum_{x \in V} |x\rangle \quad (13)$$

We will use the following result by Ďuriš et al. on binary decision diagrams (BDDs), which are QMDDs with codomain  $\{0, 1\}$ . This result concerns vector spaces, but of course, every vector space of  $\{0, 1\}^n$  is, in particular, a coset.

**Theorem 9** (Ďuriš et al.[72]). The characteristic function  $f_V : \{0, 1\}^n \rightarrow \{0, 1\}$  of a randomly chosen vector space  $V$  in  $\{0, 1\}^n$ , defined as  $f_V(x) = 1$  if  $x \in V$  and 0 otherwise, needs a BDD of size  $2^{\Omega(n)}/(2n)$  with high probability.

Our result follows by noting that if  $f$  is as above, or indeed if  $f$  is any function with codomain  $\{0, \lambda\}$  for any scalar  $\lambda$ , then the QMDD of the state  $|f\rangle = \sum_x f(x) |x\rangle$  has the same structure as the BDD of  $f$ . That is to say, in this case, the BDD and QMDD are graphs with the same number of nodes.

**Corollary 9.1.** For a random vector space  $V \subseteq \{0, 1\}^n$ , the coset state  $|V\rangle$  requires QMDDs of size  $2^{\Omega(n)}/(2n)$  with high probability.

*Proof.* We will show that the QMDD has the same number of nodes as a BDD. A BDD encodes a function  $f : \{0, 1\}^n \rightarrow \{0, 1\}$ . In this case, the BDD encodes  $f_V$ , the characteristic function of  $V$ . A BDD is a graph which contains one node for each subfunction of  $f$ . (In the literature, such a BDD is sometimes called a Full BDD, so that the term BDD is reserved for a variant where the nodes are in one-to-one correspondence with the subfunctions  $f$  which satisfy  $f_0 \neq f_1$ ).

Similarly, a QMDD representing a state  $|\varphi\rangle = \sum_x f(x) |x\rangle$  can be said to represent the function  $f : \{0, 1\}^n \rightarrow \mathbb{C}$ , and contains one node for each subfunction of  $f$  modulo scalars. We will show that,

two distinct subfunctions of  $f_V$  are never equal up to a scalar. To this end, let  $f_{V,a}, f_{V,b}$  be distinct subfunctions of  $f_V$  induced by partial assignments  $a, b \in \{0, 1\}^k$ . We will show that there is no  $\lambda \in \mathbb{C}^*$  such that  $f_{V,a} = \lambda f_{V,b}$ . Since the two subfunctions are not pointwise equal, say that the two subfunctions differ in the point  $x \in \{0, 1\}^{n-k}$ , i.e.,  $f_{V,a}(x) \neq f_{V,b}(x)$ . Say without loss of generality that  $f_{V,a}(x) = 0$  and  $f_{V,b}(x) = 1$ . Then, since  $\lambda \neq 0$ , we have  $\lambda = \lambda f_{S,b}(x) \neq f_{V,a}(x) = 0$ , so  $f_{V,a} \neq \lambda f_{V,b}$ .

Because distinct subfunctions of  $f_V$  are not equal up to a scalar, the QMDD of  $|V\rangle$  contains a node for every subfunction of  $f_V$ . We conclude that, since by [Th. 9](#) with high probability the BDD representing  $f_V$  has exponentially many nodes, so does the QMDD representing  $|V\rangle$ .  $\square$

## C How to write graph states, coset states and stabilizer states as Tower-LIMDDs

In this appendix, we prove that the families of  $\langle Z \rangle$ -,  $\langle X \rangle$ -, and Pauli-Tower-LIMDDs correspond to graph states, coset states (see [Definition 7](#) above), and stabilizer states, respectively, in [Th. 10](#), [Th. 11](#) and [Th. 14](#) below. [Definition 4](#) for reduced PAULI-LIMDDs is also valid when using  $G = \langle X \rangle$  instead of  $G = \text{PAULI}$ . Note that the proofs do not rely on the specialized definition of reduced LIMDDs, but only on [Definition 2](#) which allows parameterization of the LIM  $G$ .

A Tower-LIMDD representing an  $n$ -qubit state is a LIMDD which has  $n$  nodes, not counting the leaf.

**Theorem 10** (Graph states are  $\langle Z \rangle$ -Tower-LIMDDs). Let  $n \geq 1$ . Denote by  $\mathcal{G}_n$  the set of  $n$ -qubit graph states and write  $\mathcal{Z}_n$  for the set of  $n$ -qubit quantum states which are represented by Tower-LIMDDs which low-edge-labels  $\mathbb{I}$  and high-edge-labels  $\lambda \otimes_j P_j$  with  $P_j \in \{\mathbb{I}_2, Z\}$  and  $\lambda = 1$ . Then  $\mathcal{G}_n = \mathcal{Z}_n$ .

*Proof.* We establish  $\mathcal{G}_n \subseteq \mathcal{Z}_n$  by providing a procedure to convert any graph state in  $\mathcal{G}_n$  to a reduced Tower-LIMDD in  $\mathcal{Z}_n$ . See [Fig. 12](#) for an example of a 4-qubit graph state. We describe the procedure by induction on the number  $n$  of qubits in the graph state.

**Base case:**  $n = 1$ . We note that there is only one single-qubit graph state by definition (see [Eq. 9](#)), which is  $|+\rangle := (|0\rangle + |1\rangle)/\sqrt{2}$  and can be represented as LIMDD by a single node (in addition to the leaf node): see [Fig. 12\(a\)](#).

**Induction case.** We consider an  $(n+1)$ -qubit graph state  $|G\rangle$  corresponding to the graph  $G$ . We isolate the  $(n+1)$ -th qubit by decomposing the full state definition from [Eq. 9](#):

$$|G\rangle = \frac{1}{\sqrt{2}} \left( |0\rangle \otimes |G_{1..n}\rangle + |1\rangle \otimes \underbrace{\left[ \bigotimes_{(n+1,j) \in E} Z_j \right]}_{\text{Isomorphism B}} |G_{1..n}\rangle \right) \quad (14)$$

where  $E$  is the edge set of  $G$  and  $G_{1..n}$  is the induced subgraph of  $G$  on vertices 1 to  $n$ . Thus,  $|G_{1..n}\rangle$  is an  $n$ -qubit graph state on qubits 1 to  $n$ . Since  $|G_{1..n}\rangle$  is a graph state on  $n$  qubits, by the induction hypothesis, we have a procedure to convert it to a Tower-LIMDD  $\in \mathcal{Z}_n$ . Now we construct a Tower-LIMDD for  $|G\rangle$  as follows. The root node has two outgoing edges, both going to the node representing  $|G_{1..n}\rangle$ . The node's low edge has label  $\mathbb{I}$ , and the node's high edge has label  $B$ , as follows,

$$B = \bigotimes_{(n+1,j) \in E} Z_j \quad (15)$$

Thus the root node represents the state  $|0\rangle |G_{1..n}\rangle + |1\rangle B |G_{1..n}\rangle$ , satisfying [Eq. 14](#).

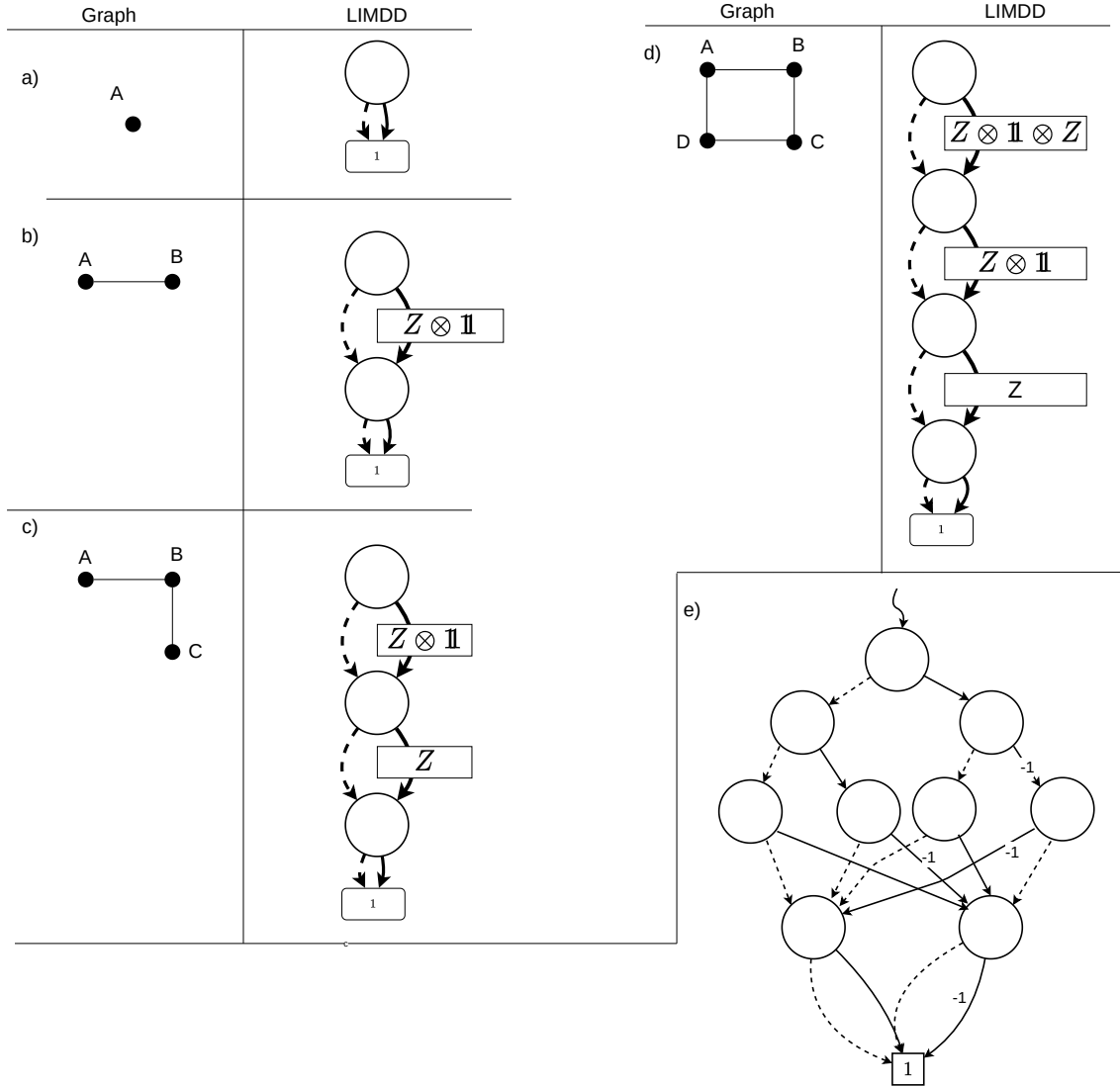


Figure 12: Construction of the Tower-LIMDD for the 4-qubit cluster state, by iterating over the vertices in the graph, as described in the proof of Th. 10. (a) First, we consider the single-qubit graph state, which corresponds to a the subgraph containing only vertex  $A$ . (b) Then, we add vertex  $B$ , which is connected to  $A$  by an edge. The resulting LIMDD is constructed from the LIMDD from (a) by adding a new root node. In the figure, the isomorphism is  $Z_B \otimes \mathbb{1}_A$ , since vertex  $C$  is connected to vertex  $B$  (yielding the  $Z$  operator) but not to  $A$  (yielding the identity operator  $\mathbb{1}$ ). (c) This process is repeated for a third vertex  $C$  until we reach the LIMDD of the full 4-qubit cluster state (d). For comparison, (e) depicts a regular QMDD for the same graph state, which has width 4 instead of 1 for the LIMDD.

To prove  $\mathcal{Z}_n \subseteq \mathcal{G}_n$ , we show how to construct the graph corresponding to a given  $\langle Z \rangle$ -Tower LIMDD. Briefly, we simply run the algorithm outlined above in reverse, constructing the graph one node at a time. Here we assume without loss of generality that the low edge of every node is labeled  $\mathbb{I}$ .

**Base case.** The LIMDD node above the Leaf node, representing the state  $|+\rangle$ , always represents the singleton graph, containing one node.

**Induction case.** Suppose that the LIMDD node  $k+1$  levels above the Leaf has a low edge labeled  $\mathbb{I}$ , and a high edge labeled  $P_k \otimes \cdots \otimes P_1$ , with  $P_j = Z^{a_j}$  for  $j = 1 \dots k$ . Here by  $Z^{a_j}$  we mean  $Z^0 = \mathbb{I}$  and  $Z^1 = Z$ . Then we add a node labeled  $k+1$  to the graph, and connect it to those nodes  $j$  with  $a_j = 1$ , for  $j = 1 \dots k$ . The state represented by this node is of the form given in Eq. 14, so it represents a graph state.

A simple counting argument based on the above construction shows that  $|\mathcal{Z}_n| = |\mathcal{G}_n| = 2^{\binom{n}{2}}$ , so the conversion is indeed a bijection. Namely, there are  $2^{\binom{n}{2}}$  graph, since there are  $\binom{n}{2}$  edges to choose, and there are  $2^{\binom{n}{2}}$  Tower  $\langle Z \rangle$ -LIMDDs, because the total number of single-qubit operators of the LIMs on the high edges  $\binom{n}{2}$ , each of which can be chosen to be either  $\mathbb{I}$  or  $Z$ , independently.  $\square$

Recall Definition 7, that a coset state is a uniform superposition over elements of a coset  $C \subseteq \{0,1\}^n$ . Aaronson showed that for some coset states, any multilinear formula representing that state requires size  $n^{\Omega(\log n)}$ . We now prove that coset states are represented by  $\langle X \rangle$ -Tower-LIMDDs.

**Theorem 11** (coset states are  $\langle X \rangle$ -Tower-LIMDDs). Let  $n \geq 1$ . Denote by  $\mathcal{V}_n$  the set of  $n$ -qubit coset states and write  $\mathcal{X}_n$  for the set of  $n$ -qubit quantum states which are represented by Tower-LIMDDs with low edge labels  $\mathbb{I}$  and high edge labels  $\lambda \otimes_j P_j$  with  $P_j \in \{\mathbb{I}, X\}$  and  $\lambda \in \{0,1\}$ . Then  $\mathcal{V}_n = \mathcal{X}_n$ .

*Proof.* We first prove  $\mathcal{V}_n \subseteq \mathcal{X}_n$  by providing a procedure for constructing a Tower-LIMDD for a coset state. We prove the statement for the case when  $C$  is a group rather than a coset; the result will then follow by noting that, by placing the label  $X^{a_n} \otimes \cdots \otimes X^{a_1}$  on the root edge, we obtain the coset state  $|C + a\rangle$ . The procedure is recursive on the number of qubits.

**Base case:**  $n = 1$ . In this case, there are two coset states:  $|0\rangle$  and  $(|0\rangle + |1\rangle)/\sqrt{2}$ , which are represented by a single node which has a low and high edge pointing to the leaf node with low/high edge labels  $1/0$  and  $1/1$ , respectively.

**Induction case.** Now consider an  $(n+1)$ -qubit coset state  $|S\rangle$  for a group  $S \subseteq \{0,1\}^{n+1}$  for some  $n \geq 1$  and assume we have a procedure to convert any  $n$ -qubit coset state into a Tower-LIMDD in  $\mathcal{X}_n$ . We consider two cases, depending on whether the first bit of each element of  $S$  is zero:

- (a) The first bit of each element of  $S$  is 0. Thus, we can write  $S = \{0x \mid x \in S_0\}$  for some set  $S_0 \subseteq \{0,1\}^n$ . Then  $0a, 0b \in S \implies 0a \oplus 0b \in S$  implies  $a, b \in S_0 \implies a \oplus b \in S_0$  and thus  $S_0$  is an length- $n$  bit string vector space. Thus by assumption, we have a procedure to convert it to a Tower-LIMDD in  $\mathcal{X}_n$ . Convert it into a Tower-LIMDD in  $\mathcal{X}_{n+1}$  for  $|S\rangle$  by adding a fresh node on top with low edge label  $\mathbb{I}_2^{\otimes n}$  and high edge label 0, both pointing to the the root  $S$ .
- (b) There is some length- $n$  bit string  $u$  such that  $1u \in S$ . Write  $S$  as the union of the sets  $\{0x \mid x \in S_0\}$  and  $\{1x \mid x \in S_1\}$  for sets  $S_0, S_1 \subseteq \{0,1\}^n$ . Since  $S$  is closed under element-wise XOR, we have  $1u \oplus 1x = 0(u \oplus x) \in S$  for each  $x \in S_1$  and therefore  $u \oplus x \in S_0$  for each  $x \in S_1$ . This implies that  $S_1 = \{u \oplus x \mid x \in S_0\}$  and thus  $S$  is the union of  $\{0x \mid x \in S_0\}$  and  $\{1u \oplus 0x \mid x \in S_0\}$ . By similar reasoning as in case (a), we can show that  $S_0$  is a vector space on length- $n$  bit strings.

We build a Tower-LIMDD for  $|S\rangle$  as follows. By the induction hypothesis, there is a Tower-LIMDD with root node  $v$  which represents  $|v\rangle = |S_0\rangle$ . We construct a new node whose two outgoing edges both go to this node  $v$ . Its low edge has label  $\mathbb{I}_2^{\otimes n}$  and its high edge has label  $P = P_n \otimes \cdots \otimes P_1$  where  $P_j = X$  if  $u_j = 1$  and  $P_j = \mathbb{I}$  if  $u_j = 0$ .

We now show  $\mathcal{V}_n \subseteq \mathcal{X}_n$ , also by induction.

**Base case:**  $n = 1$ . There are only two Tower-LIMDDs on 1 qubit satisfying the description above, namely

- (1) A node whose two edges point to the leaf. Its low edge has label 1, and its high edge has label 0. This node represents the coset state  $|0\rangle$ , corresponding to the vector space  $V = \{0\} \subseteq \{0, 1\}^1$ .
- (2) A node whose two edges point to the leaf. Its low edge has label 1 and its high edge also has label 1. This node represents the coset state  $|0\rangle + |1\rangle$ , corresponding to the vector space  $V = \{0, 1\}$ .

**Induction case.** Let  $v$  be the root node of an  $n+1$ -qubit Tower  $\langle X \rangle$ -LIMDD as described above. We distinguish two cases, depending on whether  $v$ 's high edge has label 0 or not.

- (a) The high edge has label 0. Then  $|v\rangle = |0\rangle |v_0\rangle$  for a node  $v_0$ , which represents a coset state  $|v_0\rangle$  corresponding to a coset  $V_0 \subseteq \{0, 1\}^n$ , by the induction hypothesis. Then  $v$  corresponds to the coset  $\{0x \mid x \in V_0\}$ .
- (b) the high edge has label  $P = P_n \otimes \dots \otimes P_1$  with  $P_j \in \{\mathbb{I}_2, X\}$ . Then  $|v\rangle = |0\rangle |v_0\rangle + |1\rangle \otimes P |v_0\rangle$ . By the observations above, this is a coset state, corresponding to the vector space  $V = \{0x \mid x \in V_0\} \cup \{1(ux) \mid x \in V_0\}$  where  $u \in \{0, 1\}^n$  is a string whose bits are  $u_j = 1$  if  $P_j = X$  and  $u_j = 0$  if  $P_j = \mathbb{I}_2$ , and  $V_0$  is the vector space corresponding to the coset state  $|v_0\rangle$ .

□

Lastly, we prove the stabilizer-state case. Specifically, we now define Stabilizer LIMDDs, and then we show that they represent exactly the set of stabilizer states. For this, we first need [Lemma 12](#) and [Lemma 13](#), which state that, if one applies a Clifford gate to a Stabilizer LIMDD, the resulting state is another Stabilizer LIMDD. First, [Lemma 12](#) treats the special case of applying a gate to the top qubit; then [Lemma 13](#) treats the general case of applying a gate to an arbitrary qubit.

**Definition 8** (Stabilizer LIMDD). A *Stabilizer-LIMDD* is a Tower Pauli-LIMDD (i.e., each node has exactly one unique child), in which each node is semi-reduced, and each node's high edge's label is of the form  $\lambda P$  with  $\lambda \in \{0, \pm 1, \pm i\}$  and  $P$  is a Pauli string.

**Lemma 12.** Let  $|\varphi\rangle$  be an  $n$ -qubit stabilizer state which is represented by a Stabilizer LIMDD. Let  $U$  be either a Hadamard gate or  $S$  gate on the top qubit ( $n$ -th qubit), or a downward CNOT with the top qubit as control. Then  $U|\varphi\rangle$  is still represented by a semi-reduced Pauli-Tower-LIMDD.

*Proof.* The proof is on the number  $n$  of qubits.

**Base case:**  $n = 1$ . For  $n = 1$ , there are six single-qubit stabilizer states  $|0\rangle$ ,  $|1\rangle$  and  $(|0\rangle + \alpha |1\rangle)/\sqrt{2}$  for  $\alpha \in \{\pm 1, \pm i\}$ . There are precisely represented by Pauli-Tower-LIMDDs with high edge label factor  $\in \{0, \pm 1, \pm i\}$  as follows:

- for  $|0\rangle$ :  $\textcircled{1} \times \cdot^1 \textcircled{0} \rightarrow \textcircled{1}$
- for  $|1\rangle$ :  $A \cdot \textcircled{1} \times \cdot^1 \textcircled{0} \rightarrow \textcircled{1}$  where  $A \propto X$  or  $A \propto Y$
- for  $(|0\rangle + \alpha |1\rangle)/\sqrt{2}$ :  $\textcircled{1} \times \cdot^1 \textcircled{0} \rightarrow \textcircled{\alpha}$

Since the  $H$  and  $S$  gate permute these six stabilizer states,  $U|\varphi\rangle$  is represented by a Stabilizer LIMDD if  $|\varphi\rangle$  is.

**Induction case.** For  $n > 1$ , we first consider  $U = S$  and  $U = \text{CNOT}$ . Let  $R$  be the label of the root edge. If  $U = S$ , then the high edge of the top node is multiplied with  $i$ , while a

downward CNOT (target qubit with index  $k$ ) updates the high edge label  $A \mapsto X_k A$ . Next, the root edge label is updated to  $URU^\dagger$ , which is still a Pauli string, since  $U$  is a Clifford gate. Since the high labels of the top qubit in the resulting diagram is still a Pauli string, and the high edge's weights are still  $\in \{0, \pm 1, \pm i\}$ , we conclude that both these gates yield a Stabilizer LIMDD. Finally, for the Hadamard, we decompose  $|\varphi\rangle = |0\rangle \otimes |\psi\rangle + \alpha |1\rangle \otimes P|\psi\rangle$  for some  $(n-1)$ -qubit stabilizer state  $|\psi\rangle$ ,  $\alpha \in \{0, \pm 1, \pm i\}$  and  $P$  is an  $(n-1)$ -qubit Pauli string. Now we note that  $H|\varphi\rangle \propto |0\rangle \otimes |\psi_0\rangle + |1\rangle \otimes |\psi_1\rangle$  where  $|\psi_x\rangle := (\mathbb{I} + (-1)^x \alpha P)|\psi\rangle$  with  $x \in \{0, 1\}$ . Now we consider two cases, depending on whether  $P$  commutes with all stabilizers of  $|\psi\rangle$ :

- (a) There exist a stabilizer  $g$  of  $|\psi\rangle$  which anticommutes with  $P$ . We note two things. First,  $\langle\psi|P|\psi\rangle = \langle\psi|Pg|\psi\rangle = \langle\psi|g \cdot (-P)|\psi\rangle = -\langle\psi|P|\psi\rangle$ , hence  $\langle\psi|P|\psi\rangle = 0$ . It follows from Lemma 15 of [73] that  $|\psi_x\rangle$  is a stabilizer state, so by the induction hypothesis it can be written as a Stabilizer LIMDD. Let  $v$  be the root node of this LIMDD. Next, we note that  $g|\psi_0\rangle = g(\mathbb{I}_2 + \alpha P)|\psi\rangle = (\mathbb{I}_2 - \alpha P)g|\psi\rangle = |\psi_1\rangle$ . Hence,  $\bigcirc \xrightarrow{\mathbb{I}} \bigcirc \xrightarrow{g} \bigcirc$  is the root node of a Stabilizer LIMDD for  $H|\varphi\rangle$ .
- (b) All stabilizers of  $|\psi\rangle$  commute with  $P$ . Then  $(-1)^y P$  is a stabilizer of  $|\psi\rangle$  for either  $y = 0$  or  $y = 1$ . Hence,  $|\psi_x\rangle = (\mathbb{I} + (-1)^x \alpha P)|\psi\rangle = (1 + (-1)^{x+y} \alpha)|\psi\rangle$ . Therefore,  $|\varphi\rangle = |a\rangle \otimes |\psi\rangle$  where  $|a\rangle := (1 + (-1)^y \alpha)|0\rangle + (1 + (-1)^{y+1} \alpha)|1\rangle$ . It is not hard to see that  $|a\rangle$  is a stabilizer state for all choices of  $\alpha \in \{0, \pm 1, \pm i\}$ . By the induction hypothesis, both  $|a\rangle$  and  $|\psi\rangle$  can be represented as Stabilizer LIMDDs. We construct a Stabilizer LIMDD for  $H|\varphi\rangle$  by replacing the leaf of the LIMDD of  $|a\rangle$  by the root node of the LIMDD of  $|\psi\rangle$ , and propagating the root edge label of  $|\psi\rangle$  upwards. Specifically, if the root edge of  $|a\rangle$  is  $\bigcirc \xrightarrow{A} v$  with  $v = \bigcirc \xrightarrow{1} \bigcirc \xrightarrow{\beta} \bigcirc$ , and if the root edge of  $|\psi\rangle$  is  $\bigcirc \xrightarrow{B} w$ , then a Stabilizer LIMDD for  $H|\varphi\rangle$  has root node  $\bigcirc \xrightarrow{\mathbb{I}} \bigcirc \xrightarrow{w} \bigcirc \xrightarrow{\beta \mathbb{I}} w$  and has root edge label  $A \otimes B$ .

□

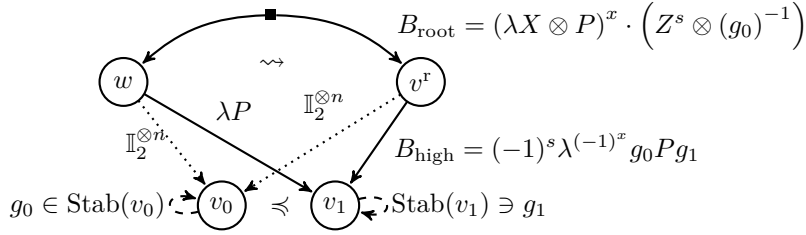
**Lemma 13.** Let  $|\varphi\rangle$  be an  $n$ -qubit state represented by a Stabilizer LIMDD, and let  $U$  be either a Hadamard gate, an  $S$  gate or a CNOT gate. Then  $U|\varphi\rangle$  is a state which is also represented by a Stabilizer LIMDD.

*Proof.* The proof is by induction on  $n$ . The case  $n = 1$  is covered by Lemma 12. Suppose that the induction hypothesis holds, and let  $|\varphi\rangle$  be an  $n+1$ -qubit state represented by a Stabilizer LIMDD. First, we note that a CNOT gate  $CX_c^t$  can be written as  $CX_c^t = (H \otimes H)CX_c^t(H \otimes H)$ , so without loss of generality we may assume that  $c > t$ . We treat two cases, depending on whether  $U$  affects the top qubit or not.

- (a)  $U$  affects the top qubit. Then  $U|\varphi\rangle$  is represented by a Stabilizer LIMDD, according to Lemma 12.
- (b)  $U$  does not affect the top qubit. Suppose  $|\varphi\rangle = |0\rangle \otimes |\varphi_0\rangle + |1\rangle \otimes \alpha P|\varphi_0\rangle$  (with  $P$  a Pauli string and  $\alpha \in \{0, \pm 1, \pm i\}$ ). Then  $U|\varphi\rangle = |0\rangle \otimes U|\varphi_0\rangle + |1\rangle \otimes (\alpha U P U^\dagger)U|\varphi_0\rangle$ . Since  $U$  is either a Hadamard,  $S$  gate or CNOT, and  $|\varphi_0\rangle$  is an  $n$ -qubit state, the induction hypothesis states that the state  $U|\varphi_0\rangle$  is represented by a Stabilizer LIMDD. Let  $\bigcirc \xrightarrow{A} v$  be the root edge of this Stabilizer LIMDD, representing  $U|\varphi_0\rangle$ . Then  $U|\varphi\rangle$  is represented by the root edge  $\bigcirc \xrightarrow{\mathbb{I} \otimes A} w$ , where  $w$  is the node  $\bigcirc \xrightarrow{\mathbb{I}} \bigcirc \xrightarrow{\alpha A^{-1} U P U^\dagger A} v$ . The label  $\alpha A^{-1} U P U^\dagger A$  is a Pauli string, and may therefore be used as the label on the high edge of  $w$ .

□

Finally, we show that stabilizer states are precisely the Stabilizer LIMDDs defined in Definition 8.



Choose  $s, x \in \{0, 1\}$ ,  $g_0 \in \text{Stab}(v_0)$ ,  $g_1 \in \text{Stab}(v_1)$  s.t.  $B_{\text{high}}$  is minimal and  $x = 0$  if  $v_0 \neq v_1$ .

Figure 13: Illustration of finding a canonical high label for a semi-reduced node  $w$ , yielding a reduced node  $v^r$ . The chosen high label is the minimal element from the set of eligible high labels based on stabilizers  $g_0, g_1$  of  $v_0, v_1$  (drawn as self loops). The minimal element holds a factor  $\lambda^{(-1)^x}$  for some  $x \in \{0, 1\}$ . There are two cases: if  $v_0 \neq v_1$  or  $x = 0$ , then the factor is  $\lambda$  and the root edge should be adjusted with an  $\mathbb{I}_2$  or  $Z$  on the root qubit. The other case,  $x = 1$ , leads to an additional multiplication with an  $X$  on the root qubit.

**Theorem 14** (Stabilizer states are Stabilizer LIMDDs). Let  $n \geq 1$ . Each  $n$ -qubit stabilizer state is represented by Stabilizer LIMDD with  $n$  nodes. Conversely, every Stabilizer LIMDD represents a stabilizer state.

*Proof.* We first prove that each stabilizer state is represented by a Pauli-Tower-LIMDD. We recall that each stabilizer state can be obtained as the output state of a Clifford circuit on input state  $|0\rangle^{\otimes n}$ . Each Clifford circuit can be decomposed into solely the gates  $H, S$  and CNOT. The state  $|0\rangle^{\otimes n}$  is represented by a Stabilizer LIMDD. According to Lemma 13, applying an  $H, S$  or CNOT gate to a Stabilizer LIMDD results a state represented by another Stabilizer LIMDD. One can therefore apply the gates of a Clifford circuit to the initial state  $|0\rangle$ , and obtain a Stabilizer LIMDD for every intermediate state, including the output state. Therefore, every stabilizer state is represented by a Stabilizer LIMDD.

For the converse direction, the proof is by induction on  $n$ . We only need to note that a state represented by a Stabilizer LIMDD can be written as  $|\varphi\rangle = |0\rangle \otimes |\varphi_0\rangle + |1\rangle \otimes \alpha P |\varphi_0\rangle = C(P)(|0\rangle + \alpha |1\rangle) \otimes |\varphi_0\rangle$  where  $C(P) := |0\rangle\langle 0| \otimes \mathbb{I} + |1\rangle\langle 1| \otimes P$  is the controlled- $(P)$  gate. Using the relations  $Z = HXH$ ,  $Y = SXS^\dagger$  and  $S = Z^2$ , we can decompose  $C(P)$  as CNOT,  $H$  and  $S$ , hence  $C(P)$  is a Clifford gate. Since both  $|0\rangle + \alpha |1\rangle$  and  $|\varphi_0\rangle$  can be written as Pauli-Tower-LIMDDs, they are stabilizer states by the induction hypothesis. Therefore, the state  $|\psi\rangle = (|0\rangle + \alpha |1\rangle) \otimes |\varphi_0\rangle$  is also a stabilizer state. Thus, the state  $|\varphi\rangle = C(P) |\psi\rangle$  is obtained by applying the Clifford gate  $C(P)$  to the stabilizer state  $|\psi\rangle$ . Therefore,  $|\varphi\rangle$  is a stabilizer state.  $\square$

## D Efficient algorithms for choosing a canonical high label

Here, we present our efficient algorithm which, on input LIMDD node  $\textcircled{v_0} \xrightarrow{\mathbb{I}_2^{\otimes n}} \textcircled{w} \xrightarrow{\lambda P} \textcircled{v_1}$ , returns a canonical choice for the high label  $B_{\text{high}}$  (algorithm GETLABELS, in Alg. 7). By *canonical*, we mean that it returns the same high label for any two nodes in the same isomorphism equivalence class, i.e., for any two nodes  $v, w$  for which  $|v\rangle \simeq_{\text{Pauli}} |w\rangle$ .

We first characterize all eligible labels  $B_{\text{high}}$  in terms of the stabilizer subgroups of the children nodes  $v_0, v_1$ , denoted as  $\text{Stab}(v_0)$  and  $\text{Stab}(v_1)$  (see Sec. 2 for the definition of stabilizer subgroup). Then, we show that GETLABELS correctly finds the lexicographically minimal eligible label (and corresponding root label), and runs in time  $O(n^3)$  where  $n$  is the number of qubits.

Fig. 13 illustrates this process. In the figure, the left node  $w$  summarizes the status of the MAKEEDGE algorithm on line 10, when this algorithm has enough information to construct the semi-reduced node  $\textcircled{v_0} \xrightarrow{\mathbb{I}_2^{\otimes n}} \textcircled{w} \xrightarrow{\lambda P} \textcircled{v_1}$ , shown on the left. The node  $v^r$ , on the right, is the canonical node, and is obtained by replacing  $w$ 's high edge's label by the canonical label  $B_{\text{high}}$ . This label

is chosen by minimizing the expression  $B_{\text{high}} = (-1)^s \lambda^{(-1)^x} g_0 P g_1$ , where the minimization is over  $s, x \in \{0, 1\}$ ,  $g_0 \in \text{Stab}(|v_0\rangle)$ ,  $g_1 \in \text{Stab}(|v_1\rangle)$ , subject to the constraint that  $x = 0$  if  $v_0 \neq v_1$ . We have  $|w\rangle \simeq_{\text{Pauli}} |v^r\rangle$  by construction as intended, namely, they are related via  $|w\rangle = B_{\text{root}} |v^r\rangle$ . [Th. 15](#) shows that this way to choose the high label indeed captures all eligible high labels, i.e., a node  $\textcircled{v_0} \xrightarrow{\mathbb{I}_2^{\otimes n}} \textcircled{v} \xrightarrow{B_{\text{high}}} \textcircled{v_1}$  is isomorphic to  $|w\rangle$  if and only if  $B_{\text{high}}$  is of this form.

**Theorem 15** (Eligible high-edge labels). Let  $\textcircled{v_0} \xrightarrow{\mathbb{I}_2^{\otimes n}} \textcircled{w} \xrightarrow{\lambda P} \textcircled{v_1}$  be a semi-reduced  $n$ -qubit node in a Pauli-LIMDD, where  $v_0, v_1$  are reduced,  $P$  is a Pauli string and  $\lambda \neq 0$ . For all nodes  $v = \textcircled{v_0} \xrightarrow{\mathbb{I}_2^{\otimes n}} \textcircled{v} \xrightarrow{B_{\text{high}}} \textcircled{v_1}$ , it holds that  $|w\rangle \simeq |v\rangle$  if and only if

$$B_{\text{high}} = (-1)^s \cdot \lambda^{(-1)^x} g_0 P g_1 \quad (16)$$

for some  $g_0 \in \text{Stab}(v_0)$ ,  $g_1 \in \text{Stab}(v_1)$ ,  $s, x \in \{0, 1\}$  and  $x = 0$  if  $v_0 \neq v_1$ . An isomorphism mapping  $|w\rangle$  to  $|v\rangle$  is

$$B_{\text{root}} = (X \otimes \lambda P)^x \cdot (Z^s \otimes (g_0)^{-1}). \quad (17)$$

*Proof.* It is straightforward to verify that the isomorphism  $B_{\text{root}}$  in eq. (17) indeed maps  $|w\rangle$  to  $|v\rangle$  (as  $x = 1$  implies  $v_0 = v_1$ ), which shows that  $|w\rangle \simeq |v\rangle$ . For the converse direction, suppose there exists an  $n$ -qubit Pauli LIM  $C$  such that  $C|w\rangle = |v\rangle$ , i.e.,

$$C(|0\rangle \otimes |v_0\rangle + \lambda |1\rangle \otimes P|v_1\rangle) = |0\rangle \otimes |v_0\rangle + |1\rangle \otimes B_{\text{high}} |v_1\rangle. \quad (18)$$

We show that if  $B_{\text{high}}$  satisfies eq. (18), then it has a decomposition as in eq. (16). We write  $C = C_{\text{top}} \otimes C_{\text{rest}}$  where  $C_{\text{top}}$  is a single-qubit Pauli operator and  $C_{\text{rest}}$  is an  $(n-1)$ -qubit Pauli LIM (or a complex number  $\neq 0$  if  $n = 1$ ). We treat the two cases  $C_{\text{top}} \in \{\mathbb{I}_2, Z\}$  and  $C_{\text{top}} \in \{X, Y\}$  separately:

- (a) **Case**  $C_{\text{top}} \in \{\mathbb{I}_2, Z\}$ . Then  $C_{\text{top}} = \begin{bmatrix} 1 & 0 \\ 0 & (-1)^y \end{bmatrix}$  for  $y \in \{0, 1\}$ . In this case, [Eq. 18](#) implies  $C_{\text{top}} |0\rangle C_{\text{rest}} |v_0\rangle = |0\rangle |v_0\rangle$ , so  $C_{\text{rest}} |v_0\rangle = |v_0\rangle$ , in other words  $C_{\text{rest}} \in \text{Stab}(|v_0\rangle)$ . Moreover, [Eq. 18](#) implies  $(-1)^y \lambda C_{\text{rest}} P |v_1\rangle = B_{\text{high}} |v_1\rangle$ , or, equivalently,  $(-1)^{-y} \lambda^{-1} P^{-1} C_{\text{rest}}^{-1} B_{\text{high}} \in \text{Stab}(v_1)$ . Hence, by choosing  $s = y$  and  $x = 0$ , we compute

$$(-1)^y \lambda^{(-1)^0} \underbrace{C_{\text{rest}}}_{\in \text{Stab}(v_0)} \underbrace{P (-1)^{-y} \lambda^{-1} P^{-1} C_{\text{rest}}^{-1} B_{\text{high}}}_{\in \text{Stab}(v_1)} = \frac{(-1)^y \lambda^{(-1)^0}}{(-1)^y \lambda} B_{\text{high}} = B_{\text{high}}$$

- (b) **Case**  $C_{\text{top}} \in \{X, Y\}$ . Write  $C_{\text{top}} = \begin{bmatrix} 0 & z^{-1} \\ z & 0 \end{bmatrix}$  where  $z \in \{1, i\}$ . Now, eq. (18) implies

$$z C_{\text{rest}} |v_0\rangle = B_{\text{high}} |v_1\rangle \quad \text{and} \quad z^{-1} \lambda C_{\text{rest}} P |v_1\rangle = |v_0\rangle. \quad (19)$$

From [Eq. 19](#), we first note that  $|v_0\rangle$  and  $|v_1\rangle$  are isomorphic, so by [Corollary 6](#), and because the diagram has merged these two nodes, we have  $v_0 = v_1$ . Consequently, we find from [Eq. 19](#) that  $z^{-1} C_{\text{rest}}^{-1} B_{\text{high}} \in \text{Stab}(v_0)$  and  $z^{-1} \lambda C_{\text{rest}} P \in \text{Stab}(v_1)$ . Now choose  $x = 1$  and choose  $s$  such that  $(-1)^s \cdot z^{-2} C_{\text{rest}}^{-1} B_{\text{high}} C_{\text{rest}} = B_{\text{high}}$  (recall that Pauli LIMs either commute or anticommute, so  $B_{\text{high}} C_{\text{rest}} = \pm C_{\text{rest}} B_{\text{high}}$ ). This yields:

$$(-1)^s \lambda^{-1} \cdot \underbrace{z^{-1} C_{\text{rest}}^{-1} B_{\text{high}}}_{\in \text{Stab}(v_0)} \cdot \underbrace{P \cdot z^{-1} \lambda P C_{\text{rest}}}_{\in \text{Stab}(v_1)} = \lambda^{-1} \cdot \lambda \cdot (-1)^s z^{-2} \cdot (C_{\text{rest}}^{-1} B_{\text{high}} C_{\text{rest}}) = B_{\text{high}}$$

where we used the fact that  $P^2 = \mathbb{I}_2^{\otimes(n-1)}$  because  $P$  is a Pauli string.

□

**Corollary 15.1.** As a corollary of [Th. 15](#), we find that taking, as in [Fig. 13](#),

$$\text{HighLabel}(\textcircled{v_0} \xrightarrow{\mathbb{I}_2^{\otimes n}} \textcircled{v} \xrightarrow{\lambda P} \textcircled{v_1}) = \min_{i, s, x \in \{0, 1\}, g_i \in \text{Stab}(v_i)} \left( \left\{ (-1)^s \cdot \lambda^{(-1)^x} \cdot g_0 \cdot P \cdot g_1 \mid x \neq 1 \text{ if } v_0 \neq v_1 \right\} \right)$$

yields a proper implementation of **HighLabel** as required by [Definition 4](#), because it considers all possible  $B_{\text{high}}$  such that  $|v\rangle \simeq_{\text{PAULI}} |0\rangle |v_0\rangle + |1\rangle \otimes \text{HighLabel}(v) |v_1\rangle$ .

A naive implementation for GETLABELS would follow the possible decompositions of eligible LIMs (see Eq. 16) and attempt to make this LIM smaller by greedy multiplication, first with stabilizers of  $g_0 \in \text{Stab}(v_0)$ , and then with stabilizers  $g_1 \in \text{Stab}(v_1)$ . To see why this does not work, consider the following example: the high edge label is  $Z$  and the stabilizer subgroups are  $\text{Stab}(v_0) = \langle X \rangle$  and  $\text{Stab}(v_1) = \langle Y \rangle$ . Then the naive algorithm would terminate and return  $Z$  because  $X, Y > Z$ , which is incorrect since the high-edge label  $X \cdot Z \cdot Y = -i\mathbb{I}_2$  is smaller than  $Z$ .

---

**Algorithm 7** Algorithm for finding LIMs  $B_{\text{high}}$  and  $B_{\text{root}}$  required by MAKEEDGE. Its parameters represent a semi-reduced node  $\textcircled{v_0} \xrightarrow{\lambda P} \textcircled{v_1}$  and it returns LIMs  $B_{\text{high}}, B_{\text{root}}$  such that  $|v\rangle = B_{\text{root}} |w\rangle$  with  $\textcircled{v_0} \xrightarrow{B_{\text{high}}} \textcircled{v_1}$ . The LIM  $B_{\text{high}}$  is chosen canonically as the lexicographically smallest from the set characterized in Th. 15. It runs in  $O(n^3)$ -time (with  $n$  the number of qubits), provided GetStabilizerGenSet has been computed for children  $v_0, v_1$  (an amortized cost).

---

```

1: procedure GETLABELS(PAULILIM  $\lambda P$ , NODE  $v_0, v_1$  with  $\lambda \neq 0$  and  $v_0, v_1$  reduced)
   Output: canonical high label  $B_{\text{high}}$  and root label  $B_{\text{root}}$ 
2:    $G_0, G_1 := \text{GetStabilizerGenSet}(v_0), \text{GetStabilizerGenSet}(v_1)$ 
3:    $(g_0, g_1) := \text{ARGLEXMIN}(G_0, G_1, \lambda P)$ 
4:   if  $v_0 = v_1$  then
5:      $(x, s) := \arg \min_{(x,s) \in \{0,1\}^2} \{(-1)^s \lambda^{(-1)^x} g_0 P g_1\}$ 
6:   else
7:      $x := 0$ 
8:      $s := \arg \min_{s \in \{0,1\}} \{(-1)^s \lambda g_0 P g_1\}$ 
9:      $B_{\text{high}} := (-1)^s \cdot \lambda^{(-1)^x} \cdot g_0 \cdot P \cdot g_1$ 
10:     $B_{\text{root}} := (X \otimes \lambda P)^x \cdot (Z^s \otimes (g_0)^{-1})$ 
11:   return  $(B_{\text{high}}, B_{\text{root}})$ 

```

---

To overcome this, we consider the group closure of *both*  $\text{Stab}(v_0)$  and  $\text{Stab}(v_1)$ . See Alg. 7 for the  $O(n^3)$ -algorithm for GETLABELS, which proceeds in two steps. In the first step (Line 3), we use the subroutine ARGLEXMIN for finding the minimal Pauli LIM  $A$  such that  $A = \lambda P \cdot g_0 \cdot g_1$  for  $g_0 \in \text{Stab}(v_0), g_1 \in \text{Stab}(v_1)$ . We will explain and prove correctness of this subroutine below in Sec. D.2. In the second step (Lines 4-8), we follow Corollary 15.1 by also minimizing over  $x$  and  $s$ . Finally, the algorithm returns  $B_{\text{high}}$ , the minimum of all eligible edge labels according to Corollary 15.1, together with a root edge label  $B_{\text{root}}$  which ensures the represented quantum state remains the same.

Below, we will explain  $O(n^3)$ -time algorithms for finding generating sets for the stabilizer subgroup of a reduced node and for ARGLEXMIN. Since all other lines in Alg. 7 can be performed in linear time, its overall runtime is  $O(n^3)$ .

## D.1 Constructing the stabilizer subgroup of a LIMDD node

In this section, we give a recursive subroutine **GetStabilizerGenSet** to construct the stabilizer subgroup  $\text{Stab}(|v\rangle) = \{A \in \text{PAULILIM}_n \mid A|v\rangle = |v\rangle\}$  of an  $n$ -qubit LIMDD node  $v$  (see Sec. 2). This subroutine is used by the algorithm GETLABELS to select a canonical label for the high edge and root edge. If the stabilizer subgroup of  $v$ 's children have been computed already, **GetStabilizerGenSet**'s runtime is  $O(n^3)$ . **GetStabilizerGenSet** returns a generating set for the group  $\text{Stab}(|v\rangle)$ . Since these stabilizer subgroups are generally exponentially large in the number of qubits  $n$ , but they have at most  $n$  generators, storing only the generators instead of all elements may save an exponential amount of space. Because any generator set  $G$  of size  $|G| > n$  can be brought back to at most  $n$  generators in time  $\mathcal{O}(|G| \cdot n^2)$  (see Sec. 2), we will in the derivation below show how to obtain generator sets of size linear in  $n$  and leave the size reduction implicit. We will also use the notation  $A \cdot G$  and  $G \cdot A$  to denote the sets  $\{A \cdot g \mid g \in G\}$  and  $\{g \cdot A \mid g \in G\}$ , respectively, when  $A$  is a Pauli LIM.



- **Find the intersection of two stabilizer subgroups, represented as generating sets  $G_0$  and  $G_1$  (Alg. 10).** First, it is straightforward to show that the intersection of two stabilizer subgroups is again a stabilizer subgroup (it is never empty since  $\mathbb{I}$  is a stabilizer of all states). Alg. 10 will find a generating set  $G_U$  for the conjugated intersection of  $\langle UG_0U^\dagger \rangle \cap \langle UG_1U^\dagger \rangle$  for a suitably chosen  $U$ , followed by returning  $U^\dagger G_U U$  as a generating set for the target intersection  $\langle G_0 \rangle \cap \langle G_1 \rangle$ . As unitary  $U$ , we choose an  $n$ -qubit unitary  $U$  which maps  $G_0$  to the generating set

$$UG_0U^\dagger = \{Z_1, Z_2, \dots, Z_{|G_0|}\}$$

where  $Z_k$  denotes a  $Z$  gate on qubit with index  $k$ , i.e.,

$$Z_k := \mathbb{I} \otimes \mathbb{I} \otimes \dots \otimes \mathbb{I} \otimes \underbrace{Z}_{\text{position } k} \otimes \mathbb{I} \otimes \dots \otimes \mathbb{I}.$$

Such a unitary always exists and can be found in time  $O(n^3)$  using Algorithm 2 from [73]. It is not hard to see that the Pauli string of all LIMs in  $\langle UG_0U^\dagger \rangle$  is a  $Z$  or  $\mathbb{I}$ . Therefore, to find the intersection of this group with  $\langle UG_1U^\dagger \rangle$ , we only need to bring  $UG_1U^\dagger$  into RREF form (see Sec. 2), followed by discarding all generators in the RREF form whose pivot corresponds to an  $X$  or an  $Y$ , i.e. its pivot is a 1 in the  $X$ -block when representing a generator as a check vector (see Sec. 2). Both the resulting generator set (called  $H_1$  in Alg. 10) and  $UG_0U^\dagger$  are subsets of the group of Pauli LIMs with scalars  $\pm 1$  and Pauli strings with only  $\mathbb{I}$  and  $Z$ . These groups are finite and abelian. We use the Zassenhaus algorithm [71] to find a generating set  $H'$  for the intersection of  $\langle H_1 \rangle \cap \langle UG_0U^\dagger \rangle$  (in particular, the groups  $\langle H_1 \rangle$  and  $\langle UG_0U^\dagger \rangle$  are group isomorphic to Boolean vector spaces, where addition corresponds to XOR-ing. Hence we may think of  $H_1$  and  $UG_0U^\dagger$  as bases of linear subspaces. The Zassenhaus algorithm computes a basis for the intersection of the two linear subspaces.) The final step is to perform the inverse conjugation map and return  $U^\dagger H' U$ . All of the above steps can be performed in  $O(n^3)$  time; in particular, the operator  $U$  as found by Algorithm 2 from [73] consists of at most  $O(n^2)$  Cliffords, each of which can be applied to a check matrix in time  $O(n)$ , yielding  $O(n^3)$  time required for evaluating  $G \mapsto UGU^\dagger$ . Hence the overall runtime of Alg. 10 is  $O(n^3)$  also.

- **IntersectIsomorphismSets: Find the intersection of two isomorphism sets, represented as single isomorphism  $(\pi_0, \pi_1)$  with a generator set of a stabilizer subgroup  $(G_0, G_1)$ , see Lemma 16.** This is the *coset intersection problem* for the PAULILIM $_n$  group. Isomorphism sets are coset of stabilizer groups (see Lemma 16) and it is not hard to see that the intersection of two cosets, given as isomorphisms  $\pi_{0/1}$  and generator sets  $G_{0/1}$ , is either empty, or a coset of  $\langle G_0 \rangle \cap \langle G_1 \rangle$  (this intersection is computed using Alg. 10). Therefore, we only need to determine an isomorphism  $\pi \in \pi_0 \langle G_0 \rangle \cap \pi_1 \langle G_1 \rangle$ , or infer that no such isomorphism exists.

We solve this problem in  $O(n^3)$  time in two steps (see Alg. 9 for the full algorithm). First, we note that  $\pi_0 \langle G_0 \rangle \cap \pi_1 \langle G_1 \rangle = \pi_0 [\langle G_0 \rangle \cap (\pi_0^{-1} \pi_1) \langle G_1 \rangle]$ , so we only need to find an element of the coset  $S := \langle G_0 \rangle \cap (\pi_0^{-1} \pi_1) \langle G_1 \rangle$ . Now note that  $S$  is nonempty if and only if there exists  $g_0 \in \langle G_0 \rangle, g_1 \in \langle G_1 \rangle$  such that  $g_0 = \pi_0^{-1} \pi_1 g_1$ , or, equivalently,  $\pi_0^{-1} \pi_1 \cdot g_1 \cdot g_0^{-1} = \mathbb{I}$ . We show in Lemma 17 that such  $g_0, g_1$  exist if and only if  $\mathbb{I}$  is the smallest element in the set  $S \pi_0^{-1} \pi_1 \langle G_1 \rangle \cdot \langle G_0 \rangle$ . Hence, for finding out if  $S$  is empty we may invoke the LEXMIN algorithm we have already used before in GETLABELS and we will explain below in Sec. D.2. If it is not empty, then we obtain  $g_0, g_1$  as above using ARGLEXMIN, and output  $\pi_0 \cdot g_0$  as an element in the intersection. Since LEXMIN and ARGLEXMIN take  $O(n^3)$  time, so does Alg. 9.

**Lemma 17.** The coset  $S := \langle G_0 \rangle \cap \pi_0^{-1} \pi_1 \langle G_1 \rangle$  is nonempty if and only if the lexicographically smallest element of the set  $S = \pi_0^{-1} \pi_1 \langle G_1 \rangle \cdot \langle G_0 \rangle = \{\pi_0^{-1} \pi_1 g_1 g_0 \mid g_0 \in G_0, g_1 \in G_1\}$  is  $1 \cdot \mathbb{I}$ .

*Proof.* (Direction  $\rightarrow$ ) Suppose that the set  $\langle G_0 \rangle \cap \pi_0^{-1} \pi_1 \langle G_1 \rangle$  has an element  $a$ . Then  $a = g_0 = \pi_0^{-1} \pi_1 g_1$  for some  $g_0 \in \langle G_0 \rangle, g_1 \in \langle G_1 \rangle$ . We see that  $\mathbb{I} = \pi_0^{-1} \pi_1 g_1 g_0^{-1} \in \pi_0^{-1} \pi_1 \langle G_1 \rangle \cdot \langle G_0 \rangle$ , i.e.,

$\mathbb{I} \in S$ . Note that  $\mathbb{I}$  is, in particular, the lexicographically smallest element, since its check vector is the all-zero vector  $(\vec{0}|\vec{0}|00)$ .

(Direction  $\leftarrow$ ) Suppose that  $\mathbb{I} \in \pi_0^{-1}\pi_1 \langle G_1 \rangle \cdot \langle G_0 \rangle$ . Then  $\mathbb{I} = \pi_0^{-1}\pi_1 g_1 g_0$ , for some  $g_0 \in \langle G_0 \rangle, g_1 \in \langle G_1 \rangle$ , so we get  $g_0^{-1} = \pi_0^{-1}\pi_1 g_1 \in \langle G_0 \rangle \cap \pi_0^{-1}\pi_1 \langle G_1 \rangle$ , as promised.  $\square$

The four algorithms above allow us to evaluate each of the four individual terms in eq. (23). To finish the evaluation of eq. (23), one would expect that it is also necessary that we find the union of isomorphism sets. However, we note that if  $\pi G$  is an isomorphism set, with  $\pi$  an isomorphism and  $G$  an stabilizer subgroup, then  $P_n \otimes (\pi g) = (P_n \otimes \pi)(\mathbb{I}_2 \otimes g)$  for all  $g \in G$ . Therefore, we will evaluate eq. (23), i.e. find (a generating set) for all stabilizers of node  $v$  in two steps. First, we construct the generating set for the first term, i.e.  $\mathbb{I}_2 \otimes (\text{Stab}(|v_0\rangle) \cap \text{Stab}(B_{\text{high}}|v_1\rangle))$ , using the algorithms above. Next, for each of the other three terms  $P_n \otimes (\pi G)$ , we add only *a single* stabilizer of the form  $P_n \otimes \pi$  for each  $P_n \in \{X, Y, Z\}$ . We give the full algorithm in Alg. 8 and prove its efficiency below.

**Lemma 18** (Efficiency of function `GetStabilizerGenSet`). Let  $v$  be an  $n$ -qubit node. Assume that generator sets for the stabilizer subgroups of the children  $v_0, v_1$  are known, e.g., by an earlier call to `GetStabilizerGenSet`, followed by caching the result (see Line 27 in Alg. 8). Then Alg. 8 (function `GetStabilizerGenSet`), applied to  $v$ , runs in time  $O(n^3)$ .

*Proof.* If  $n = 1$  then Alg. 8 only evaluates Line 2–4, which run in constant time. For  $n > 1$ , the algorithm performs a constant number of calls to `GetIsomorphism` (which only multiplies two Pauli LIMs and therefore runs in time  $O(n)$ ) and four calls to `IntersectIsomorphismSets`. Note that the function `IntersectIsomorphismSets` from Alg. 9 invoke  $O(n^3)$ -runtime external algorithms (the Zassenhaus algorithm [71], RREF algorithm from Sec. 2, and Algorithm 2 from [73]), making its overall runtime  $O(n^3)$  also. Therefore, `GetStabilizerGenSet` has runtime is  $O(n^3)$ .  $\square$

## D.2 Efficiently finding a minimal LIM by multiplying with stabilizers

Here, we give  $O(n^3)$  subroutines solving the following problem: given generators sets  $G_0, G_1$  of stabilizer subgroups on  $n$  qubits, and an  $n$ -qubit Pauli LIM  $A$ , determine  $\min_{(g_0, g_1) \in \langle G_0, G_1 \rangle} A \cdot g_0 \cdot g_1$ , and also find the  $g_0, g_1$  which minimize the expression. We give an algorithm for finding both the minimum (`LEXMIN`) and the arguments of the minimum (`ARGLEXMIN`) in Alg. 12. The intuition behind the algorithms are the following two steps: first, the lexicographically minimum Pauli LIM *modulo scalar* can easily be determined using the scalar-ignoring `DivisionRemainder` algorithm from Sec. 2. Since in the lexicographic ordering, the scalar is least significant (Sec. 2), the resulting Pauli LIM has the same Pauli string as the the minimal Pauli LIM *including scalar*. We show below in Lemma 19 that if the scalar-ignoring minimization results in a Pauli LIM  $\lambda P$ , then the only other eligible LIM, if it exists, is  $-\lambda P$ . Hence, in the next step, we only need to determine whether such LIM  $-\lambda P$  exists and whether  $-\lambda < \lambda$ ; if so, then  $-\lambda P$  is the real minimal Pauli LIM  $\in \langle G_0 \cup G_1 \rangle$ .

**Lemma 19.** Let  $v_0$  and  $v_1$  be LIMDD nodes,  $R$  a Pauli string and  $\nu, \nu' \in \mathbb{C}$ . Define  $G = \text{Stab}(v_0) \cup \text{Stab}(v_1)$ . If  $\nu R, \nu' R \in \langle G \rangle$ , then  $\nu = \pm \nu'$ .

*Proof.* We prove  $g \in \langle G \rangle$  and  $\lambda g \in \langle G \rangle$  implies  $\lambda = \pm 1$ . Since Pauli LIMs commute or anticommute, we can decompose both  $g$  and  $\lambda g$  as  $g = (-1)^x g_0 g_1$  and  $\lambda g = (-1)^y h_0 h_1$  for some  $x, y \in \{0, 1\}$  and  $g_0, h_0 \in \text{Stab}(v_0)$  and  $g_1, h_1 \in \text{Stab}(v_1)$ . Combining these yields  $\lambda(-1)^x g_0 g_1 = (-1)^y h_0 h_1$ . We recall that, if  $g \in \text{Stab}(|\varphi\rangle)$  is a stabilizer of any state, then  $g^2 = \mathbb{I}$ . Therefore, squaring both sides of the equation, we get  $\lambda^2 (g_0 g_1)^2 = (h_0 h_1)^2$ , so  $\lambda^2 \mathbb{I} = \mathbb{I}$ , so  $\lambda = \pm 1$ .  $\square$

The central procedure in Alg. 12 is `ARGLEXMIN`, which, given a LIM  $A$  and sets  $G_0, G_1$  which generate stabilizer groups, finds  $g_0 \in \langle G_0 \rangle, g_1 \in \langle G_1 \rangle$  such that  $A \cdot g_0 \cdot g_1$  reaches its lexicographic minimum over all choices of  $g_0, g_1$ . It first performs the scalar-ignoring minimization (Line 5) to find

---

**Algorithm 8** Algorithm for constructing the Pauli stabilizer subgroup of a Pauli-LIMDD node

---

```

1: procedure GetStabilizerGenSet(EDGE  $e_0 \xrightarrow{\mathbb{I}_2^{\otimes n}} v_0, e_1 \xrightarrow{B_{\text{high}}} v_1$  with  $v_0, v_1$  reduced)
2:   if  $n=1$  then
3:     if there exists  $P \in \pm 1 \cdot \{X, Y, Z\}$  such that  $P|v\rangle = |v\rangle$  then return  $P$ 
4:     else return None
5:   else
6:     if  $v \in \text{STABCACHE}[v]$  then return  $\text{STABCACHE}[v]$ 
7:      $G_0 := \text{GetStabilizerGenSet}(v_0)$ 
8:     if  $B_{\text{high}} = 0$  then
9:       return  $\{\mathbb{I}_2 \otimes g, \mathbb{Z} \otimes g \mid g \in G_0\}$ 
10:    else
11:       $G := \emptyset$   $\triangleright$  Add all stabilizers of the form  $\mathbb{I}_2 \otimes \dots$ 
12:       $G_1 := \{A_1^\dagger g A_1 \mid g \in \text{GetStabilizerGenSet}(v_1)\}$ 
13:       $(\pi, B) := \text{IntersectIsomorphismSets}((\mathbb{I}_2^{\otimes n-1}, G_0), (\mathbb{I}_2^{\otimes n-1}, G_1))$ 
14:       $G := G \cup \{\mathbb{I}_2 \otimes g \mid g \in B\}$ 
15:
16:       $\pi_0, \pi_1 := \mathbb{I}_2^{\otimes n-1}, \text{GetIsomorphism}(e_1, -1 \cdot e_1)$ 
17:       $(\pi, B) := \text{IntersectIsomorphismSets}((\pi_0, G_0), (\pi_1, G_1))$ 
18:      if  $\pi \neq \text{None}$  then  $G := G \cup \{Z \otimes \pi\}$   $\triangleright$  Add stabilizer of form  $Z \otimes \dots$ 
19:
20:       $\pi_0, \pi_1 := \text{GetIsomorphism}(e_0, e_1), \text{GetIsomorphism}(e_1, e_0)$ 
21:       $(\pi, B) := \text{IntersectIsomorphismSets}((\pi_0, G_0), (\pi_1, G_1))$ 
22:      if  $\pi \neq \text{None}$  then  $G := G \cup \{X \otimes \pi\}$   $\triangleright$  Add stabilizer of form  $X \otimes \dots$ 
23:
24:       $\pi_0, \pi_1 := \text{GetIsomorphism}(e_0, -i \cdot e_1), \text{GetIsomorphism}(-i \cdot e_1, e_0)$ 
25:       $(\pi, B) := \text{IntersectIsomorphismSets}((\pi_0, G_0), (\pi_1, G_1))$ 
26:      if  $\pi \neq \text{None}$  then  $G := G \cup \{Y \otimes \pi\}$   $\triangleright$  Add stabilizer of form  $Y \otimes \dots$ 
27:       $\text{STABCACHE}[v] := G$ 
28:      return  $G$ 

```

---



---

**Algorithm 9** An  $O(n^3)$  algorithm for computing the intersection of two sets of isomorphisms, each given as single isomorphism with a stabilizer subgroup (see [Lemma 16](#)).

---

```

1: procedure INTERSECTISOMORPHISMSets(stabilizer subgroup generating sets  $G_0, G_1$ ,
   Pauli-LIMs  $\pi_0, \pi_1$ )
   Output: Pauli LIM  $\pi$ , stabilizer subgroup generating set  $G$  s.t.  $\pi\langle G \rangle = \pi_0\langle G_0 \rangle \cap \pi_1\langle G_1 \rangle$ 
2:    $\pi := \text{LexMin}(G_0, G_1, \pi_1^{-1}\pi_0)$ 
3:   if  $\pi = \mathbb{I}$  then
4:      $(g_0, g_1) = \text{ArgLexMin}(G_0, G_1, \pi_1^{-1}\pi_0)$ 
5:      $\pi := \pi_0 \cdot g_0$ 
6:      $G := \text{IntersectStabilizerGroups}(G_0, G_1)$ 
7:     return  $(\pi, G)$ 
8:   else
9:     return None

```

---



---

**Algorithm 10** Algorithm for finding the intersection of two stabilizer subgroup generating sets.

---

```

1: procedure INTERSECTSTABILIZERGROUPS(stabilizer subgroup generating sets  $G_0, G_1$ )
   Output: a generating set for  $\langle G_0 \rangle \cap \langle G_1 \rangle$ 
2:   Compute  $U$  s.t.  $H_0 := UG_0U^\dagger = \{Z_1, \dots, Z_{|G_0|}\}$   $\triangleright$  Using Algorithm 2 from [73]
3:    $H_1 := UG_1U^\dagger$ 
4:   Bring  $H_1$  into RREF form  $\triangleright$  See also Sec. 2
5:   Discard any generators from  $H_1$  whose check vector has a 1 in the  $X$  block as pivot
6:    $H' :=$  generating set for  $\langle H_0 \rangle \cap \langle H_1 \rangle$   $\triangleright$  Using Zassenhaus' algorithm [71]
7:   return  $U^\dagger H' U$ 

```

---

---

**Algorithm 11** Algorithm for constructing a single isomorphism between the quantum states represented by two Pauli-LIMDD edges, each pointing to a canonical node.

---

```

1: procedure GetIsomorphism(EDGE  $\xrightarrow{A} \bigcirc_v$ ,  $\xrightarrow{B} \bigcirc_w$  with  $v, w$  reduced,  $A \neq 0 \vee B \neq 0$ )
2:   if  $v = w$  and  $A, B \neq 0$  then
3:     return  $B \cdot A^{-1}$ 
4:   return None

```

---

$g_0, g_1$  modulo scalar. The algorithm LEXMIN simply invokes ARGLEXMIN to get the arguments  $g_0, g_1$  which yield the minimum and uses these to compute the actual minimum.

The subroutine FINDOPPOSITE finds an element  $g \in G_0$  such that  $-g \in G_1$ , or infers that no such  $g$  exists. It does so in a similar fashion as INTERSECTSTABILIZERGROUPS from [Sec. D.1](#): by conjugation with a suitably chosen unitary  $U$ , it maps  $G_1$  to  $\{Z_1, Z_2, \dots, Z_{|G_1|}\}$ . Analogously to our explanation of INTERSECTSTABILIZERGROUPS, the group generated by  $UG_1U^\dagger$  contains precisely all Pauli LIMs which satisfy the following three properties: (i) the scalar is 1; (ii) its Pauli string has an  $\mathbb{I}$  or  $Z$  at positions  $1, 2, \dots, |G_1|$ ; (iii) its Pauli string has an  $\mathbb{I}$  at positions  $|G_1| + 1, \dots, n$ . Therefore, the target  $g$  only exists if there is a LIM in  $\langle UG_0U^\dagger \rangle$  which (i') has scalar  $-1$  and satisfies properties (ii) and (iii). To find such a  $g$ , we put  $UG_0U^\dagger$  in RREF form and check all resulting generators for properties (i'), (ii) and (iii). (By definition of RREF, it suffices to check only the generators for this property) If a generator  $h$  satisfies these properties, we return  $U^\dagger h U$  and **None** otherwise. The algorithm requires  $O(n^3)$  time to find  $U$ , the conversion  $G \mapsto UGU^\dagger$  can be done in time  $O(n^3)$ , and  $O(n)$  time is required for checking each of the  $O(n^2)$  generators. Hence the runtime of the overall algorithm is  $O(n^3)$ .

## E Advanced algorithms

### E.1 Measuring an arbitrary qubit

[Alg. 13](#) allows one to measure a given qubit. Specifically, given a quantum state  $|e\rangle$  represented by a LIMDD edge  $e$ , a qubit index  $k$  and an outcome  $b \in \{0, 1\}$ , it computes the probability of observing  $|b\rangle$  when measuring the  $k$ -th significant qubit of  $|e\rangle$ . The algorithm proceeds by traversing the LIMDD with root edge  $e$  at [Line 7](#). Like [Alg. 2](#), which measured the top qubit, this algorithm finds the probability of a given outcome by computing the squared norm of the state when the  $k$ -th qubit is projected onto  $|0\rangle$ , or  $|1\rangle$ . The case that is added, relative to [Alg. 2](#), is the case when  $n > k$ , in which case it calls the procedure SQUAREDNORMPROJECTED. On input  $e, y, k$ , the procedure SQUAREDNORMPROJECTED outputs the squared norm of  $\Pi_k^y |e\rangle$ , where  $\Pi_k^y = \mathbb{I}_{n-k} \otimes |y\rangle \langle y| \otimes \mathbb{I}_{k-1}$  is the projector which projects the  $k$ -th qubit onto  $|y\rangle$ .

After measurement of a qubit  $k$ , a quantum state is typically projected to  $|0\rangle$  or  $|1\rangle$  ( $b = 0$  or  $b = 1$ ) on that qubit, depending on the outcome. [Alg. 14](#) realizes this. It does so by traversing the LIMDD until a node  $v$  with  $\text{idx}(v) = k$  is reached. It then returns an edge to a new node by calling MAKEEDGE(FOLLOW<sub>0</sub>( $e$ ), 0) to project onto  $|0\rangle$  or MAKEEDGE(0, FOLLOW<sub>1</sub>( $e$ )) to project onto  $|1\rangle$ , on [Line 5](#), recreating a node on level  $k$  in the backtrack on [Line 7](#). The projection operator  $\Pi_k^b$  commutes with any LIM  $P$  when  $P_k$  is a diagonal operator (i.e.,  $P_k \in \{\mathbb{I}_2, Z\}$ ). Otherwise, if  $P_k$  is an antidiagonal operator (i.e.,  $P_k \in \{X, Y\}$ ), have  $\Pi_k^b \cdot P = P \Pi_k^{(1-b)}$ . The algorithm applies this correction on [Line 2](#).

**Sampling.** To sample from a quantum state in the computational basis, simply repeat the three-step measurement procedure outlined in [Sec. 3.3.1](#)  $n$  times: once for each qubit.

---

**Algorithm 12** Algorithms LEXMIN and ARGLEXMIN for computing the minimal element from the set  $A \cdot \langle G_0 \rangle \cdot \langle G_1 \rangle = \{Ag_0g_1 | g_0 \in G_0, g_1 \in G_1\}$ , where  $A$  is a Pauli LIM and  $G_0, G_1$  are generating sets for stabilizer subgroups. The algorithms make use of a subroutine FINDOPPOSITE for finding an element  $g \in \langle G_0 \rangle$  such that  $-g \in \langle G_1 \rangle$ . A canonical choice for the ROOTLABEL (see Sec. 3.3.3) of an edge  $e$  pointing to a node  $v$  is  $\text{LEXMIN}(G, \{\mathbb{I}\}, \text{label}(e))$  where  $G$  is a stabilizer generator group of  $\text{Stab}(v)$ .

---

```

1: procedure LEXMIN(stabilizer subgroup generating sets  $G_0, G_1$  and Pauli LIM  $A$ )
   Output:  $\min_{(g_0, g_1) \in \langle G_0 \cup G_1 \rangle} A \cdot g_0 \cdot g_1$ 
2:    $(g_0, g_1) := \text{ARGLEXMIN}(G_0, G_1, A)$ 
3:   return  $A \cdot g_0 \cdot g_1$ 

4: procedure ARGLEXMIN(stabilizer subgroup generating sets  $G_0, G_1$  and Pauli LIM  $A$ )
   Output:  $\arg \min_{g_0 \in G_0, g_1 \in G_1} A \cdot g_0 \cdot g_1$ 
5:    $(g_0, g_1) := \arg \min_{(g_0, g_1) \in \langle G_0 \cup G_1 \rangle} \{h \mid h \propto A \cdot g_0 \cdot g_1\}$  ▷ Using the scalar-ignoring
   DivisionRemainder algorithm from Sec. 2,
6:    $g' := \text{FINDOPPOSITE}(G_0, G_1, g_0, g_1)$ 
7:   if  $g'$  is None then
8:     return  $(g_0, g_1)$ 
9:   else
10:     $h_0, h_1 := g_0 \cdot g', (-g') \cdot g_1$  ▷  $g_0g_1 = -h_0h_1$ 
11:    if  $A \cdot h_0 \cdot h_1 <_{\text{lex}} A \cdot g_0 \cdot g_1$  then return  $(h_0, h_1)$ 
12:    else return  $(g_0, g_1)$ 

13: procedure FINDOPPOSITE(stabilizer subgroup generating sets  $G_0, G_1$ )
   Output:  $g \in G_0$  such that  $-g \in G_1$ , or None if no such  $g$  exists
14:   Compute  $U$  s.t.  $UG_1U^\dagger = \{Z_1, Z_2, \dots, Z_{|G_1|}\}$ , using Algorithm 2 from [73] ▷  $Z_j$  is the  $Z$ 
   gate applied to qubit with index  $j$ 
15:    $H_0 := UG_0U^\dagger$ 
16:    $H_0^{\text{RREF}} := H_0$  in RREF form
17:   for  $h \in H_0^{\text{RREF}}$  do
18:     if  $h$  satisfies all three of the following: (i)  $h$  has scalar  $-1$ ; the Pauli string of  $h$  (ii)
       contains only  $\mathbb{I}$  or  $Z$  at positions  $1, 2, \dots, |G_1|$ , and (iii) only  $\mathbb{I}$  at positions  $|G_1| + 1, \dots, n$  then
19:       return  $U^\dagger h U$ 
20:   return None

```

---

---

**Algorithm 13** Compute the probability of observing  $|y\rangle$  when measuring the  $k$ -th qubit of the state  $|e\rangle$ . Here  $e$  is given as LIMDD on  $n$  qubits,  $y$  is given as a bit, and  $k$  is an integer index. For example, to measure the top-most qubit, one calls  $\text{MEASURE}(e, 0, n)$ . The procedure  $\text{SQUAREDNORM}(e, y, k)$  computes the scalar  $\langle e | (\mathbb{I} \otimes |y\rangle \langle y| \otimes \mathbb{I}) | e \rangle$ , i.e., computes the squared norm of the state  $|e\rangle$  after the  $k$ -th qubit is projected to  $|y\rangle$ . For readability, we omit calls to the cache, which implement dynamic programming.

---

```

1: procedure MEASUREMENTPROBABILITY(EDGE  $e \xrightarrow{\lambda P_n \otimes P'} \textcircled{v}$ ,  $y \in \{0, 1\}$ ,  $k \in \mathbb{Z}_{\geq 1}$ )
2:   if  $n = k$  then
3:      $p_0 := \text{SQUAREDNORM}(\text{FOLLOW}_0(e))$ 
4:      $p_1 := \text{SQUAREDNORM}(\text{FOLLOW}_1(e))$ 
5:     return  $p_j / (p_0 + p_1)$  where  $j = 0$  if  $P_n \in \{\mathbb{I}, Z\}$  and  $j = 1$  if  $P_n \in \{X, Y\}$ 
6:   else
7:      $p_0 := \text{SQUAREDNORMPROJECTED}(\text{FOLLOW}_0(e), y, k)$ 
8:      $p_1 := \text{SQUAREDNORMPROJECTED}(\text{FOLLOW}_1(e), y, k)$ 
9:     return  $(p_0 + p_1) / \text{SQUAREDNORM}(e)$ 
10: procedure SQUAREDNORM(EDGE  $e \xrightarrow{\lambda P} \textcircled{v}$ )
11:   if  $n = 0$  then return  $|\lambda|^2$ 
12:   if  $v \in \text{NORM-CACHE}$  then
13:      $s := \text{ADD}(\text{SQUAREDNORM}(\text{FOLLOW}_0(\textcircled{v})), \text{SQUAREDNORM}(\text{FOLLOW}_1(\textcircled{v})))$ 
14:   return  $|\lambda|^2 s$ 
15: procedure SQUAREDNORMPROJECTED(EDGE  $e \xrightarrow{\lambda P_n \otimes P'} \textcircled{v}$ ,  $y \in \{0, 1\}$ ,  $k \in \mathbb{Z}_{\geq 1}$ )
16:    $b := (P_n \in \{X, Y\})$   $\triangleright$  i.e.,  $b = 1$  iff  $P_n$  is Anti-diagonal
17:   if  $n = 0$  then
18:     return  $|\lambda|^2$ 
19:   else if  $n = k$  then
20:     return  $\text{SQUAREDNORM}(\text{FOLLOW}_{b \oplus y}(e))$ 
21:   else
22:      $\alpha_0 := \text{SQUAREDNORMPROJECTED}(\text{FOLLOW}_0(\textcircled{v}), b \oplus y, k)$ 
23:      $\alpha_1 := \text{SQUAREDNORMPROJECTED}(\text{FOLLOW}_1(\textcircled{v}), b \oplus y, k)$ 
24:   return  $|\lambda|^2 \cdot (\alpha_0 + \alpha_1)$ 

```

---

**Strong simulation.** To compute the probability of observing a given bit-string  $x = x_n \dots x_1$ , first compute the probability  $p_n$  of observing  $|x_n\rangle$ ; then update the LIMDD to outcome  $x_n$ , obtaining a new, smaller LIMDD. On this new LIMDD, compute the probability  $p_{n-1}$  of observing  $|x_{n-1}\rangle$ , and so forth. Note that, because the LIMDD was updated after observing the measurement outcome  $|x_n\rangle$ ,  $p_{n-1}$  is the probability of observing  $x_{n-1}$  given that the top qubit is measured to be  $x_n$ . Then the probability of observing the string  $x$  is the product  $p = p_1 \dots p_n$ .

## E.2 Applying Hadamards to stabilizer states in polynomial time

We show that, using the algorithms that we have given, a Hadamard can be applied to a stabilizer state in polynomial time. Together with the results of [Sec. 3.3.2](#), this shows that all Clifford gates can be applied to stabilizer states in polynomial time. We emphasize that our algorithms do not invoke existing algorithms that are tailored to applying a Hadamard to a stabilizer state; instead, the LIMDD algorithms are inherently polynomial-time for this use case. The key ingredient is [Lemma 21](#), which describes situations in which the ADD procedure adds two stabilizer states in polynomial time. It shows that only  $5n$  distinct calls to ADD are made. Our algorithms are polynomial-time because of the dynamic programming effected by the caching of previously computed results, as described in [Sec. 4.3](#), which, in this case, makes sure only  $5n$  recursive calls are made.

**Theorem 20.** When  $\text{APPLYGATE}(H, |\psi\rangle)$  ([Alg. 3](#)) is used to apply a Hadamard gate to a stabilizer state  $|\psi\rangle$ , it runs in polynomial time.

---

**Algorithm 14** Project LIMDD  $\xrightarrow{A} \textcircled{v}$  to  $|b\rangle$  for qubit  $k$ , i.e.,  $(\mathbb{I}_{n-k} \otimes |b\rangle \langle b| \otimes \mathbb{I}_{k-1}) \cdot |Av\rangle$ .

---

```

1: procedure UPDATEPOSTMEAS(EDGE  $\xrightarrow{\lambda P_n \otimes \dots \otimes P_1} \textcircled{v}$ ,  $k \leq n = \text{idx}(v)$ ,  $b \in \{0, 1\}$ )
2:    $b' := x \oplus b$  where  $x = 0$  if  $P_k \in \{\mathbb{I}, Z\}$  and  $x = 1$  if  $P_k \in \{X, Y\}$   $\triangleright$  flip  $b$  if  $P_k$  is anti-diagonal
3:   if  $(v, k, b') \in \text{CACHE}$  then return  $\text{CACHE}[v, k, b']$ 
4:   if  $n = k$  then
5:      $e := \text{MAKEEDGE}((1 - b') \cdot \text{low}(v), b' \cdot \text{high}(v))$   $\triangleright$  Project  $|v\rangle$  to  $|b'\rangle \langle b'| \otimes \mathbb{I}_2^{\otimes n-1}$ 
6:   else  $\triangleright n \neq k$ :
7:      $e := \text{MAKEEDGE}(\text{UPDATEPOSTMEAS}(\text{low}(v), k, b'), \text{UPDATEPOSTMEAS}(\text{high}(v), k, b'))$ 
8:      $\text{CACHE}[v, k, b'] := e$ 
9:   return  $e$ 

```

---

*Proof.* Let  $|\varphi\rangle$  be a stabilizer state, represented by a LIMDD with root edge  $\xrightarrow{P} \textcircled{v}$ . By Th. 14, this LIMDD is a Tower Pauli-LIMDD. If the Hadamard gate is applied to the top qubit, then APPLYGATE (Alg. 3) makes two calls to ADD, on Line 5 and Line 6. Both calls are of the form  $\text{ADD}(\xrightarrow{\lambda P} \textcircled{v}, \xrightarrow{\lambda Q} \textcircled{v})$  where  $\lambda \in \mathbb{C}$  is a scalar,  $P$  and  $Q$  are Pauli strings, and  $v$  is a node representing a stabilizer state. Lemma 21 tells us that at most  $\mathcal{O}(n)$  recursive calls to ADD are made. Each recursive call to ADD may invoke the MAKEEDGE procedure, which runs in time  $\mathcal{O}(n^3)$ , yielding a total worst-case running time of  $\mathcal{O}(n^4)$ . Otherwise, if the Hadamard is not applied to the top qubit, then Hadamard gate is propagated downward in recursive calls to APPLYGATE until the target qubit is encountered, at which point the above reasoning guarantees a polynomial runtime.  $\square$

We now prepare Lemma 21, which is the main technical ingredient. The idea is to look closely at the recursive calls made by ADD – since this call does all the work – and to look closely at when a cache hit is achieved, in order to give precise descriptions of both. We then use these descriptions to show that all the recursive calls to ADD effect only five different cache entries at any given level of the LIMDD.

To understand the recursive calls to ADD, we note that each call to ADD makes two recursive calls. Specifically, when it is called with parameters  $\text{ADD}(\xrightarrow{P} \textcircled{v}, \xrightarrow{R} \textcircled{v})$ , it makes two recursive calls, of the following form,

$$\text{ADD}(\text{FOLLOW}_x(\xrightarrow{P} \textcircled{v}), \text{FOLLOW}_x(\xrightarrow{Q} \textcircled{v})) \quad \text{for } x \in \{0, 1\} \quad (24)$$

These calls subsequently call ADD again, recursively; therefore, if we ignore the fact that some of these calls don't happen because a cache hit preempts it, then the cumulative effect is that the total set of recursive calls to ADD is described by the set of tuples of the form  $(\text{FOLLOW}_x(\xrightarrow{P} \textcircled{v}), \text{FOLLOW}_x(\xrightarrow{Q} \textcircled{v}))$  for  $x \in \{0, 1\}^\ell$  for  $0 \leq \ell \leq n$ . Inspecting ADDCACHELOOKUP and ADDCACHESTORE in Alg. 6, we see that a call to ADD with parameters  $(\xrightarrow{A} \textcircled{v}, \xrightarrow{B} \textcircled{v})$  effects a cache hit if and only if ADD was previously called with  $(\xrightarrow{C} \textcircled{v}, \xrightarrow{D} \textcircled{v})$  satisfying  $A^{-1}B|v\rangle = C^{-1}D|v\rangle$ . Thus, each call to  $\text{ADD}(\xrightarrow{P} \textcircled{v}, \xrightarrow{Q} \textcircled{v})$  can be associated with the Pauli operator  $P^{-1}Q$ , which is equal to  $PQ$  since  $P^{-1} = P$ .

We now turn briefly to the FOLLOW procedure. The procedure  $\text{FOLLOW}_x(\xrightarrow{P} \textcircled{v})$  traverses a path of length  $\ell = |x|$ , and outputs an edge  $\xrightarrow{A} \textcircled{t}$  with some label  $A$ . The path starts at  $v$  and ends at  $t$ . Here  $A$  is the product of the LIMs on the edges that were traversed (including the label  $P$  on the root edge), after which we discard the most significant  $\ell$  qubits of the result. Let  $L(x, P)$  be the function which outputs this label  $A$ . For any Pauli string  $P = P_n \otimes \dots \otimes P_1$ , let  $P^{(\ell)} = P_{n-\ell} \otimes \dots \otimes P_1$  be the last  $(n - \ell)$  gates of  $P$ , so that, e.g.,  $P = P_n \otimes P_{n-1} \otimes P^{(2)}$ . Thus, if the procedure traverses edges  $e_1, e_2, \dots, e_\ell$ , labeled with LIMs  $A_1, A_2, \dots, A_\ell$ , respectively, then  $A = \lambda A_1^{(\ell)} \cdot A_2^{(\ell)} \dots A_\ell^{(\ell)}$  for some  $\lambda \in \mathbb{C}$ . Here the factor  $\lambda$  depends only on the operators that were discarded and on the weights on the edges that were traversed. For example, if  $x = 1$  and  $P_n = Z$ ,

and  $v$ 's high edge is labeled with 5, then  $\lambda = -5$ . Moreover, the  $\ell$  most significant operators of  $P$  influence which path is traversed in the following way. Let  $u = u_1 \dots u_\ell$  be the string defined by  $u_j = 0$  if  $P_{n-j+1} \in \{I, Z\}$  and  $u_j = 1$  otherwise, i.e., if  $P_{n-j+1} \in \{X, Y\}$ . Then we have

$L(x, P) = \lambda L(x \oplus u, \mathbb{I}^{\otimes \ell} \otimes P^{(\ell)})$  for some  $\lambda \in \mathbb{C}$ . Thus,  $\text{FOLLOW}_x(\xrightarrow{P} \textcircled{v}) = \frac{\lambda L(x \oplus u, \mathbb{I}^{\otimes \ell} \otimes P^{(\ell)})}{\lambda L(x \oplus u, \mathbb{I}^{\otimes \ell} \otimes P^{(\ell)})} \xrightarrow{P} \textcircled{v}$  for some  $\lambda \in \mathbb{C}$ , where  $t$  is the destination of the path traversed by  $\text{FOLLOW}_x(\xrightarrow{P} \textcircled{v})$ . Lastly, we note that  $L(x, \mathbb{I}^{\otimes \ell} \otimes P^{(\ell)}) = P^{(\ell)} \cdot L(x, \mathbb{I}^{\otimes n})$ .

**Lemma 21.** Let  $v$  be a node in a Tower Pauli-LIMDD representing a stabilizer state,  $\alpha, \beta \in \{0, \pm 1, \pm i\}$  scalars and  $P, R$  Pauli strings. Then a call to  $\text{ADD}(\xrightarrow{\alpha P} \textcircled{v}, \xrightarrow{\beta R} \textcircled{v})$  invokes only at most  $5n$  recursive calls to  $\text{ADD}$ .

*Proof.* Let  $v_1, \dots, v_{n+1}$  be the nodes in the Tower Pauli-limdd, with  $v = v_1$  the top node and  $v_{n+1}$  the Leaf node (so that node  $v_\ell$  is on layer  $\ell$ ).

When  $\text{ADD}$  is called with parameters  $\text{ADD}(\xrightarrow{P} \textcircled{v_0}, \xrightarrow{R} \textcircled{v_0})$ , the parameters to the recursive calls are all of the form  $(\text{FOLLOW}_x(\xrightarrow{P} \textcircled{v_0}), \text{FOLLOW}_x(\xrightarrow{R} \textcircled{v_0}))$ , for some  $x \in \{0, 1\}^\ell$  and  $0 \leq \ell \leq n$ . Using the insights above, we have  $\text{FOLLOW}_x(\xrightarrow{P} \textcircled{v_0}) = \frac{\lambda L(x \oplus u, \mathbb{I}^{\otimes \ell} \otimes P^{(\ell)})}{\lambda L(x \oplus u, \mathbb{I}^{\otimes \ell} \otimes P^{(\ell)})} \xrightarrow{P} \textcircled{v_\ell} = \frac{\lambda P^{(\ell)} L(x, \mathbb{I})}{\lambda P^{(\ell)} L(x, \mathbb{I})} \xrightarrow{P} \textcircled{v_\ell}$  for some  $\lambda$  and  $\text{FOLLOW}_x(\xrightarrow{R} \textcircled{v_0}) = \frac{\omega L(x \oplus u, \mathbb{I}^{\otimes \ell} \otimes R^{(\ell)})}{\omega L(x \oplus u, \mathbb{I}^{\otimes \ell} \otimes R^{(\ell)})} \xrightarrow{R} \textcircled{v_\ell} = \frac{\omega R^{(\ell)} L(x, \mathbb{I})}{\omega R^{(\ell)} L(x, \mathbb{I})} \xrightarrow{R} \textcircled{v_\ell}$  for some  $\omega$ . This call to  $\text{ADD}$  can be associated with the operator  $(\lambda P^{(\ell)} L(x \oplus u, \mathbb{I}))^{-1} \cdot \omega R^{(\ell)} L(x \oplus u, \mathbb{I}) = \lambda^{-1} \omega P^{(\ell)} R^{(\ell)} L(x \oplus u, \mathbb{I})^{-1} L(x \oplus u, \mathbb{I}) = \lambda^{-1} \omega P^{(\ell)} R^{(\ell)} \in \{\pm 1, \pm i\}$ . Thus,  $\text{ADD}$  is called with parameters

$$\left( \xrightarrow{\lambda P^{(\ell)} L(x, \mathbb{I})} \textcircled{v_\ell}, \xrightarrow{\omega R^{(\ell)} L(x, \mathbb{I})} \textcircled{v_\ell} \right) \quad \text{for some } \lambda, \omega \in \{\pm 1, \pm i\} \quad (25)$$

Recall that a LIMDD representing a stabilizer state only has edge weights in  $\{0, \pm 1, \pm i\}$ . Therefore, since  $\lambda$  and  $\omega$  depend on the weights on the edges, and depend on the path traversed, we have  $\lambda, \omega \in \{0, \pm 1, \pm i\}$ , so we have  $\lambda^{-1} \omega \in \{0, \pm 1, \pm i\}$ . Thus, since  $P^{(\ell)}$  and  $R^{(\ell)}$  are fixed, the cache only stores at most four distinct recursive calls, and will achieve a cache hit on all other recursive calls, at level  $\ell$ . When a cache hit is achieved, the algorithm does not recurse further, and instead terminates the current call. Since the diagram contains  $n$  levels, there are at most  $5n$  recursive calls in total.  $\square$

## F LIMDDs prepare the $W$ state efficiently

In this section, we show that LIMDDs can efficiently simulate a circuit family given by McClung [46], which prepares the  $|W\rangle$  state when initialized to the  $|0\rangle$  state. We thereby show a separation between LIMDD and the Clifford+ $T$  simulator, as explained in Sec. 3.2.3. Figure Fig. 14 shows the circuit for the case of 8 qubits.

A sketch of the proof is as follows. First, we establish that the LIMDD of each intermediate state (Lemma 24), as well as of each gate (Lemma 25), has polynomial size. Second, we establish that the algorithms presented in Sec. 3.3 can apply each gate to the intermediate state in polynomial time (Th. 29). To this end, we observe that the circuit only produces relatively simple intermediate states. Specifically, each intermediate and output state is of the form  $|\psi_t\rangle = \frac{1}{\sqrt{n}} \sum_{k=1}^n |x_k\rangle$  where the  $x_k \in \{0, 1\}^n$  are computational basis vectors (Lemma 23). For example, the output state has  $|x_k\rangle = |0\rangle^{k-1} |1\rangle |0\rangle^{\otimes n-k}$ . The main technical tool we will use to reason about the size of the LIMDDs of these intermediate states, are the *subfunction rank* and *computational basis rank* of a state. Both these measures are upper bounds of the size of a LIMDD (in Lemma 22), and also allow us to upper bound the time taken by the  $\text{APPLYGATE}$  and  $\text{ADD}$  algorithms (in Lemma 26 for  $\text{APPLYGATE}$  and Lemma 27  $\text{ADD}$ ).

Fig. 14 shows the circuit for the case of  $n = 8$  qubits. For convenience and without loss of generality, we only treat the case when the number of qubits is a power of 2, since the circuit is simplest in

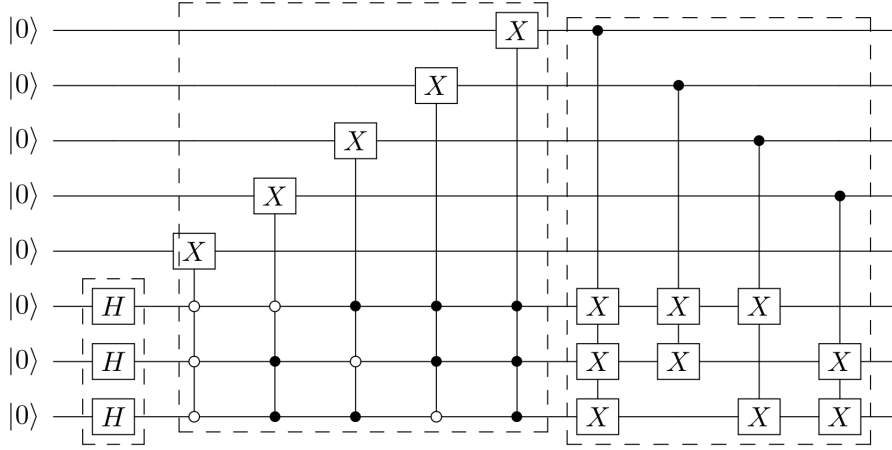


Figure 14: Reproduced from McClung [46]. A circuit on eight qubits ( $n = 8$ ) which takes as input the  $|0\rangle^{\otimes 8}$  state and outputs the  $|W_8\rangle$  state. In the general case, it contains  $\log n$  Hadamard gates, and its Controlled- $X$  gates act on one target qubit and at most  $\log n$  control qubits.

that case. In general, the circuit works as follows. The qubits are divided into two registers; register  $A$ , with  $\log n$  qubits, and register  $B$ , with the remaining  $n - \log n$  qubits. First, the circuit applies a Hadamard gate to each qubit in register  $A$ , to bring the state to the superposition  $|+\rangle^{\otimes \log n} |0\rangle^{n-\log n}$ . Then it applies  $n - \log n$  Controlled- $X$  gates, where, in each gate, each qubit of register  $A$  acts as the control qubits and one qubit in register  $B$  is the target qubit. Lastly, it applies  $n - \log n$  Controlled- $X$  gates, where, in each gate, one qubit in register  $B$  is the control qubit and one or more qubits in register  $A$  are the target qubits. Each of the three groups of gates is highlighted in a dashed rectangle in Fig. 14. On input  $|0\rangle^{\otimes n}$ , the circuit's final state is  $|W_n\rangle$ . We emphasize that the Controlled- $X$  gates are permutation gates (i.e., their matrices are permutation matrices). Therefore, these gates do not influence the number of non-zero computational basis state amplitudes of the intermediate states. We refer to the  $t$ -th gate of this circuit as  $U_t$ , and the  $t$ -th intermediate state as  $|\psi_t\rangle$ , so that  $|\psi_{t+1}\rangle = U_t |\psi_t\rangle$  and  $|\psi_0\rangle = |0\rangle$  is the initial state.

We refer to the number of computational basis states with nonzero amplitude as a state's *computational basis rank*, denoted  $\chi_{\text{comp}}(|\psi\rangle)$ .

**Definition 9.** (Computational basis rank) Let  $|\psi\rangle = \sum_{x \in \{0,1\}^n} \alpha(x) |x\rangle$  be a quantum state defined by the amplitude function  $\alpha: \{0,1\}^n \rightarrow \mathbb{C}$ . Then the *computational basis rank* of  $|\psi\rangle$  is  $\chi_{\text{comp}}(|\psi\rangle) = |\{x \mid \alpha(x) \neq 0\}|$ , the number of nonzero computational basis amplitudes.

Recall that, for a given function  $\alpha: \{0,1\}^n \rightarrow \mathbb{C}$ , a string  $a \in \{0,1\}^\ell$  induces a *subfunction*  $\alpha_y: \{0,1\}^{n-\ell} \rightarrow \mathbb{C}$ , defined as  $\alpha_y(x) = \alpha(y, x)$ . We refer to the number of subfunctions of a state's amplitude function as its *subfunction rank*. The following definition makes this more precise.

**Definition 10.** (Subfunction rank) Let  $|\psi\rangle = \sum_{x \in \{0,1\}^n} \alpha^\psi(x) |x\rangle$  be a quantum state defined by the amplitude function  $\alpha^\psi: \{0,1\}^n \rightarrow \mathbb{C}$ , as above. Let  $\chi_{\text{sub}}(|\psi\rangle, \ell)$  be the number of unique non-zero subfunctions induced by strings of length  $\ell$ , as follows,

$$\chi_{\text{sub}}(|\psi\rangle, \ell) = |\{\alpha_y^\psi: \{0,1\}^{n-\ell} \rightarrow \mathbb{C} \mid \alpha_y \neq 0, y \in \{0,1\}^\ell\}| \quad (26)$$

We define the *subfunction rank* of  $|\psi\rangle$  as  $\chi_{\text{sub}}(|\psi\rangle) = \max_{\ell=0, \dots, n} \chi_{\text{sub}}(|\psi\rangle, \ell)$ . We extend these definitions in the natural way for an  $n$ -qubit matrix  $U = \sum_{r,c \in \{0,1\}^n} \alpha^U(r, c) |r\rangle \langle c|$  defined by the function  $\alpha^U: \{0,1\}^{2n} \rightarrow \mathbb{C}$ .

It is easy to check that  $\chi_{\text{sub}}(|\psi\rangle) \leq \chi_{\text{comp}}(|\psi\rangle)$  holds for any state.

For the next lemma, we use the notion of a *prefix* of a LIMDD node. This lemma will serve as a tool which allows us to show that a LIMDD is small when its computational basis rank is low. We apply this tool to the intermediate states of the circuit in Lemma 24.

**Definition 11** (Prefix of a LIMDD node). For a given string  $x \in \{0, 1\}^\ell$ , consider the path traversed by the  $\text{FOLLOW}_x(\xrightarrow{R}\textcircled{r})$  subroutine, which starts at the diagram's root edge and ends at a node  $v$  on level  $\ell$ . We will say that  $x$  is a *prefix* of the node  $v$ . We let  $\text{Labels}(x)$  be the product of the LIMs on the edges of this path (i.e., including the root edge). The set of prefixes of a node  $v$  is denoted  $\text{pre}(v)$ .

**Lemma 22.** If a LIMDD represents the state  $|\varphi\rangle$ , then its width at any given level (i.e., the number of nodes at that level) is at most  $\chi_{\text{comp}}(|\varphi\rangle)$ .

*Proof.* For notational convenience, let us number the levels so that the root node is on level 0, its children are on level 1, and so on, with the Leaf on level  $n$  (contrary to Fig. 3). Let  $r$  be the root node of the LIMDD, and  $R$  the root edge's label. By construction of a LIMDD, the state represented by the LIMDD can be expressed as follows, for any level  $\ell \geq 0$ ,

$$R|r\rangle = \sum_{x \in \{0,1\}^\ell} |x\rangle \otimes \text{FOLLOW}_x(\xrightarrow{R}\textcircled{r}) \quad (27)$$

Since  $\xrightarrow{R}\textcircled{r}$  is the root of our diagram, if  $x$  is a prefix of  $v$ , then

$$\text{FOLLOW}_x(\xrightarrow{R}\textcircled{r}) = \text{Labels}(x) \cdot |v\rangle \quad (28)$$

A string  $x \in \{0, 1\}^\ell$  can be a prefix of only one node; consequently, the prefix sets of two nodes on the same level are disjoint, i.e.,  $\text{pre}(v_p) \cap \text{pre}(v_q) = \emptyset$  for  $p \neq q$ . Moreover, each string  $x$  is a prefix of *some* node on level  $\ell$  (namely, simply the node at which the  $\text{FOLLOW}_x(\xrightarrow{R}\textcircled{r})$  subroutine arrives). Say that the  $\ell$ -th level contains  $m$  nodes,  $v_1, \dots, v_m$ . Therefore, the sets  $\text{pre}(v_1), \dots, \text{pre}(v_m)$  partition the set  $\{0, 1\}^\ell$ . Therefore, by putting Eq. 28 and Eq. 27 together, we can express the root node's state in terms of the nodes  $v_1, \dots, v_m$  on level  $\ell$ :

$$R|r\rangle = \sum_{k=1}^m \sum_{x \in \text{pre}(v_k)} |x\rangle \otimes \text{FOLLOW}_x(\xrightarrow{R}\textcircled{r}) \quad (29)$$

$$= \sum_{k=1}^m \sum_{x \in \text{pre}(v_k)} |x\rangle \otimes \text{Labels}(x) \cdot |v_k\rangle \quad (30)$$

We now show that each term  $\sum_{x \in \text{pre}(v_k)} |x\rangle \otimes \text{Labels}(x) \cdot |v_k\rangle$  contributes a non-zero vector. It then follows that the state has computational basis rank at least  $m$ , since these terms are vectors with pairwise disjoint support, since the sets  $\text{pre}(v_k)$  are pairwise disjoint. Specifically, we show that each node has at least one prefix  $x$  such that  $\text{Labels}(x) \cdot |v\rangle$  is not the all-zero vector. This can fail in one of three ways: either  $v$  has no prefixes, or all prefixes  $x \in \text{pre}(v_k)$  have  $\text{Labels}(x) = 0$  because the path contains an edge labeled with the 0 LIM, or the node  $v$  represents the all-zero vector (i.e.,  $|v\rangle = \vec{0}$ ). First, we note that each node has at least one prefix, since each node is reachable from the root, as a LIMDD is a connected graph. Second, due to the zero edges rule (see Definition 4), for any node, at least one of its prefixes has only non-zero LIMs on the edges. Namely, each node  $v$  has at least one incoming edge labeled with a non-zero LIM, since, if it has an incoming edge from node  $w$  labeled with 0, then this must be the high edge of  $w$  and by the zero edges rule the low edge of  $w$  must also point to  $v$  and moreover must be labeled with  $\mathbb{I}$  by the low factoring rule. Together, via a simple inductive argument, there must be at least one non-zero path from  $v$  to the root. Lastly, no node represents the all-zero vector, due to the low factoring rule (in Definition 4). Namely, if  $v$  is a node, then by the low factoring rule, the low edge has label  $\mathbb{I}$ . Therefore, if this edge points to node  $v_0$ , and the high edge points to  $\xrightarrow{P}\textcircled{v_1}$ , then the node  $v$  represents  $|v\rangle = |0\rangle|v_0\rangle + |1\rangle P|v_1\rangle$  with possibly  $P = 0$ , so, if  $|v_0\rangle \neq \vec{0}$ , then  $|v\rangle \neq \vec{0}$ . An argument by induction now shows that no node in the reduced LIMDD represents the all-zero vector.

Therefore, each node has at least one prefix  $x$  such that  $\text{FOLLOW}_x(\frac{R}{r} \circ r) \neq \vec{0}$ . We conclude that the equation above contains at least  $m$  non-zero contributions. Hence  $m \leq \chi_{\text{comp}}(R|r)$ , at any level  $0 \leq \ell \leq n$ .  $\square$

**Lemma 23.** Each intermediate state in the circuit in Fig. 14 has  $\chi_{\text{comp}}(|\psi\rangle) \leq n$ .

*Proof.* The initial state is  $|\psi_0\rangle = |0\rangle^{\otimes n}$ , which is a computational basis state, so  $\chi_{\text{comp}}(|\psi_0\rangle) = 1$ . The first  $\log n$  gates are Hadamard gates, which produce the state

$$|\psi_{\log n}\rangle = H^{\otimes \log n} \otimes \mathbb{I}^{n-\log n} |0\rangle = |+\rangle^{\otimes \log n} \otimes |0\rangle^{\otimes n-\log n} = \frac{1}{\sqrt{n}} \sum_{x=0}^{n-1} |x\rangle |0\rangle^{\otimes n-\log n} \quad (31)$$

This is a superposition of  $n$  computational basis states, so we have  $\chi_{\text{comp}}(|\psi_{\log n}\rangle) = n$ . All subsequent gates are controlled- $X$  gates; these gates permute the computational basis states, but they do not increase their number.  $\square$

**Lemma 24.** The reduced LIMDD of each intermediate state in the circuit in Fig. 14 has polynomial size.

*Proof.* By Lemma 22, the width of a LIMDD representing  $|\varphi\rangle$  is at most  $\chi_{\text{comp}}(|\varphi\rangle)$  at any level. Since there are  $n$  levels, the total size is at most  $n\chi_{\text{comp}}(|\varphi\rangle)$ . By Lemma 23, the intermediate states in question have polynomial  $\chi_{\text{comp}}$ , so the result follows.  $\square$

**Lemma 25.** The LIMDD of each gate in the circuit in Fig. 14 has polynomial size.

*Proof.* Each gate acts on at most  $k = \log n + 1$  qubits. Therefore, the width of any level of the LIMDD is at most  $4^k = 4n^2$ . The height of the LIMDD is  $n$  by definition, so the LIMDD has at most  $4n^3$  nodes.  $\square$

The APPLYGATE procedure handles the Hadamard gates efficiently, since they apply a single-qubit gate to a product state. The difficult part is to show that the same holds for the controlled- $X$  gates. To this end, we show a general result for the speed of LIMDD operations (Lemma 26). Although this worst-case upper bound is tight, it is exponentially far removed from the best case, e.g., in the case of Clifford circuits, in which case the intermediate states can have exponential  $\chi_{\text{sub}}$ , yet the LIMDD simulation is polynomial-time, as shown in Sec. E.2.

**Lemma 26.** The number of recursive calls made by subroutine  $\text{APPLYGATE}(U, |\psi\rangle)$ , is at most  $n\chi_{\text{sub}}(U)\chi_{\text{sub}}(|\psi\rangle)$ , for any gate  $U$  and any state  $|\psi\rangle$ .

*Proof.* Inspecting Alg. 3, we see that every call to  $\text{APPLYGATE}(U, |\psi\rangle)$  produces four new recursive calls, namely  $\text{APPLYGATE}(\text{FOLLOW}_{rc}(U), \text{FOLLOW}_c(|\psi\rangle))$  for  $r, c \in \{0, 1\}$ . Therefore, the set of parameters in all recursive calls of  $\text{APPLYGATE}(U, |\psi\rangle)$  is precisely the set of tuples  $(\text{FOLLOW}_{rc}(U), \text{FOLLOW}_c(|\psi\rangle))$ , with  $r, c \in \{0, 1\}^\ell$  with  $\ell = 0 \dots n$ . The terms  $\text{FOLLOW}_{rc}(U)$  and  $\text{FOLLOW}_c(|\psi\rangle)$  are precisely the subfunctions of  $U$  and  $|\psi\rangle$ , and since there are at most  $\chi_{\text{sub}}(U)$  and  $\chi_{\text{sub}}(|\psi\rangle)$  of these, the total number of distinct parameters passed to  $\text{APPLYGATE}$  in recursive calls at level  $\ell$ , is at most  $\chi_{\text{sub}}(U, \ell) \cdot \chi_{\text{sub}}(|\psi\rangle, \ell) \leq \chi_{\text{sub}}(U) \cdot \chi_{\text{sub}}(|\psi\rangle)$ . Summing over the  $n$  levels of the diagram, we see that there are at most  $n\chi_{\text{sub}}(U)\chi_{\text{sub}}(|\psi\rangle)$  distinct recursive calls in total. As detailed in Sec. 4.3, the APPLYGATE algorithm caches its inputs in such a way that it will achieve a cache hit on a call  $\text{APPLYGATE}(U', |\psi'\rangle)$  when it has previously been called with parameters  $U, |\psi\rangle$  such that  $U = U'$  and  $|\psi\rangle = |\psi'\rangle$ . Therefore, the total number of recursive calls that is made, is equal to the number of *distinct* calls, and the result follows.  $\square$

In our case, both  $\chi_{\text{sub}}(U)$  and  $\chi_{\text{sub}}(|\psi\rangle)$  are polynomial, so a polynomial number of recursive calls to  $\text{APPLYGATE}$  is made. We now show that also the ADD subroutine makes only a small number of recursive calls every time it is called from  $\text{APPLYGATE}$ . First, Lemma 27 shows expresses a worst-case upper bound on the number of recursive calls to  $\text{ADD}$  in terms of  $\chi_{\text{sub}}$ . Then Lemma 28 uses this result to show that, in our circuit, the number of recursive calls is polynomial in  $n$ .

**Lemma 27.** The number of recursive calls made by the subroutine  $\text{ADD}(|\alpha\rangle, |\beta\rangle)$  is at most  $n\chi_{\text{sub}}(|\alpha\rangle) \cdot \chi_{\text{sub}}(|\beta\rangle)$ , if  $|\alpha\rangle, |\beta\rangle$  are  $n$ -qubit states.

*Proof.* Inspecting [Alg. 4](#), every call to  $\text{ADD}(|\alpha\rangle, |\beta\rangle)$  produces two new recursive calls, namely  $\text{ADD}(\text{FOLLOW}_0(|\alpha\rangle), \text{FOLLOW}_0(|\beta\rangle))$  and  $\text{ADD}(\text{FOLLOW}_1(|\alpha\rangle), \text{FOLLOW}_1(|\beta\rangle))$ . It follows that the set of parameters on  $n-\ell$  qubits with which  $\text{ADD}$  is called is the set of tuples  $(\text{FOLLOW}_x(|\alpha\rangle), \text{FOLLOW}_x(|\beta\rangle))$ , for  $x \in \{0, 1\}^\ell$ . This corresponds precisely to the set of subfunctions of  $\alpha$  and  $\beta$  induced by length- $\ell$  strings, of which there are  $\chi_{\text{sub}}(|\alpha\rangle, \ell)$  and  $\chi_{\text{sub}}(|\beta\rangle, \ell)$ , respectively. Because the results of previous computations are cached, as explained in [Sec. 4.3](#), the total number of recursive calls is the number of *distinct* recursive calls. Therefore, we get the upper bound of  $\chi_{\text{sub}}(|\alpha\rangle) \cdot \chi_{\text{sub}}(|\beta\rangle)$  for each level of the LIMDD. Since the LIMDD has  $n$  levels, the upper bound  $n\chi_{\text{sub}}(|\alpha\rangle) \cdot \chi_{\text{sub}}(|\beta\rangle)$  follows.  $\square$

**Lemma 28.** The calls to  $\text{ADD}(|\alpha\rangle, |\beta\rangle)$  that are made by the recursive calls to  $\text{APPLYGATE}(U_t, |\psi_t\rangle)$ , satisfy  $\chi_{\text{sub}}(|\alpha\rangle), \chi_{\text{sub}}(|\beta\rangle) = \text{poly}(n)$ .

*Proof.* We have established that the recursive calls to  $\text{APPLYGATE}$  are all called with parameters of the form  $\text{APPLYGATE}(\text{FOLLOW}_{r,c}(U_t), \text{FOLLOW}_c(|\psi_t\rangle))$  for some  $r, c \in \{0, 1\}^\ell$ . Inspecting [Alg. 3](#), we see that, within such a call, each call to  $\text{ADD}(|\alpha\rangle, |\beta\rangle)$  has parameters which are both of the form  $|\alpha\rangle, |\beta\rangle = \text{APPLYGATE}(\text{FOLLOW}_{r,c}(U_t), \text{FOLLOW}_{cy}(|\psi_t\rangle))$  for some  $x, y \in \{0, 1\}$ ; therefore, the parameters  $|\alpha\rangle, |\beta\rangle$  are of the form  $|\alpha\rangle, |\beta\rangle = \text{FOLLOW}_{r,c}(U_t) \cdot \text{FOLLOW}_r(|\psi_t\rangle)$ . Here  $\text{FOLLOW}_{cy}(|\psi_t\rangle)$  is a quantum state on  $n - (\ell + 1)$  qubits.

The computational basis rank of a state is clearly non-increasing under taking subfunctions; that is, for any string  $x$ , it holds that,  $\chi_{\text{comp}}(\text{FOLLOW}_x(|\psi\rangle)) \leq \chi_{\text{comp}}(|\psi\rangle)$ . In particular, we have  $\chi_{\text{comp}}(\text{FOLLOW}_{cy}(|\psi_t\rangle)) \leq \chi_{\text{comp}}(|\psi_t\rangle) = \mathcal{O}(n)$ . The matrix  $\text{FOLLOW}_{r,c}(U_t)$  is a subfunction of a permutation gate, and applying such a matrix to a vector cannot increase its computational basis rank, so we have

$$\chi_{\text{sub}}(|\alpha\rangle) = \chi_{\text{sub}}(\text{FOLLOW}_{r,c}(U_t) \cdot \text{FOLLOW}_{cy}(|\psi_t\rangle)) \quad (32)$$

$$\leq \chi_{\text{comp}}(\text{FOLLOW}_{r,c}(U_t) \cdot \text{FOLLOW}_{cy}(|\psi_t\rangle)) \leq \chi_{\text{comp}}(\text{FOLLOW}_{cy}(|\psi_t\rangle)) \quad (33)$$

$$\leq \chi_{\text{comp}}(|\psi_t\rangle) = \mathcal{O}(n) \quad (34)$$

This proves the lemma.  $\square$

**Theorem 29.** Each call to  $\text{APPLYGATE}(U_t, |\psi_t\rangle)$  runs in polynomial time, for any gate  $U_t$  in the circuit in [Fig. 14](#).

*Proof.* If  $U_t$  is a Hadamard gate, then LIMDDs can apply this in polynomial time by [Th. 20](#), since  $|\psi_t\rangle$  is a stabilizer state. Otherwise,  $U_t$  is one of the controlled- $X$  gates. In this case there are a polynomial number of recursive calls to  $\text{APPLYGATE}$ , by [Lemma 26](#). Each recursive call to  $\text{APPLYGATE}$  makes two calls to  $\text{ADD}(|\alpha\rangle, |\beta\rangle)$ , where both  $\alpha$  and  $\beta$  are states with polynomial subfunction rank, by [Lemma 28](#). By [Lemma 27](#), these calls to  $\text{ADD}$  all complete in time polynomial in the subfunction rank of its arguments.  $\square$

**Corollary 29.1.** The circuit in [Fig. 14](#) can be simulated by LIMDDs in polynomial time.

## G Numerical search for the stabilizer rank of Dicke states

Given the separation between the Clifford + T simulator – a specific stabilizer-rank based simulator – and Pauli-LIMDDs, it would be highly interesting to theoretically compare Pauli-LIMDDs and general stabilizer-rank simulation. However, proving an exponential separation would require us to find a family of states for which we can prove its stabilizer rank scales exponentially, which is a major open problem. Instead, we here take the first steps towards a numerical comparison by choosing a family of circuits which Pauli-LIMDDs can efficiently simulate and using Bravyi et

al.’s heuristic algorithm for searching the stabilizer rank of the circuits’ output states [10]. If the stabilizer rank is very high (specifically, if it grows superpolynomially in the number of qubits), then we have achieved the goal of showing a separation. We cannot use  $W$  states for showing this separation because the  $n$ -qubit  $W$  state  $|W_n\rangle$  has linear stabilizer rank, since it is a superposition of only  $n$  computational basis states. Instead we focus on their generalization, Dicke states  $|D_w^n\rangle$ , which are equal superpositions of all  $n$ -qubit computational-basis states with Hamming weight  $w$  (note  $|W_n\rangle = |D_1^n\rangle$ ),

$$|D_w^n\rangle = \frac{1}{\sqrt{\binom{n}{w}}} \sum_{x:|x|=w} |x\rangle \quad (35)$$

We implemented the algorithm by Bravyi et al.: see [74] for our open-source implementation. Unfortunately, the algorithm’s runtime grows significantly in practice, which we believe is due to the fact that it acts on sets of quantum state vectors, which are exponentially large in the number of qubits. Our implementation allowed us to go to at most 9 qubits using the SURF supercomputing cluster. We believe this is a limitation of the algorithm and not of our implementation, since Bravyi et al. do not report beyond 6 qubits while Calpin uses the same algorithm and reaches at most 10 qubits [75]. Table 3 shows the heuristically found stabilizer ranks of Dicke states with our implementation. Although we observe the maximum found rank over  $w$  to grow quickly in  $n$ , the feasible regime (i.e. up to 9 qubits) is too small to draw a firm conclusion on the stabilizer ranks’ scaling.

Since our heuristic algorithm finds only an upper bound on the stabilizer rank, and not a lower bound, by construction we cannot guarantee any statement on the scaling of the rank itself. However, our approach could have found only stabilizer decompositions of very low rank, thereby providing evidence that Dicke states have very slowly growing rank, meaning that stabilizer-rank methods can efficiently simulate circuits which output Dicke states. This is not what we observe; at the very least we can say that, if Dicke states have low stabilizer rank, then the current state-of-the-art method by Bravyi et al. does not succeed in finding the corresponding decomposition. Further research is needed for a conclusive answer.

We now explain the heuristic algorithm by Bravyi et al. [10], which has been explained in more detail in [75]. The algorithm follows a simulated annealing approach: on input  $n, w$  and  $\chi$ , it performs a random walk through sets of  $\chi$  stabilizer states. It starts with a random set  $V$  of  $\chi$  stabilizer states on  $n$  qubits. In a single ‘step’, the algorithm picks one of these states  $|\psi\rangle \in V$  at random, together with a random  $n$ -qubit Pauli operator  $P$ , and replaces the state  $|\psi\rangle$  with  $|\psi'\rangle := c(\mathbb{I} + P)|\psi\rangle$  with  $c$  a normalization constant (or repeats if  $|\psi'\rangle = 0$ ), yielding a new set  $V'$ . The step is accepted with certainty if  $F_V < F_{V'}$ , where  $F_V := |\langle D_w^n | \Pi_V | D_w^n \rangle|$  with  $\Pi_V$  the projector on the subspace of the  $n$ -qubit Hilbert space spanned by the stabilizer states in  $V$ . Otherwise, it is accepted with probability  $\exp(-\beta(F_{V'} - F_V))$ , where  $\beta$  should be interpreted as the inverse temperature. The algorithm terminates if it finds  $F_V = 1$ , implying that  $|D_w^n\rangle$  can be written as linear combination of  $V$ , outputting the number  $\chi$  as (an upper bound on) the stabilizer rank of  $|\psi\rangle$ . For a fixed  $\chi$ , we use identical values to Bravyi et al. [10] and vary  $\beta$  from 1 to 4000 in 100 steps, performing 1000 steps at each value of  $\beta$ .

Table 3: Heuristically-found upper bounds on the stabilizer rank  $\chi$  of Dicke states  $|D_w^n\rangle$  (eq. (35)) using the heuristic algorithm from Bravyi et al. [10], see text in App. G for details. We investigated up to 9 qubits using the SURF supercomputing cluster (approximately the same as the number of qubits reached in the literature as described in the text). Empty cells indicate non-existing or not-investigated states. In particular, we have not investigated  $w > \lfloor \frac{n}{2} \rfloor$  since  $|D_w^n\rangle$  and  $|D_{n-w}^n\rangle$  have identical stabilizer rank because  $X^{\otimes n} |D_w^n\rangle = |D_{n-w}^n\rangle$ . For  $|D_3^8\rangle$  and  $|D_4^9\rangle$ , we have run the heuristic algorithm to find sets of stabilizers up to size 11 (theoretical upper bound) and 10, respectively, but the algorithm has not found sets in which these two Dicke states could be decomposed. We emphasize that the algorithm is heuristic, so even if there exists a stabilizer decomposition of a given rank, the algorithm might not find it.

#qubits $n$	Hamming weight $w$				
	0	1	2	3	4
<b>1</b>	1				
<b>2</b>	1	1			
<b>3</b>	1	2			
<b>4</b>	1	2	2		
<b>5</b>	1	3	2		
<b>6</b>	1	3	4	2	
<b>7</b>	1	4	7	4	
<b>8</b>	1	4	8	$\leq 11$	5
<b>9</b>					$> 10?$